Three-Dimensional Imaging of Ventricular Electrical Activity: Method, Animal Validation and Clinical Evaluation

A DISSERTATION SUBMITTED TO THE GRDUATE SCHOOL AND FACULTY OF UNIVERISTY OF MINESOTA BY

Long Yu

IN PARTIAL FULFILLMENT OF THE REQUIREMENTS FOR THE DEGREE OF DOCTOR OF PHILOSOPHY

Prof, Bin He, Advisor

February 2017

Acknowledgement

Here in the first place above all, I would like to address my most sincere gratitude to my advisor Dr. Bin He. The teachings from Dr. He have far exceeded purely technical or scientific knowledge in the research lectures or discussions. Dr. He, as a role model, has been and still is teaching me what the world should be like in the eye of the a scientist, what a scientist means and how one should make his contribution to the world. It is his philosophy, together with his knowledge, that guided me through my study and help me overcome the difficulties along the course. It has been a great journey to be a student of his and make the scientific progress under his supervision. I would also like to express my thanks to my committee members: Dr. Paul Iaizzo, Dr. Author Erdman, Dr. Shai Ashkenazi and Dr. Hubert Lim. The discussions with my committee have always been very inspiring and leading to further improvement to my dissertational research.

I would very much like to acknowledge Dr. Steven Pogwizd, who has been more a mentor of me rather than a collaborator in research, of the useful discussions, the resources and most importantly the skills I learned from him along the years of studies. Also, I would like to thank Dr. Liqun Wu and Dr. Qi Jin for the help in the clinical studies as collaborators, which significantly contribution to the clinical part of the dissertation.

A very significant part of my acknowledgement should be addressed to the other members of the team. I would like to give my special thanks to Dr. Chengzong han, Dr. Chenguang Liu and Dr. Zhaoye Zhou. With great patience

and passion have they trained me and prepared me in almost every aspect of the research and scientific thinking. Without their help, finishing the dissertational study will be extremely challenging. I would also like to thank Ms. Ting Yang for being key part of the research team, who will for sure bring the technology to an entirely new level.

Without any doubt, my appreciation goes to the whole lab, a long list of outstanding researchers carrying on excellent research on different scientific front lines. The very environment built by all is such a benefiting one for me to conduct scientific and technical explorations. More than that, I am grateful for the friendship and interactions with these extraordinary minds over the years.

Dedication

This dissertation is dedicated to my patients, Zhengjun Yu and Xiaoping Sun as they have taught me how to be a decent human being with an independent mind before all the academic training can ever happen and all the scientific finding can be ever be made.

The dissertation is also dedicated to my life-long companion, Disi, whose love and support has helped me through all the challenges and given me courage to pursue further and higher goals.

The dissertation is, last but not least, to all my friends who I do not manage to mention in the acknowledgement. I will not be who I am, for the better or worse but for sure uniquely , without all of you.

Abstract

Non-invasive cardiac electrical imaging techniques aim to directly visualize the intra-cardiac electrical activities and promise to assist in clinical diagnosis and treatment of cardiac arrhythmias, a family of highly dangerous disease leading to a hundreds of thousands of deaths and disabilities in the United States alone. In this dissertation, a line of investigations is included regarding cardiac electrical sparse imaging - a novel three dimensional cardiac imaging technique – from mathematical formulation of the imaging problem to validations studies covering numerical models, animal healthy and pathological models and patients with ventricular arrhythmias both during and before cardiac ablative procedures.

With its spatiotemporal sparse problem, the novel imaging method incorporate cardiac electrophysiological features into the imaging process in order to achieve improvements in spatiotemporal resolution and, consequentially, general performance of the imaging technique. Simulation studies were conducted using a cardia automaton based heart-torso numerical model to verify the performance of the technique against various disturbances resembling the clinical challenges. Based on the numerical studies, rigorous animal studies using intra-cardiac simultaneous mapping technique were conducted to further validate the technique in biological systems such as canine and swine under healthy and pathological conditions such as myocardial infarction and congestive heart failure. Moreover, to evaluate the performance and compatibility of the technique in real life clinical challenges, further in-

procedural and pre-procedural clinical studies were carried out on patients with ventricular arrhythmias.

High accuracy and strong robustness can be observed by comparing the imaged activations with the mapped ones. The imaging technique achieved good performance not only in numerical simulations, but also in animal models with complex pathological conditions. Strong correlation was observed from the comparisons on ventricular arrhythmias with both focal and reentrant patterns. In further clinical studies, the technique also achieved good performance in localizing the arrhythmia foci and imaging the 3D activation pattern during the arrhythmias.

The promising results shown in the studies indicate that the technique has good capability in visualizing the whole heart electrical activities and in providing key information such as arrhythmia foci and reentry pathways to assist in clinical practice in various pathological conditions.

Contents

List of Figures

List of Tables

Chapter 1

Introduction

1.1. Overview

Contraction of the cardiac muscle is coordinated by a proper electrical activation throughout the myocardium. However, in a situation where the electrical activation fails to propagate normally, the cardiac function will be compromised and possibly leading to severe syndrome such as sudden cardiac arrest(Go et al. 2014; Mozaffarian et al. 2015). The condition where healthy cardiac rhythm is disrupted electrically is called cardiac arrhythmia. Each year, more than 400,000 cases of sudden cardiac arrest have been reported, causing numerous deaths and disabilities. As a routine procedure anti-arrhythmic drugs have been administered to the patients with arrhythmias(Mozaffarian et al. 2015). In the recent years, direct substrate modification achieved by catheter ablation is becoming a widely adopted procedure to eliminate the arrhythmia syndromes.

Naturally, the success of the clinical management – both diagnosis and treatment - of cardiac arrhythmia relies heavily on the information regarding the electrical activation inside the heart(Nademanee et al. 2011). Efforts from various perspective have been put to obtain direct information during the arrhythmic activities. Cardiac electrophysiological mapping techniques emerged as a key tool to aid in both the fundamental research of cardiac electrophysiological mechanism and the clinical management of cardiac

arrhythmia such as catheter ablation or cardiac resynchronization therapies(Nademanee and Kosar 1998; Nademanee et al. 2011). Compared to open chest direct mapping, minimally invasive catheter based mapping techniques have been utilized with increasing popularity. Successful as the catheter based techniques have been since, they are subjected to some intrinsic limitations such as long mapping time, limited mapping area and difficulties in mapping unstable arrhythmias. Therefore, there is strong need for techniques that can map the cardiac electrical activities in a fast and beat-to-beat manner.

Non-invasive approaches have been pursued for decades in the aim of visualizing the intra-cardiac electricity based on body surface observations. As a standard procedure, 12 lead ECG recordings have been widely used in the diagnosis and the treatment planning of cardiac arrhythmias. The standard procedural enjoys the strength of the simplicity and relatively low cost in hardware setup(Yamada et al. 2015). However, due to its lack in number of measurements, the observed ECG recordings are a projection of the complicated electrical activity of cardiac conduction and limited by the very simplification of system, especially in arrhythmic conditions. Body surface mapping techniques employ more electrodes than standard 12 lead ECG technique in order to extend the observation space for more information. The techniques have shown promising results in identifying further detailed features during various arrhythmia, but yet this kind of visualization is still indirect and the cardiac electrical signal is heavily convoluted travelling through the body, a volume conductor.

In order to solve the volume conduction problem and further exploit the information hiding in the body surface observations, non-invasive imaging techniques have been developed over the years in the pursuit of applying numerical methods to model the electrical conduction and inverse calculated the intra-cardiac electrical activity based on body surface ECG recordings(Y. Wang et al. 2011; Berger et al. 2006; Zhang et al. 2005; Z. Liu, Liu, and He 2006; Yu, Zhou, and He 2015). The epicardial imaging technique seeks to reconstruct the epicardial potential maps to identify the activation sequence. Modeled based surface activation imaging technique was also developed to determine the surface activation using a pre-defined depolarization model. Three dimensional cardiac imaging techniques, in contrast to epicardial or surface imaging techniques, have been developed to visualize the whole heart electricity throughout the myocardium. Various approaches, both physical based 3D imaging and physiological model based estimation approaches have been investigated. With the goal of direct identifying the critical area and mechanism of cardiac arrhythmias, the techniques have demonstrated significant potential and promising performance in further applications.

1.2 Goals and Significance

The goal of the dissertation study is to further develop the 3D Cardiac Electrical Imaging (3DCEI) technique and thoroughly validate and evaluate the method in numerical, animal and clinical studies as detailed below:

1. By integrating electrophysiological knowledge in the originally physical-model based 3D imaging technique, the imaging problem formulation is to

be extended into 4D spatiotemporally in order to achieve improved performance and optimized using numerical simulations.

2. The developed technique will be validated using the 3D intra-cardiac mapping technique in experimental animals such as rabbit, canine and swine under various pathological conditions such congestive heart failure and myocardial infarction. The imaged activation is to be compared directly with 3D intra-cardiac recorded electrical activation mapped during simultaneous mapping study to quantitatively validate the method in a rigorous manner.
3. The imaging technique is to be further evaluated on the performance and the compatibility in the clinical scenarios. Both pre-procedural and in-procedural simultaneous studies are to be conducted to test the developed technique against real-life challenges.

The success of cardiac ablation procedure depends heavily on how accurate the crus of the arrhythmia can be localized and targeted for ablation. The foci of the automatic cardiac arrhythmia or reentry isthmus can emerge from various locations and depths in the myocardium, from epicardium to transmural area to endocardium. Failing to pinpoint the arrhythmic foci or reentry pathway preciously in 3D can results in failure to eliminate the arrhythmias. Therefore, an imaging technique that can provide accurate knowledge three dimensionally can provide significant assistance in clinical management of the cardiac arrhythmia given the catheter electrophysiological mapping can only measure cardiac electrical activities on limited area. For a medical imaging technique,

rigorous validation plays a vital role in the assessment of accuracy and robustness in well controlled and clinically relevant scenarios. In this dissertation study, 3D intra-cardiac mapping technique, where intra-cardiac transmural electrode needles were inserted into the myocardium to monitor the electrical activities throughout the myocardium, was utilized to validate the developed imaging technique quantitatively in a rigorous manner. A line of animal models – rabbits, canine and swine – were employed as animal models in the simultaneous study. Various types of arrhythmias such as automatic and reentrant arrhythmias were induced on different pathological models such as heart failure and congestive heart failure. The broad spectrum of animal model can provide significant insight on the performance of the medical imaging technique against the highly dynamic clinical challenges. Moreover, in-procedure and pre-procedure clinical studies were conducted to directly evaluate the capability of the technique as a clinical tool in both pre-ablation diagnostics and potentially assisting the ablation in the EP lab. The clinical study fully examined the performance and the compatibility of the imaging technique on patients with ventricular arrhythmias to test the imaging technique against real clinical challenges and verify the potential of the imaging technique to fully function in a clinical environment.

1.3 Scope of the Dissertation

In chapter 2, a brief review is made on the general electrophysiology and related non-invasive imaging techniques. Important previous efforts on the topic are also discussed.

In chapter 3, the technique details of the developed Cardiac Electrical Sparse Imaging (CESI) technique are presented together with numerical simulations conducted for preliminary evaluation and optimization of the method. Single site and dual site pacing simulations were conducted with various noise/error disturbances such as Gaussian noise, hospital recorded noise, geometrical model error and registration error etc. Some preliminary results on rabbit pace mapping is also shown.

In chapter 4, a series of animal validation study are presented to evaluate the performance of the imaging technique against automatic arrhythmias such as PVC and VTs in both healthy and congestive heart failure conditions. Simultaneous study using 3D intra-cardiac mapping technique was performed on rabbit and canine models to quantitatively validate the method. Further animal study on swine with myocardial infarction are shown. Reentrant arrhythmias were induced using programmed pacing stimulations. Imaged activation sequences during the reentry were compared with the measured one to evaluate the capability of the imaging technique to identify the reentry pathway and localize the reentry isthmus in the highly dynamic arrhythmia.

In chapter 5, clinical investigation was carried out to evaluate the performance of the imaging technique to identify the arrhythmic foci in patient with Premature Ventricular Complex (PVC), a most common type of ventricular arrhythmia. The imaging results were compared with the CARTO invasive mapping results for quantitative evaluation. Furthermore, the clinical investigations are extended to in-procedure simultaneous mapping study

carried out in EP labs on patient during the catheter ablation of ventricular arrhythmias such as PVC and VT. Both the performance of the imaging technique against the highly dynamic rhythms in VT and the compatibility of the imaging system with the current standing equipment are examined in the clinical setup. Deep learning technique to identify the depth of the arrhythmic foci is introduced and evaluated in numerical and clinical studies. The deep learning neuro network is trained using the personalized simulation framework and tested in both simulations and clinical rhythms such as paced beats and PVCs.

In chapter 6, the major contributions of the dissertation study is discussed. Discussions on potential future work is also presented.

Chapter 2

Background

2.1 Cardiac Electrical Activity and Arrhythmias

The electrical activity in the heart plays a key role in organizing the contracting movement and maintaining the cardiac output to support the lungs and peripheral organs. Within a cardiac cycle, the normal intrinsic electrical conduction of the heart allows electrical impulse propagation to be initiated from the sinoatrial node through the atria and then forward to the atrial ventricular junction. Normal physiology allows further propagation along purkinje fibers, their respective bundle branches, and activates the ventricular myocardium in proper order. This electrical conduction system initiates a depolarization wave front that spread throughout the myocardium tissue and thus causes efficient and coordinated contraction of the cardiac muscle tissue to provide blood perfusion through the rest of the system.

The cardiac electrical activities are generated thorough the ion flow through the cell membrane ion channel during depolarization and repolarization. The depolarization occurs due to an inflow of sodium ions through the cell membranes ion channels. A repolarization phrase subsequently follows due to the potassium ion outflow. The transient shift from a resting state to an excited state of cardiac cell defines the action potential, a time dependent voltage function, travels from excited, or depolarized, cells to neighboring resting cells via low resistance intercellular junctions.

In the abnormal conditions, the cardiac activation sequence can be disturbed – by ectopic initiation site or structural damage cause by disease – and is described as cardiac arrhythmias. The abnormal rhythm can be faster or slower than normal conditions, or neither but ineffective in pumping blood due to ill-ordered activation. The disease affect numerous people and constitutes a major threat to the public health. Among all kinds of arrhythmias, ventricular arrhythmias is a kind of repetitive fast heart rhythm which originates in the ventricles of the heart and has a high risk deteriorating into sudden cardiac arrest, a life threatening condition. As a regular approach to manage arrhythmias, anti-arrhythmic drugs have been administered for the past decades. However, it has been shown that pharmacological treatment is difficult considering the significant proarrhythmic effects of many antiarrhythmic agents. As an alternative approach, electrical intervening devices, including implantable and wearable defibrillators, cardiac pacemakers and cardiac resynchronization leads, have been developed and investigated to suppress the lethal syndromes and mitigate the malignant effect of cardiac arrhythmias. More recently, substrate modification approaches, such as radiofrequency based catheter ablation procedure, have been increasingly relied on to eliminate the lethal arrhythmias. Naturally, the success of this kind of targeted therapy heavily relied on the accuracy of the knowledge regarding the mechanism of the arrhythmia and the potential ablation targets such as arrhythmic foci and reentry isthmus.

2.2 Electrophysiological Mapping

Electrophysiological mapping emerges as an important tool to characterize the electrophysiological state of the arrhythmic heart and to localize the potential ablation targets, providing significant assistance in both research to understand arrhythmic mechanism and the clinical management of cardiac arrhythmia such as catheter ablation and configuration of cardiac resynchronization therapy(Nademanee and Kosar 1998). More recently, technical advancement has been made allowing the physicians to identify the intra-cardiac electrical activity and intervene using minimal invasive catheter based ablation procedure. One of the wide used EP mapping system, the non-fluorescent electroanatomic catheter mapping technique, or CARTO system, has been developed using electromagnetic guidance of the catheter positioning to achieve activation mapping by performing sequential mapping on the endocardium(Yamada et al. 2015; Nademanee and Kosar 1998; Nademanee et al. 2011). Another widely applied approach is the cavitary non-contact endocardial mapping technique, or Ensite Velocity(Thiagalingam et al. 2004). The Ensite system reconstruct endocardial potentials from its multiple electrodes non-contact sensing array in the chamber of interest during the arrhythmias. Widely applied as the catheter based techniques have been recently, the procedure remains invasive and need fluoroscopy and magnetic guidance to properly function, indicating major demand in resource, time and expertise to successfully identify the key ablation targets. In some cases such as hemodynamic instability or special arrhythmic location, the catheter based

mapping techniques can be difficult to perform. Other than the minimal invasive approaches, open chest epicardiac or intra-cardiac contact mapping can also provide detailed information on the electrical activity by directly measuring the local potential during arrhythmias. However, limited by the invasiveness, open chest mapping has a relatively limited role in clinical practice but represents a good approach in understanding arrhythmic mechanism in animal studies.

2.3 Noninvasive Mapping and Imaging of Cardiac Electricity

The thoracic detection of the electrical activity of the heart over a period of time, as recorded by electrodes attached to the outer surface of the skin is the electrocardiogram (ECG). Current clinically routine noninvasive detection of the cardiac electrical activity is widely performed using 12-lead ECG system. The standard 12-Lead ECG system includes three bipolar limb leads, six unipolar thoracic electrodes and three segmented unipolar leads. As a standard procedure in clinical practice, one can derive important diagnostic information based on the 12 lead ECG readings.

By employing more electrodes rather than just six on the thorax, Body Surface Potential Mapping (BSPM) explores to acquire more information than the original 12 lead approach. In the past decades, BSPMs and its variant have been shown by many experimental and clinical studies to have higher diagnostic power benefiting from the expanded sensing space. However, the body surface measurements, regardless of number of measurements adopted, suffer from

the limitation that body surface observation, however, dense, is an indirect reflection of electrical event occurring inside the heart. Much information can be lost in the smoothing and distorting process when the electrical activity travels from the myocardium to the body surface.

The cardiac electrical imaging techniques include ECG forward problem and ECG inverse problem (Figure 1). The ECG forward problem lays foundations for noninvasive cardiac electrical imaging techniques through mathematically modeling the electrical field between heart and torso. The ECG forward problem entails the calculation of densely sampled body surface potentials, starting from the assumed equivalent cardiac sources models (e.g., equivalent current density, transmembrane potential, or epicardial/pericardial potentials) to represent the cardiac electrical activity.

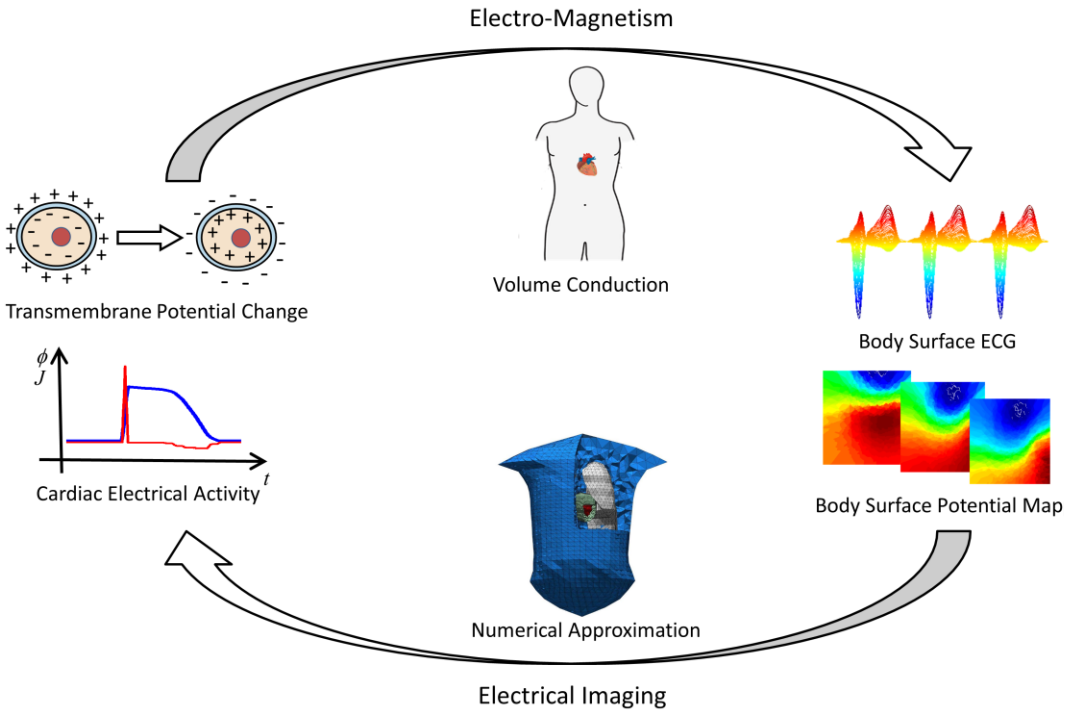

Figure 1: Illustrations of the principles of cardiac electrical imaging. When a cell activates, the transmembrane potential change rapidly and generates electrical activity that can travel through the body and be detected by ECG electrodes. With numerical methods such as the boundary element method, the electrical activity can be reconstructed in the form of equivalent current densities inside the myocardium to visualize the activation pattern of the cardiac depolarization process.

The ECG imaging problem is to reconstruct the source distribution over specified volume conductor from body surface potentials through certain mathematical manipulation. The solutions to the imaging problem give one direct insight into the electrical activity of the heart without invasive assess to the myocardium. One of the major challenge of the imaging problem is the ill-posedness of the problem, rendering the direct solution of the imaging problem without a unique solution. In the past decades, many investigations have been made to overcome the difficulty of non-uniqueness of ECG inverse problem by

using different formulations of equivalent cardiac electrical generators. A direct solution, naturally, is to reduce the presentation of the complex electrical process of the heart in dimension, fitting the scope of the measurements. By presenting the heart with a few electrical dipoles, the dipole localization seeks to pinpoint the key activity noninvasively. However, due to the distributed nature of the cardiac electrical activity, the moving dipole solution tends to oversimplify the cardiac activation at the arrhythmic conditions. Epicardial imaging techniques advance the imaging object from a single site to the whole epicardial surface by incorporating structural information into reconstruction. Geometries from structural imaging modalities like CT and MR are used to relate epicardial and body surface potential distribution based on bidomain theory. Activation sequences on epicardial surface can be reconstructed with this kind of technique on realistic geometry and thus more information is provided. But for many arrhythmias whose origins or abnormal pathways lie deep into the myocardium, a direct visualization of cardiac electrical activities on these regions of interests become difficult.

For higher efficiency in ablation surgery and better understanding of arrhythmia in human, a 3D approach to investigate cardiac electrical activity on a beat-to-beat basis is necessary and of great importance. Imaging cardiac electrical activity three dimensionally based on physiological prior knowledge has been developed and evaluated on animal model. The inverse solution was computed with nonlinear optimization method to minimize model error and maximize correlation.

Recently, a novel three dimension (3D) cardiac electrical imaging (3DCEI) technique based on physical model has been proposed to inversely solve equivalent current density distribution and thus generate the electrical activation sequence of the entire myocardium. In this method, electrical activity, represented as a distributed equivalent current density model, was linearly related to body surface potential drop with boundary element model solely based on physical principles. Reconstruction of the electrical activity, or specifically current density in the model, was done through inversion of the linear system constrained by minimum energy principle. Activation time of myocardium was computed for each source point according to the peak criterion, generating a whole heart activation sequence with the activation propagation pattern shown in a 3D manner. This approach has been validated on various animal models such as rabbit and canine in comparison with 3D intra-cardiac mapping results. Previous study has shown that the method has demonstrated good concordance with direct measurement under both healthy and pathological conditions.

Reliable and computational efficient as the method is, the method does not take temporal dynamic of cardiac electrical activity into consideration. According to cardiac electrophysiology, a myocardial cell cannot fire constantly and a plateau followed the depolarization which indicates that the electrical activity in a certain location has a sparse property in temporal domain [15, 58]. This temporal dynamic information can be added to current 3DCEI and help to

improve the imaging accuracy. Details of the method will be discussed in later sections.

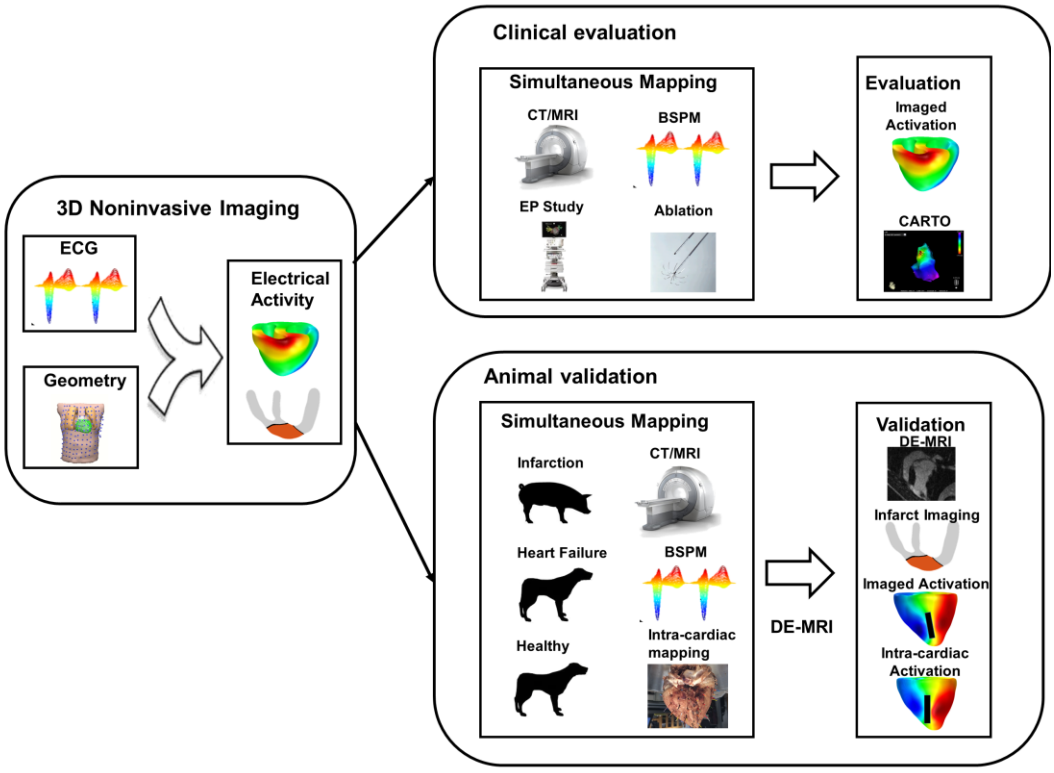

Figure 2: general schematic diagram of the experimental validation study. Simultaneous mapping studies were conducted on both patients and experimental animals with structure imaging conducted prior to the mapping study. Imaging activations were directly compared with the intra-cardiac recordings and the imaged infarction substrates were compared with DE-MRI segmentation results.

To sum up, imaging cardiac electrical activity three dimensionally has shown a good potential to provide additional important information in comparison to current mapping and imaging techniques in a clinical condition. With temporal information added into reconstruction, performance of 3DCEI can be further improved and demonstrate greater capability both in assistance of

clinical practice like ablation surgery and to help understand mechanism of ventricular arrhythmia in human patient.

Chapter 3

Formulation and Reconstruction of Temporal Sparse Promoting Cardiac Electrical Imaging

Cardiac disease is a significant challenge to public health and a leading killer in the United States, costing more than 270 billion dollars annually in the United States alone (Go et al. 2014). Each year, about 400, 000 sudden cardiac deaths are reported in the United States while a major portion of them are induced by ventricular arrhythmias (Go et al. 2014). In clinical practice, anti-arrhythmic medications are usually administered to suppress the life-threatening syndromes. For the medically refractory cases, catheter ablation has become a standard procedure to eliminate the arrhythmias (Nademanee and Kosar 1998; Ben-Haim et al. 1996; Nademanee et al. 2011). The success of such catheter ablation relies on information regarding the arrhythmogenesis. Contact and non-contact intra-cardiac mapping technologies have been employed to guide catheter ablative procedures (Ben-Haim et al. 1996; Thiagalingam et al. 2004). However, limited by its invasive nature, these approaches are often time consuming and can only map cardiac electrical activity on the endocardium of a single or only partial ventricular chamber. Therefore, there is a clinical need to develop noninvasive imaging modalities that can image cardiac electrical activity throughout the three-dimensional (3D) myocardial volume which shall play an important role in improving the effectiveness and efficiency of catheter ablation treatment and also help elucidate the mechanisms of ventricular arrhythmias.

Efforts have been made pursuing noninvasive approaches of mapping cardiac electrical activity by solving the inverse problem of electrocardiography (ECG) (Barr and Spach 1978; Berger et al. 2006; Oster et al. 1998; Z. Liu, Liu, and He 2006; Han et al. 2008; Li and He 2001; Greensite 2005; Liebman et al. 1991; Tilg et al. 2002; Bin He and Wu 2001; Bin He, Li, and Zhang 2002; Okamoto, Teramachi, and Musha 1983; Y. Wang et al. 2011; Bin He, Li, and Zhang 2003). Moving dipole localization techniques seek to represent whole heart electrical activity with either one or several moving dipoles (Gulrajani, Roberge, and Savard 1984; Armoundas et al. 2003). Epicardial imaging techniques expand the solution space from few dipole sources to potential distributions over the epicardial surface (Barr and Spach 1978; Oster et al. 1998; Y. Wang et al. 2011; Yamashita and Geselowitz 1985; Barr, Ramsey, and Spach 1977; Jamison et al. 2011). Heart surface activation imaging, alternatively, directly solves myocardial activation time on the heart surfaces based on a physiological model (Berger et al. 2006; Tilg et al. 2002). These methods have been shown to provide potentially valuable information noninvasively, although they estimate cardiac electrical activity over the epicardium or the heart surfaces (including epicardial and endocardial surfaces) instead of over the 3D myocardium (Barr and Spach 1978; Greensite 2005; Greensite and Huiskamp 1998).

Over the past decade, cardiac electrical imaging approaches considering the whole myocardium have been pursued. Physiological model based methods incorporate a priori knowledge based physiological model into inverse solutions to solve the ECG inverse problem (Li and He 2001; Bin He, Li, and Zhang 2003; Bin He, Li, and Zhang 2002; Zhang et al. 2005). Recently, a physical-model based 3D Cardiac Electrical Imaging (3DCEI) approach has been developed (Z. Liu, Liu, and He 2006) and validated on various animal models such as rabbits and canines (Han et al. 2008;

Han et al. 2012; Han et al. 2013; Han et al. 2011), in which good concordance was observed with 3D intra-cardiac mapping results (Han et al. 2011; Han et al. 2012; Han et al. 2013). However, the minimum energy based Weighted Minimum Norm (WMN) method employed by 3DCEI limits the spatial-temporal resolution and robustness against non-Gaussian disturbance such as geometrical modeling errors and electrode registration errors, which can be introduced in realistic scenarios due to limited quality in raw data. The minimum energy constraints (which is a physical constraint instead of electrophysiological constraint) imposed may become dominant in reconstruction, leading to a smoothed and distorted imaged activation sequence.

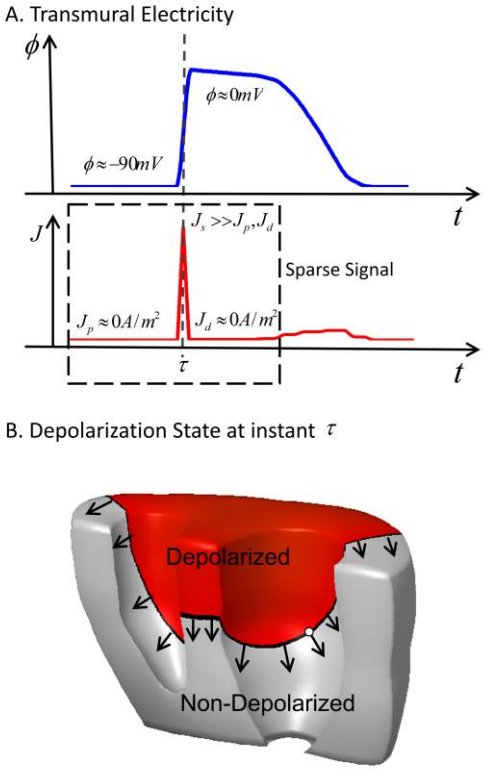

Figure 3: Temporal Sparse Property of myocardial electrical activity. Panel A shows the transmural potential ϕ and J, the magnitude of coresponding current density at the myocardium marked by the white dot in penal B. The depolarization state in the myocardium at instant τ, marked by dash lines, in A. Current density at the depolarization, J_s, is much larger than those at resting or plateau potential, represented by J_p and J_d due to the rapid transition of the transmural potential and therefore, the current density inside the rectangle can be assumed as sparse signal. However, this sparsity only holds in temporal domain.

In this chapter of dissertation, we propose a weighted group sparse promoting strategy based on a physical model to exploit the sparse properties of cardiac electrical activity and therefore improve the spatial-temporal resolution and the robustness in imaging 3D cardiac electrical activity. We conducted computer simulations to evaluate the performance of the proposed Cardiac Electrical Sparse Imaging (CESI) technique and further demonstrated the feasibility by using 3D intra-cardiac mapping data in a rabbit model.

3.1 Forward Formulation of the Imaging Problem

When a myocardial cell is activated, the TMP has a transient rise from the -90mV resting state to the plateau potential at around 0 mV. Regardless of individual variations in the resting or plateau potential, the impulse of trans-membrane current flow, corresponding to the temporal derivative of TMP, can indicate the timing of cell activation by sharp peaks while during the remainder of the cardiac cycle, the cell is nearly electrically silent. This indicates a sparse property of cardiac electrical activity in the temporal domain that can potentially be exploited for enhancement in imaging.

The spatial derivative of the TMP, equivalently, can be an indicator of activation propagation throughout the spatial domain of the myocardium. Activation propagates through the heart and generates a wave front between the resting and the depolarized myocardial tissue. For each myocardial cell, the TMP time course consists of two distinguished phases and a rapid transition between them. Figure 3 illustrates the temporal sparse property of cardiac electrical activity. The rapid potential shift from the polarized -90 mV to the depolarized 0 mV during propagation can generate an excitation wave front as well as a spike in current density for the myocardium at the wave front. On the other hand, the current density during the relatively stable potential in both resting and plateau stage is much smaller and can be considered as electrically silent compared with the spike. Therefore, the current density in each site of the myocardium can be assumed as a sparse signal. However, this sparsity can only hold in the temporal domain. Although each myocardial cell in a cardiac

cycle is activated only once, a considerably large portion of the heart can possibly be excited at the same time as excitation propagates. Note that the spatial derivative of TMP along a certain direction can be directly measured by bipolar recordings, a well-established mapping technique, allowing us to validate the performance of the cardiac electrical imaging results in a rigorous manner.

At location r and time instant t, equivalent current density J_{eq} can be defined as

$$J_{eq}(r,t) = -G_i(r)\nabla\Phi_m(r,t) \quad (1)$$

Where $G_i(r)$ stands for the intracellular effective conductivity tensor at location r and $\Phi_m(r,t)$ is the transmembrane potential.

Based on the bidomain theory and distributed ECD model, the discrete architechture of the myocardial cell can be generalized into a model on a macroscopic continuum where the electrical activity in myocardium can be represented with two component: intracellular and extracellular domains divided by a theoretical membrane. The electrical behavior of assumed quasi-static state electrical field is governed by(Miller and Geselowitz 1978; Tung 1978)(Miller and Geselowitz 1978; Tung 1978)(Miller and Geselowitz 1978; Tung 1978):

$$\nabla\cdot[(G_i(r)+G_e(r))\nabla\Phi_e(r,t)] = \nabla\cdot J_{eq}(r,t) \quad (2)$$

Where $G_e(r)$ and $G_i(r)$ are the extracellular and intracellular effective conductivity tensors and $\Phi_e(r,t)$ is the extracellular potential at location r and time instant t. The differential equation (2), with boundary element model approximation and a distributed

grid point ventricular geometrical model, can be linearized into a matrix-vector transfer function shown as:

$$\vec{\Phi} = L\vec{J} \tag{3}$$

Where L stands for the transfer matrix and $\vec{\Phi}, \vec{J}$ are vectors of body surface potentials and equivalent current density at the source grid points inside the myocardium, respectively. Matrix L is an $M \times 3N$ matrix connecting M electrode measurements and the current density dipole momentums on N myocardial grid points. On each grid point, 3 momentums are considered in equivalence of a rotating current density dipole. Eq. (3) depicts the linear relation between body surface ECG and equivalent current density on each grid point of the myocardium source at a certain time instant. To expand this to the entire time course, Eq. (3) can be reformed into:

$$\vec{\Phi}_T = L_T \vec{J}_T \tag{4}$$

$$L_T = \begin{bmatrix} L & & & \\ & L & & \\ & & \ddots & \\ & & & L \end{bmatrix} \tag{5}$$

where L_T is a $MT \times 3NT$ matrix which connects the body surface potentials over a period of time, Φ_T, and the equivalent current density over a period of time J_T. In Eq. (4), a transfer function from the electrical activity on a time course for each myocardial voxel to the body surface potential for the time window T is constructed. The temporal dynamics of cardiac electrical activity and its sparse property can be described in J_T and shown in the reconstructed solutions in subsequent sections.

3.2 Temporal Sparse Promoting Reconstruction of Equivalent Current Density

Eq. (4) formulates a forward problem that connects the spatiotemporal dynamics of cardiac electrical activity with the body surface potential maps (BSPMs). However, the formulated problem is ill-posed and cannot be solved by direct matrix inversion. Minimum energy based inverse regularization have been investigated for cardiac electrical imaging (Oster et al. 1998; Berger et al. 2006; Z. Liu, Liu, and He 2006) while the pure physical constraints imposed to achieve direct inverse fail to incorporate physiological knowledge and each timeframe is computed independently, leading to a smoothing effect that decreases temporal resolution and distorts the activation sequence. Sparse constraints can be applied to the inverse problem formulation in order to produce solutions with sparse features (Cotter et al. 2005). However, simple sparse constraints are sensitive to noise and cannot present the temporal dynamics in the heart properly. In our proposed CESI method, a novel dipole-wise temporal weighted sparse reconstructing strategy is applied as:

$$\hat{J}_T = \arg\min(\left\| L_T \vec{J}_T - \vec{\Phi}_T \right\|_2^2) \tag{6}$$

$$s.t. \sum_t^T W_{t,i} \left\| \vec{J}_{t,i} \right\|_2^1 < \mu \mathrm{E}_i \ \ for \quad all \quad i = 1 \ldots N \tag{7}$$

where $W_{t,i}$ represents the soft temporal weights of time instant t at myocardial source grid point i. $\vec{J}_{t,i}$ stands for the current density vector $[J_x, J_y, J_z]$ at instant t and myocardial source grid i. E_i represents the estimated energy of the equivalent current density within the time window T at location i. $W_{t,i}$ and E_i can be derived by:

$$W_{t,i} = \exp(-C_{i,t} / C_{\max,i}) \tag{8}$$

$$E_i = \sqrt{\sum_T C_{t,i}^2} \tag{9}$$

$$J_w = \arg\min \left\| LJ_w - \Phi \right\|_2^2 + \left\| W_w J_w \right\|_2^2 \tag{10}$$

where $C_{t,i} = \left\| J_{w,x,t,i}, J_{w,y,t,i}, J_{w,z,t,i} \right\|_2^1$ is the amplitude of WMN reconstructed current density $J_{w,i} = [J_{w,i,1}, J_{w,i,2}, J_{w,i,3} \cdots J_{w,i,T}, J_{w,i,T}, J_{w,i,T}]$ at instant t and myocardial source grid i solved with the weighted minimum norm method as described in (Z. Liu, Liu, and He 2006; J.-Z. Wang, Williamson, and Kaufman 1992). $C_{\max,i}$ is the maximum value of $C_{i,t}$ along the time course T at each location i. $W_{t,i}$ is designated to help stabilize the sparse solutions at the same time evading the smearing effect and distortion a minimum norm solution may have. When $C_{i,t}$ gets smaller, indicating a smaller likelihood that the activation may occur, $W_{t,i}$ becomes larger, imposing a larger penalty and the final electrical spikes are less likely to occur at the instant. All the current density time course from Eq. (10) are normalized so that the total penalty on each site will be approximately the same. The constraints in Eq. (7) has a soft guiding effect on the final temporal sparse results: when the weighted minimum norm is "confident" about the reconstructed result, namely a distinguished peak is reconstructed, the penalty for disagreeing will be larger. On the other hand, in the situation where only smoothed waveform or multiple peaks are generated due to noisy background or modeling error, which is the major source of error in the WMN methods, the CESI will seek for activation in a larger range and rely more on the information from BSPM and other "confident" results. In this way, the merit of WMN can be preserved

while the weakness can be avoided. E, on the opposite side of the constraints, is directly linked to the energy of the weighted minimum norm solutions and the effect of distributing lead-field energy can be canceled out. Note that Eq. (6) serves as the dominating term in reconstruction while in Eqs. (8) to 10 minimum norm inverse solutions are introduced as secondary guiding information. In contrast to the minimum energy based constraints from which most entries in the solution vector can be non-zero to compensate the residual term in Eq. (6), the sparse constraints in Eq. (7) designed in the proposed method enforce electrical silence except for the very instant of activation. Therefore, the tendency for loss of temporal resolution and distortion will be heavily penalized by the residual term due to the total absence of electrical activity in other instants and the information from BSPM can be efficiently reflected in the reconstructed results without compromise to a stronger regularization term as the disturbance from noise or modeling errors become more serious. At the same time, the sensitivity of sparse reconstruction to sensor noise can be overcome by weighting based on the Gaussian-noise-robust minimum energy solutions. Instead of a direct L1, the sparse constraints in Eq. (7) adapt a grouped sparse formulation in which the three momentums in $\vec{J}_{t,i}$ are considered grouped and only the amplitude of $\vec{J}_{t,i}$ will be sparse and only in the temporal domain. The μ in Eq. (7) can be determined by a data driven approach such as the L-curve method (Hansen 1992; Pascual-Marqui 1995). Eqs. (6) to (9) defines a convex constrained problem and can be solved equivalently using various methods and in this study, solved with CVX, a software package for specifying and solving convex programs (M. Grant, Boyd, and Ye 2012; M. C. Grant and Boyd 2008). Activation time, according to the peak criterion (Z. Liu, Liu, and He 2006), is computed based on the CESI imaged electrical activity and the 3D activation sequence throughout the myocardium is generated accordingly.

3.3 Numerical Study using Excitable Automaton based Heart-Torso Model

In order to evaluate the performance of the proposed method on human applications in a realistic scenario, a cellular automaton heart model embedded in a realistic heart-torso volume conductor model was used. A generalized cardiac anisotropy was incorporated into the heart model and the myocardial fiber rotated counterclockwise over 120 degree from the outermost layer to the innermost layer. The conduction velocity is 0.8 m/s along the fiber and 0.3 m/s transverse. The myocardium consists of a total of 30,085 cardiac automatons and 4,096 torso surface vertices were constructed. Two hundred electrodes were evenly distributed on both the chest and the back in the computer simulation. Pacing simulations on various locations were employed, including the basal anterior (BA), basal left wall (BLW), basal right wall (BRW), basal posterior (BP), basal Septum (BS), middle left wall (MLW), middle right wall (MRW), middle anterior (MA), mid-septum (MS), middle posterior (MP), apical anterior (AA) and Apical posterior(AP). Dual site pacing was also simulated in the present study with seven pairs of pacing sites selected throughout the ventricular myocardium. One pacing site was fixed at the mid lateral RV free wall while the other one gradually moved towards the mid left wall. BSPMs were computed by means of the Boundary Element Method (BEM) with simulated cardiac electrical sources using the cellular automaton model.

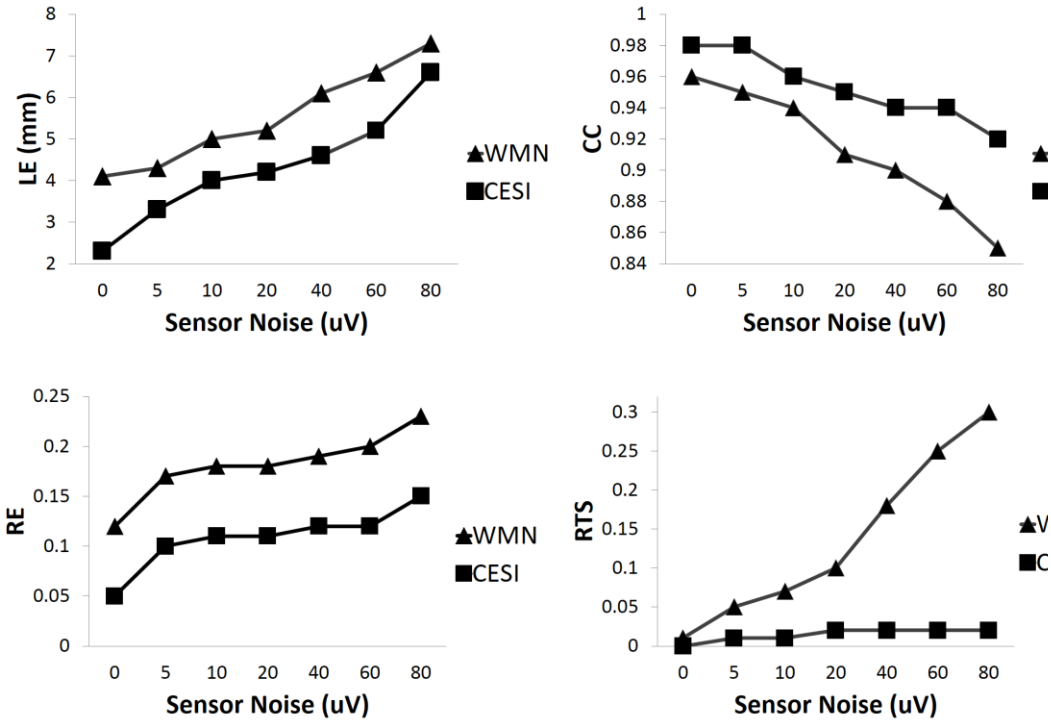

Figure 4: Comparison of imaging statistics between CESI and WMN for 12 site single pacing simulations. The four panels show the averaged statistics of CC (top left), RE (top right), LE (bottom left) and RTS (bottom right).

Various kinds of experimental noise and modeling errors were considered to simulate noise-contaminated measurements in a clinical setting. White Gaussian noise of different levels (20 - 80 uV) was utilized as the sensor noise. Noise signal that randomly selected from hospital ECG recordings with ECG waveform rejected was also used to simulate realistic noise such as power line interference, medical device interference and movement drift. Heart and torso modeling errors were simulated where the size of the torso was inflated by 10% and the location of the heart was moved 4 mm towards the lung. To simulate the electrode localization errors that could occur in realistic applications, such

as electrode-CT geometrical co-registration, the electrodes were moved 1cm upward from its original locations.

	WMN	CESI
CC	0.83±0. 05	0.91±0. 03
RE	0.26±0. 05	0.15±0. 02
LE (mm)	7±1.4	4±1.4
RTS	0.21±0. 08	0.02±0. 004

Table 1: 12 single site pacing simulation results with hospital recorded noise.

Correlation Coefficient (CC), Relative Error (RE), Localization Error (LE) and Relative Temporal Shrinkage (RTS) were computed for both computer simulation data and animal experimental data, as defined below:

$$CC = \frac{\sum_i (AT_i - MT_i) \cdot (ATA_i - MT_i)}{\sqrt{\sum_i (AT_i - MT_i)^2} \bullet \sqrt{\sum_i (ATA_i - MT_i)^2}}$$

$$RE = \sqrt{\frac{\sum_i (AT_i - MT_i)^2}{\sum_i MT_i^2}}$$

$$RTS = \frac{T_s - T_I}{T_s}$$

where is the activation time of grid point in the imaged activation sequence whereas is the measured activation time at the identical position from the measured activation map. is the simulated or measured total activation time

and is the imaged total activation time. Localization Error is defined as the spatial distance between the imaged activation initiation and the pacing site in simulation and animal study.

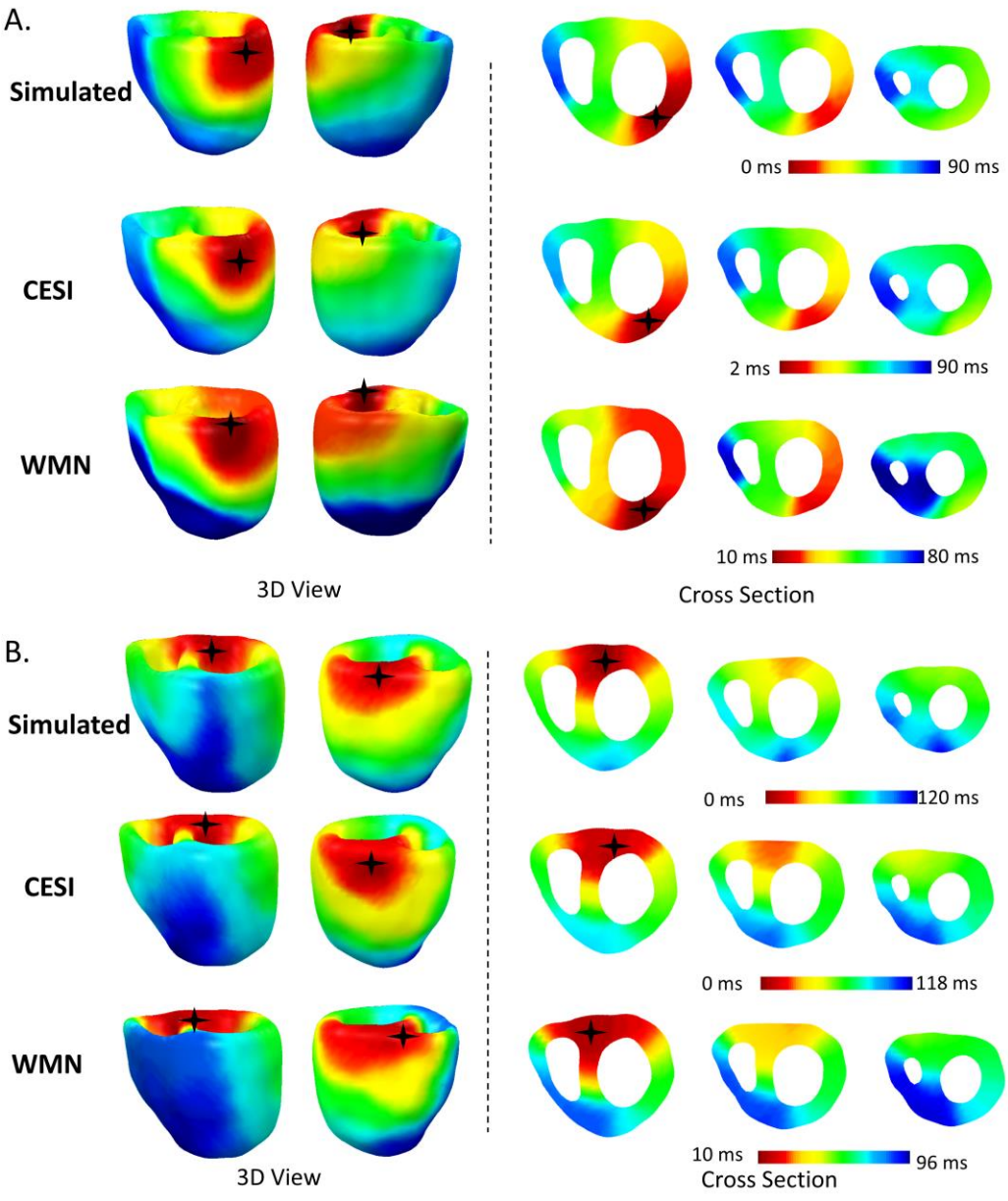

Figure 5: Comparison between simulated activation sequence and the imaged activation sequences from CESI and WMN.

The Weighted Minimum Norm (WMN) method has been used in the previous 3D cardiac electric imaging studies and has shown to have a generally good performance in imaging accuracy among the minimum norm based methods. Therefore, in this study we evaluated the performance of the proposed CESI method as compared with the WMN method. In all computer simulation and animal experiments, both CESI and WMN methods were performed independently and the results from both approaches were compared.

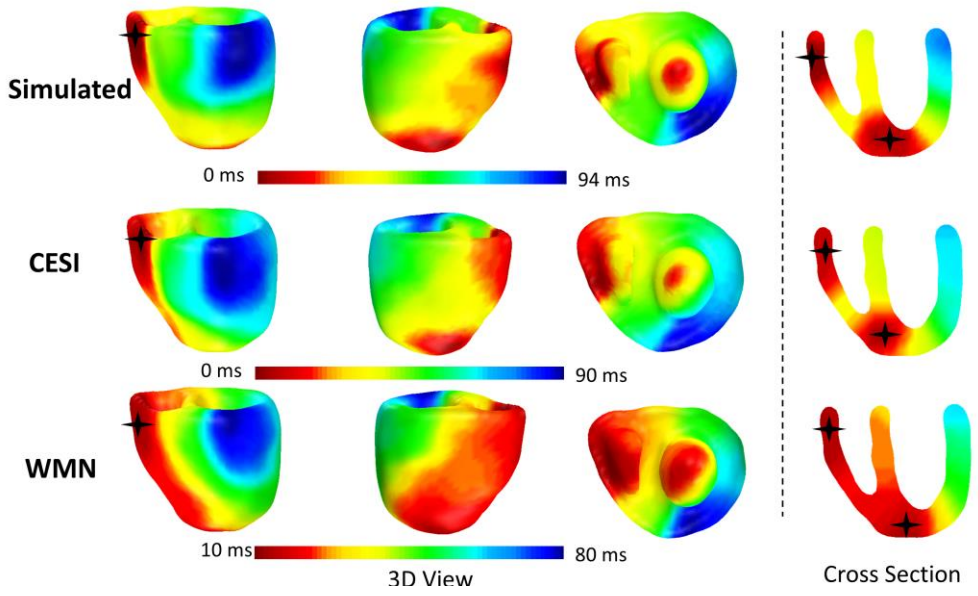

Figure 6: Comparison between simulated activation sequence and the imaged activation sequences from CESI and WMN on double pacing..

Twelve different pacing sites were used in the single pacing paradigm. For each pacing site, various levels of Gaussian white noise were added to the computed BSPM to simulate noise-contaminated measurements. The statistics of averaged CC, RE, LE and RTS on 12 pacing sites are summarized in Figure 4, and Table 1. The standard deviations of Gaussian white noise added to the

BSPMs were 0, 5 10, 20, 40, 60, 80 uV, respectively. Results in Figure 4 and Table 1 show that the CESI has demonstrated a general improvement over WMN in all four statistics. The imaging accuracy such as CC, RE and LE degrades slower than WMN while the noise level goes up and the CESI can still maintain CCs as high as 0.92 and 0.94 even under the noise level as high as 60 and 80 uV. As for RTS, the CESI was barely affected by the noise and maintains the temporal resolution under each of the noisy circumstances. Dual site pacing simulations were also performed to evaluate the CESI method and the statistics are summarized in Table 2.

	20μV Gaussian White Noise		**Hospital Recorded Noise**	
	WMN	CESI	WMN	CESI
CC	0.85±0.08	0.89±0.07	0.80±0.07	0.89±0.07
RE	0.25±0.06	0.12±0.06	0.30±0.05	0.14±0.08
LE (mm)	4.2±2.1	3.9±2.0	5.6±3.2	4.1±1.7
RTS	0.2±0.03	0.02±0.004	0.25±0.06	0.02±0.005

Table 2: Dual site pacing simulation results from the 7 pairs of pacing sites.

Figure 5 and figure 6 presents examples of single and dual site pacing computer simulation results. All figures are color coded from red (early activation) to green and to blue (late activation). For each activation sequence, the color code is adapted to the length of the activation and marked in the color bar. Simulated activation sequences are presented in the first row of each panel in the figure. The generated BSPMs were contaminated with realistic noise recorded from the hospital setting filtered with a 1-30 Hz band pass FIR filter. The results from both approaches (CESI and WMN) are shown in the middle and the bottom row in each panel. Panel A-C show single site pacing

simulations on the LV basal anterior wall (panel A), basal posterior wall (panel B), and RV free wall (panel C), while panel D shows an example of dual site pacing simulation on the RV free wall and apical septum. The CESI imaged activation sequences only showed a minimal loss of temporal resolution (~1 ms) and demonstrated better accuracy on the general propagation pattern, in comparison to the delay of WMN estimated initial activation. For single pacing sites, CESI results demonstrated higher concordance to the simulated results and suffered less of a blurring effect compared with the WMN results. The blurring effect shown in the WMN solutions in the figures is most significant at the earliest and the latest period of activation, indicating a non-linear distortion on imaged activation time which can be observed to be much relieved in the CESI results. It can be seen from Figure 7 that the CESI can image the early activation region clearly and the initiation is shown to be in good agreement with the simulated activation pattern. The propagation pathway is also well depicted both on the myocardial walls, close to epicardial surface, and the deep region inside the heart along the septum. The termination of the beat was also localized correctly, only with minor differences in the late activation pattern. In panel D, the dual site pacing simulation, the contrast of CESI imaged activation to distinguish two pacing sites is significantly higher than WMN results. The two pacing sites can be clearly identified from the CESI imaged results and the propagation pattern is in better agreement with the simulated pattern than WMN results. The activation pattern in the myocardium around the two pacing sites is better imaged as a result of temporal resolution preservation. Both the pacing

sites were imaged to be initiated independently at 0 ms, at the very beginning of the beat without interfering each other regardless of their differences in location. The activation pattern between the pacing sites is also well imaged whereas that in WMN the result is smeared due to the loss of temporal resolution. The statistics of simulation results with hospital recorded noise are summarized in Table 1 (single site pacing) and Table 2 (dual site pacing).

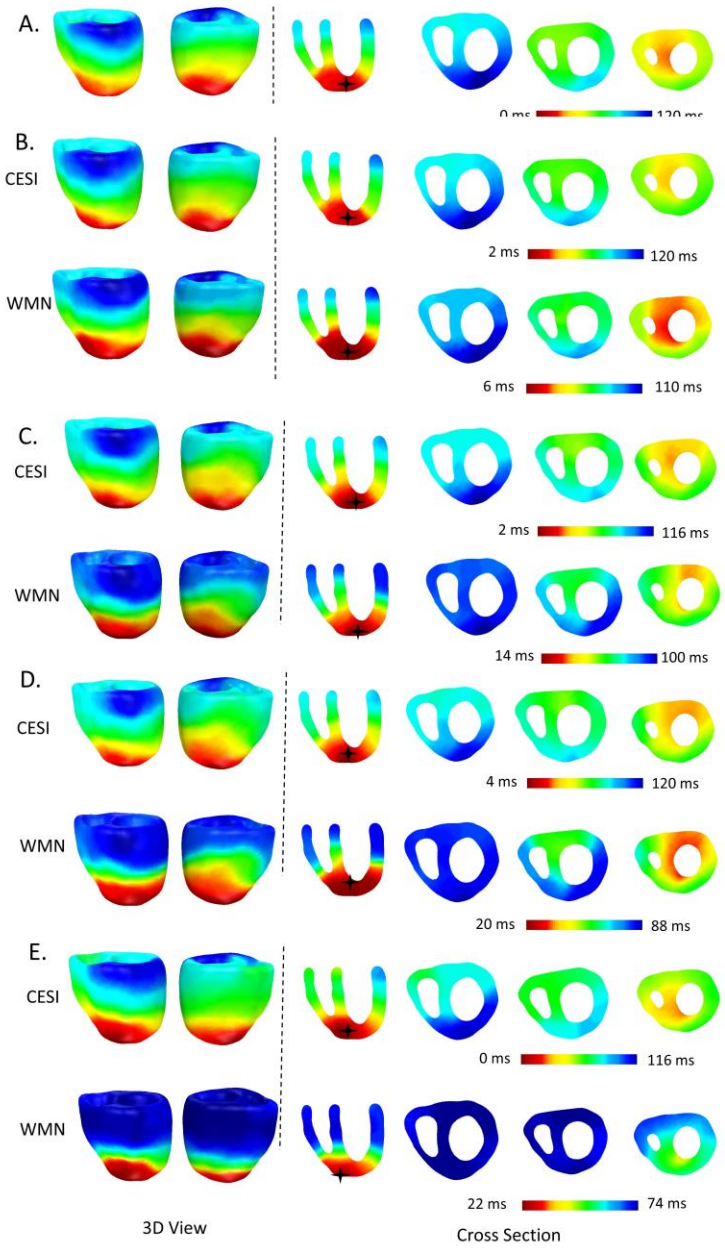

Figure 7: Comparison of imaged results between CESI and WMN imaged from pacing simulation with various modeling errors. Black star represents the initiation of each activation map. A: simulated activation sequence. B: Torso 10% dilated. C: heart position 4mm moved towards left lung. D: torso 10% dilated and heart position moved 4mm. E: body surface electrodes moved 10 mm right.

To evaluate the robustness of the CESI method, various modeling errors and co-registration errors were also simulated with 20 uV Gaussian white sensor noise. In Figure 7, examples of imaging results from a pacing simulation with various kinds of modeling and co-registration error are shown. All of the activation sequences are color coded from red (early activation) to blue (late activation) as marked in color bars. Panel A presents the computer simulated activation sequence. Panels B-E display the imaging results and the comparisons of both CESI and WMN methods under various erroneous circumstances. Panel B shows the results with torso geometry uncertainty where torso geometry is 10% dilated. Panel C shows the results with heart position uncertainty where the whole myocardium is moved 4 mm towards the left lung. Panel D shows a situation in which both errors in B and C occur together. Panel E shows the results with electrode-torso co-registration errors where all of the electrodes are 10mm upward. The imaged results showed that the CESI was maintaining the temporal resolution (shrinkage ~1ms) and the activation pattern was barely affected by the modeling errors or co-registration errors. The CESI maintains a stable overall pattern against modeling errors and little distortion was observed. The initiations of the beats are well localized by the CESI with a clearly depicted early activation pattern. In Panel D, and E, where relatively heavy disturbance is imposed, the CESI can still image the activation pattern with good accuracy. On the other hand, the WMN results, due to its physical constraints, are heavily distorted and losing details in activation pattern. In the early activation area in panel B and D as well as the late activation

in panel D and E, the smearing effect is obvious due to the minimum-energy constraints, that promote the smoothness. The statistics of the simulations are summarized in Figure 8. The CESI is much less affected by the modeling and co-registration errors than the WMN. CC, RE and RTS were maintained within a relatively small range under all those erroneous conditions while LE is increased due to the modeling and co-registration errors but still lower than WMN.

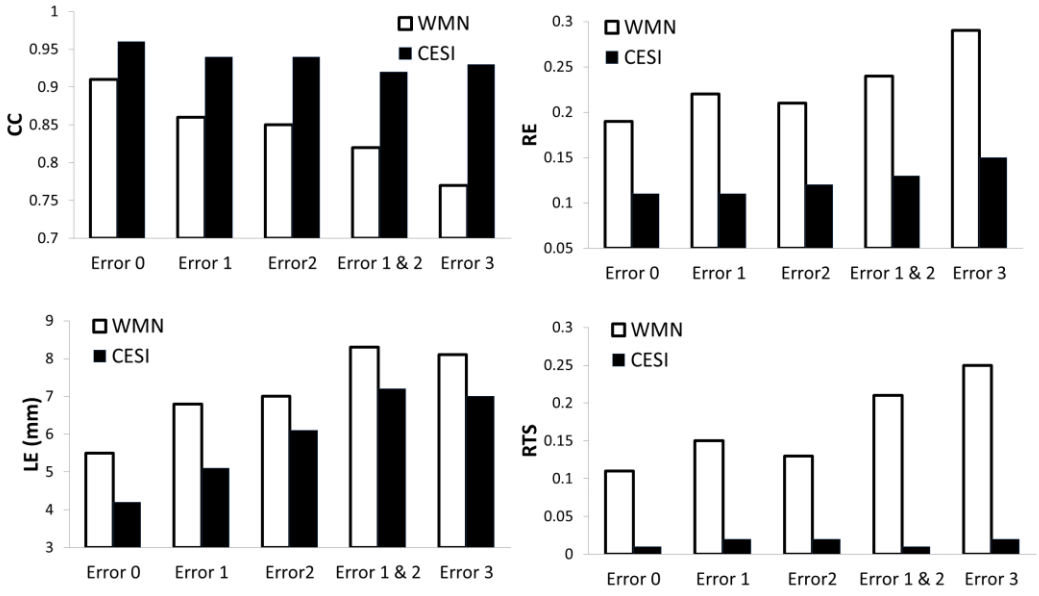

Figure 8: Comparison of the averaged statistics between CESI and WMN on single site pacing simulations with modeling errors on 12 single pacing sites. Error 0: 20 μV Gaussian white noise. Error 1: torso geometry dilated 10%. Error 2: heart position moved 4mm towards left lung. Error 3: body surface electrodes move 10 mm towards right hand.

3.4 Pace Mapping Study in Rabbit

To validate the proposed imaging method, we evaluated the proposed imaging methods in experimental data collected in two healthy New Zealand rabbits. The animal protocol was approved by the Institutional Animal Care and Use Committees. The detailed experimental protocol has been demonstrated in the previous studies (Zhang et al. 2005; Han et al. 2011). In brief, cardiac CT and torso CT were performed on the experimental rabbits prior to in vivo mapping. About 60 BSPM electrodes were uniformly placed covering the anterior and lateral rabbit. 20-25 transmural needles were inserted in the left and right ventricles of the rabbit after median sternotomy with each needle carrying 8 bipolar sensors 500 □m distant to each other. The chest and skin were carefully closed after needle insertion. Bipolar electrograms were recorded from all electrodes continuously and simultaneously with body surface ECG mapping. After the recording, electrode needles were replaced with metallic label. CT scans were performed on the excised and fixed hearts to obtain precise 3D localization of the transmural electrodes. A Gaussian interpolation was performed on the activation time detected from intra-cardiac bipolar recording according to the CT geometry to generate a 3D measured activation map. The rabbit myocardium was tessellated into around 10,000 grid points evenly located within the 3D ventricular myocardium. There were around 160-200 intra-cardiac bipolar electrodes placed in both the ventricles for intra-cardiac mapping. The ventricular activation sequences were imaged from the BSPM and quantitatively compared with those recorded simultaneously.

Intra-cardiac transmural bipolar mapping has been established as an effective approach to measure the electrical activity and as a suitable approach to evaluate 3D cardiac imaging techniques (Han et al. 2008; Han et al. 2011; Han et al. 2013). In this study, 10 single pacing sites were employed in the pacing paradigm with simultaneous

body surface and intra-cardiac mapping. Representative examples and statistics of the imaging results and comparisons are shown in Figure 7. Panel A and Panel B present two imaging examples with single pacing at RV (A) and LV (B), respectively. The activation sequences are color-coded from red (early) to blue (late). The black star represents the earliest activation site in both the imaged and measured activation maps. The focal pattern of the activation as well as its initiation has been well captured by the proposed method. The initiation is close to the pacing site and the early activation region is well focused and clear. The CESI imaged activation has good consistency with the measured results along the time course, from the early phase to the end of the beat. The CESI imaged results, in comparison with those from the WMN approach, are in higher temporal resolution with only little distortion especially in estimating the initial activation in the temporal domain. Statistics of quantitative evaluations and comparisons between the CESI and WMN are summarized in Figure 9. It can be observed that CC, RE, and LE are generally improved. The RTS of CESI remains at 0.02, showing that the CESI approach is able to maintain high temporal resolution in an experimental setting.

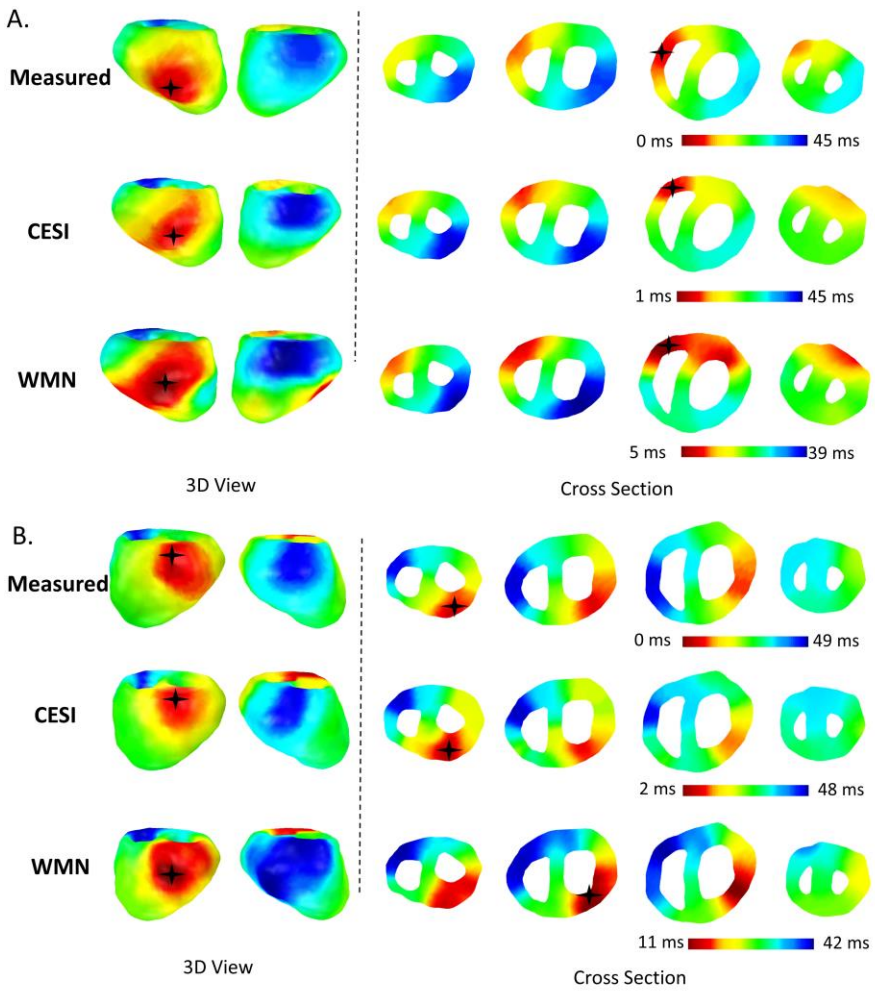

Figure 9: Comparison of imaging results between CESI and WMN during pacing experiments in rabbit. A) RV pacing. B) LV pacing.

3.5 Discussion

In the present study, a novel cardiac electrical imaging technique, Cardiac Electrical Sparse Imaging (CESI), has been proposed and evaluated with computer simulations and animal experiments. The CESI employs a novel four-dimensional (4D) inverse problem formulation to exploit the temporal sparse property of cardiac electrical activity to preserve the temporal resolution and detailed activation information for improved

accuracy and robustness. Computer simulations of both single and dual site pacing have shown that the CESI technique has promising capability in imaging cardiac electrical activities with high spatiotemporal resolution and improved performance. The CESI is able to image the activation sequence with higher CC and lower RE, LE and RTS in comparison to conventional minimum norm based methods, represented by the WMN in the simulated pacing paradigms. In addition, imaging accuracy can be well maintained against various types of modeling error, indicating robustness in realistic environments. Initial evaluation using experimental data in two rabbits with simultaneous BSPM and 3D intra-cardiac mapping further validated the CESI technique in a quantitative and realistic manner. Comparisons between the CESI and WMN based imaging results show that the proposed method is able to outperform conventional minimum energy techniques both in theoretical and experimental evaluation. Both computer simulation and animal experiments show that the CESI results are in good agreement with simulated activation sequence and experimentally measured cardiac activation.

Efforts have been made in pursuit for high resolution noninvasive imaging of cardiac electrical activity [6], [7], [9]–[11], [15], [16], [28], [29], [39]–[53]. The proposed 4D inverse problem formulation in the CESI technique can image the whole cardiac electrical process and the weighted sparse constraints incorporate the temporal sparse property of cardiac electrical dynamics into reconstruction. This is the first time that a sparse problem formulation is constructed specifically for cardiac electrical imaging with dipole based temporal weighted constraints that can reflect the electrophysiological dynamics. In section II, the sparse property of the cardiac electrical activity has been demonstrated. The temporal sparse property of cardiac electrical dynamics is derived directly from general electrophysiological knowledge of myocardial

cellular depolarization. To our best knowledge, it is the first time when cellular cardiac electrophysiological property as guiding information is incorporated into the reconstructing mathematical framework of a cardiac electrical imaging approach as temporal constraints. The property is based on a universal phenomenon that is not only observed in healthy but also in many pathological conditions. Moreover, this property is different from an electrophysiological model that requires certain individualized physiological knowledge which can vary as the condition changes(Li and He 2001; Bin He, Li, and Zhang 2003; B. He and Li 2002; Zhang et al. 2005)(Li and He 2001; Bin He, Li, and Zhang 2003; B. He and Li 2002; Zhang et al. 2005)(Li and He 2001; Bin He, Li, and Zhang 2003; B. He and Li 2002; Zhang et al. 2005). The inverse reconstruction of CESI still employs a physical-model based strategy but incorporates general physiological knowledge. The cardiac electrical inverse problem, by its nature, is often heavily ill-posed and thus not all the information can be directly reconstructed from the measurements (Hansen 1992). By incorporating the whole BSPM time course as input and temporal sparse constraints to pinpoint the activation time, the CESI is able to decrease the severity of ill-posedness and allows for a better representation of the information reflected in BSPM. The present results indicate that the CESI can achieve a spatial resolution of 1.5 mm and a temporal resolution of 1 ms. Unlike the energy based physical constraints such as minimum norm and singular value truncation, sparse constrained solution attempts to not omit the detailed information in the solutions but to utilize the sparse property of the cardiac electrical activity for its reconstruction. With these constraints, the reconstruction algorithm will search for the solution that can fit the measurements well and at the same time has an electrophysiologically based sparse property that will help prevent the loss of detailed information. Also, as can be found in the problem formulation, the CESI defines a constrained convex problem and has a unique solution which can be obtained

equivalently with different optimization methods. The reconstruction strategy in CESI seeks for a balance between the physical model based techniques and their physiological model based counterparts. The results shown in Section III demonstrate that CESI is capable of imaging cardiac electrical activation more accurately and robustly while at the same time works without any individual based physiological information.

Sparse-promoting has been applied on various imaging modalities (Ding et al. 2011; Nebel et al. 2005). Sparse properties in 3D spatial distribution have been exploited in EEG source imaging and fMRI imaging. Those methods were based on spatial features on a certain event-related instant. Our proposed method, with its novel formulation, stressing sparsity in the temporal domain, incorporates the whole 4D spatiotemporal cardiac dynamics in reconstruction. This is the first time, to our knowledge, that the temporal dynamic specific sparse formulation is applied in the imaging of a 4D functional process allowing sparse and non-sparse properties to cooperate in imaging for a higher accuracy and spatiotemporal resolution. The proposed method does not promote sparsity in spatial domain but only in temporal domain. Thus the imaging result of the proposed method can better image the spatial cardiac activation in a spatial sparse or non-sparse manner. Due to the temporal sparse constraints, the spatial area of electrical activation at a specific instant is mainly determined by the information from the residual term in Eq (6). In contrast, the minimum norm method can only generate a smoothed waveform along the time course and a large portion of the myocardium will appear electrically active during most of the beat. Therefore, the effective spatial resolution of CESI is improved even with the same source grid resolution by avoiding spatial smoothing effects. This property in spatiotemporal domain improves the method's compatibility and performance for both

the early phase, where the activation is sparse, and the later phase, where a major portion of the myocardium is in activation, of the cardiac cycle.

The CESI incorporates raw data from various modalities to image the electrical activation in the 3D myocardium. In clinical practice, the quality of raw data is limited. In section III, various disturbances were simulated and tested with the CESI. Compared to the simulated white noise, the hospital recorded noise allows to examine the performance of the imaging technique in a more realistic condition. The simulations with both generated white noise and hospital recorded sensor noise show that the CESI was capable of imaging cardiac electrical activation with higher accuracy than the WMN methods. The CESI was able to image with a CC = 0.92, RE = 0.15, LE = 7mm and RTS = 0.02 under the white noise disturbance as strong as 80 □V. In the simulations utilizing the hospital recorded noise, the CESI obtained a CC as high as 0.91, RE, LE and RTS were controlled as low as 0.16, 3.8 mm and 0.02, respectively. The results demonstrate that the CESI is capable of producing stable and accurate imaging results in relatively realistic conditions. In addition to sensor noise, imaging results with various modeling errors that could occur in clinical conditions also demonstrate the robustness of the CESI technique. Over the 4 kinds of modeling error, the proposed method maintained a CC of 0.93, RE of 0.12, LE of 0.63 mm and RTS of 0.017, respectively. By comparing the modeling error results and the modeling error free statistics shown in figure 8, one can find that the CESI is robust against the modeling errors and demonstrate the capability of functioning in complicated circumstances where the quality, and accuracy of raw data may be limited.

The present implementation of CESI employs a boundary element model based forward problem formulation and in this way does not require pre-assumed information on cardiac anisotropy. The electrical activity in anisotropic cardiac activation sequence

will travel through the volume conductor and be reflected on body surface ECG, which, with the physic based reconstruction method, can yet still be imaged based on the information in anisotropy-featured body surface ECG. The activation, as can be observed in both numerical and animal study results, did not propagate in an isotropic manner. Instead, variations in propagation speed along different directions were well reflected. Without forcing predefined anisotropy in forward problem, CESI is still capable of imaging the anisotropic activation with its temporal sparse formulation to better exploit the information underlying in the BSPM.

Rigorous evaluation in biological systems is crucial for the assessment of an imaging technique. Simultaneous recording of BSPM and intra-cardiac electrograms have been demonstrated as an effective approach to evaluate the performance of non-invasive imaging techniques in a realistic condition (Han et al. 2011; Han et al. 2013; Han et al. 2013). The post experiment CT scan can provide detailed information on the spatial location of intra-cardiac electrodes and therefore the electrical activity of the entire myocardium can be mapped over the 3D space. The results in section III show that the CESI can image the cardiac activation sequences in good concordance with the measured activation sequence via intracardiac mapping. The imaged activation initiation sites lie close to the measured initiation sites and the early activation area was clearly imaged. The animal experiment can evaluate the method in a condition that is similar to clinical practice but still have direct measurements on the electrical activity throughout the myocardial volume. Shown in Figure 7, CESI can image the paced beat with good accuracy and localization of the initiation and therefore is anticipated to function with similar performance in realistic clinical conditions on focal arrhythmias. The comparisons between CESI and WMN show that the CESI imaged results suffer less distortion in activation time (averaged CC>0.8, RE< 0.2, LE~5mm) and can

maintain temporal resolution (RTS< 0.02). The animal experiment results have demonstrated that the CESI has the capability of imaging induced cardiac activation sequences in good concordance with those found from intra-cardiac mapping.

In the clinical management of focal arrhythmias, such as Premature Ventricular Complex and Automatic Ventricular Tachycardia, catheter ablation is usually performed on the suspected initiations of the ectopic beats to terminate the arrhythmias. Therefore, the capability in correctly imaging the activation patterns in early phase of the ectopic beat is of clinical importance. Shown in Figure 4, the proposed method outperformed traditional minimum energy based method especially in early activation, identifying a clear initiation site and evading the smearing effect that the (weighted) minimum norm methods usually impose on the results and also leading to a more accurate localization of ectopic initiations with error around 4 mm. The animal experiments, compared to computer simulation, can demonstrate the potential clinical performance of CESI from a more realistic scope. The CESI promotes sparse electrical activities in the temporal domain in order to improve temporal resolution and accuracy of imaging. Results show that the CESI is capable of localizing the pacing sites, which can generate an ectopic pattern similar to focal arrhythmias, within 5 mm. Also, as can be observed, CESI capable of preserving the temporal resolution and the detailed in the propagation of the activation. The loss of temporal resolution was smaller than 2% in the pacing and the CC was also improved to 0.8 due to the preserved detail the temporal domain.

The temporal sparse formulation in CESI seeks to reconstruct electrical activity with a temporal sparse feature. However, it does not force each site of the myocardium to activate only once. The temporal constraints in Eq. (7) require the results to have as many zeros and still satisfy the residual term Eq. (6). The absence of a second major

spike in reconstructed ECD will be heavily penalized by the residual term and replaced by a multi-spike ECD that can best represent the body surface ECG. Therefore, there is no theoretical difficulty in imaging the activation sequence with multiple activation. However, to fully address the performance of CESI in these scenarios, further investigation is needed.

The CESI incorporates the temporal sparse property of myocardial electrical activity into reconstruction in aim of improving the performance of activation imaging. In this presented study, 4D problem formulation based on equivalent current density model in 3D myocardium is proposed and validated. However, the concept of sparse imaging is based on the general electrophysiology and therefore is not limited in 3D ventricular myocardium imaging but as well applicable in epicardial or surface imaging techniques and other cardiac imaging targets such as atrial electrical activity. Various applications based on different problem formulations under the general cardiac temporal sparse imaging framework will be explored in the future studies.

In sum, we have proposed a novel Cardiac Electrical Sparse Imaging (CESI) approach and evaluated it with a series of computer simulations and animal experiments. The present simulation and animal results have demonstrated that the CESI can image the cardiac electrical activation more accurately and better than traditional linear inverse methods in various conditions and in a realistic experimental setup. The promising performance of CESI suggests its potential application to map cardiac electrical activity and aid catheter ablation of arrhythmia in a clinical setting.

Chapter 4

Animal Validation Studies on Automatic and Reentrant Ventricular Tachycardia s in Canine and Swine model using 3D intra-cardiac mapping technique

With more than 400,000 cases of out-of-hospital sudden cardiac deaths yearly in the US alone, ventricular arrhythmia poses itself as a severe and direct threat to the lives and living standard across the globe(Mozaffarian et al. 2015). To manage this leading cause of death and disability, anti-arrhythmic drugs have been widely administered as a routine practice. In recent years, the treatment of the arrhythmias has been increasingly relying on Electrophysiology (EP) study with ablation(Shpun et al. 1997; Soejima et al. 2001; Wittkampf and Nakagawa 2006; Go et al. 2014; Thiagalingam et al. 2004). The success of the therapy, by its very nature, is relying on how well the pathological substrate can be localized and understood(Shpun et al. 1997). While the contact sequential and non-contact intra-cardiac mapping techniques have demonstrated the capability in determining the origin and mechanism of the arrhythmias on partial endocardium, the highly invasive nature inevitably make the techniques demanding in clinical resources and consequentially lead to prolonged period of time in procedure and hospitalization. In addition, invasive sequential mapping techniques require repetitive activation patterns and hemodynamic stability during the continuous arrhythmic rhythms. However, in the arrhythmias such as polymorphic ventricular tachycardia (PVT) and reentrant monomorphic VT, scarcity in certain pattern and hemodynamic instability may prevent the intra-cardiac mapping

catheters to properly identify the ablation targets. Therefore, a noninvasive imaging technique that can provide beat-to-beat electrical activity in 3D can potentially provide significant assistance to the clinical management of cardiac arrhythmia.

Non-invasive techniques seek to offer alternative approaches for insights into the heart based on body surface recordings. Various approaches have been investigated to solve the intra-cardiac electrical activity from body surface ECG. Such efforts, involving moving dipole localization, epicardial potential imaging and surface activation imaging, have demonstrated the potentials to provide important information that is closely relevant to clinical management(Armoundas et al. 2003; Gulrajani, Roberge, and Savard 1984; Barr and Spach 1978; Barr, Ramsey, and Spach 1977; Oster and Rudy 1992; Ramanathan et al. 2004; Vijayakumar et al. 2014; Skipa et al. 2002; Greensite 2005; Greensite 2003; Tilg et al. 2002; Berger et al. 2006; Messnarz et al. 2004; Han et al. 2015; Liebman et al. 1991; Y. Wang et al. 2011; L. Wang et al. 2013; D. Wang et al. 2013). More recently, techniques in aim of imaging the activation sequence throughout the myocardium three dimensionally (3D) have been proposed and validated in an array of numerical and animal studies(Han et al. 2012; Han et al. 2011; Han et al. 2008; Han et al. 2013; Zhang et al. 2005; Y. Wang et al. 2011; L. Wang et al. 2013; C. Liu et al. 2012; Zhou et al. 2014). As a further development of the 3D Cardiac Electrical Imaging (3DCEI) technique, Cardiac Electrical Sparse Imaging (CESI) incorporates the temporal sparse property in cardiac electrophysiology and has been shown to be capable of outperforming the conventional minimal norm based technique in numerical and healthy rabbit model(Yu, Zhou, and He 2015).

In the previous chapter, CESI, a new 3D cardiac electrical imaging method has been developed with evaluated in numerical model and preliminary pacing studies in rabbits. In this chapter of the dissertation, I would like to

discuss a first and to our knowledge most comprehensive validation study of 3D cardiac electrical imaging method using a 3D intra-cardiac mapping system and delay enhancement magnetic resonance imaging (DE-MRI). The capability of the CESI technique to identify the arrhythmic activation pattern of automatic and reentrant arrhythmias is thoroughly validated quantitatively in various pathological models such as heart failure and myocardial infarction for the first time. The non-invasive imaging technique is also applied to swine with myocardial infarction, representing a first animal investigation of 3D electrical infarct imaging validation using DE-MRI. The clinical capability of the 3D non-invasive imaging method is thoroughly investigated in a rigorous way.

4.1 Automatic Ventricular Arrhythmias in Healthy and Heart Failure Canine

The experiment animals were studied under a protocol of simultaneous body surface potential and 3D intra-cardiac mapping procedure. The protocol was previously described in detail and was approved by the Institution of Animal Care and Use Committees of University of Minnesota and University of Alabama at Birmingham(Han et al. 2013)(Han et al. 2015).

Figure 10 presents the schematic paradigm of the mapping study. Computed Tomography (Phillips, Amsterdam, Netherlands) scanning was conducted before and after the mapping study (0.33 x 0.33 x 3 mm for torso and 0.33 x 0.33 x 0.33 mm with contrast agent for heart). All the electrodes were digitized with a 3D magnetic digitization device (Fastrek, Polhemus Inc, Colchester, VT) and also identified through post mapping study CT scans. The canines were anesthetized with 0.04mg/kg intramuscular atropine and about 20 mg/kg intravenous Pentothal and the state was

maintained by 2% to 3% isoflurane per 100% oxygen. Up to 128 body surface electrodes (3M, St. Paul, MN) were distributed on the chest of the back uniformly. Up to 42 transmural plunge-in needles were inserted in the Left Ventricle (LV) and Right Ventricle (RV), providing up to 216 bipolar recording sites covering the whole heart in 3D. The chest and skin was closed carefully with silk suture, externalizing the intra-cardiac mapping device through the incision of the sternotomy. Bipolar ECG recordings were obtained at the sampling frequency of 1K Hz using a 256-channel recording system (Crescent Electronics, Salt Lake City, UT). Up to 128 body surface electrodes(1 KHz sampling rate) were placed on the front and the back of the canine after the animal had been anaesthetized. The electrodes were uniformly placed covering both the anterior and posterior chest. BSPM recording was started and continued throughout the process till the study was finished. Norepinephrine (NE) was infused to induce arrhythmias such as PVC, MVT and PVT during the mapping study.

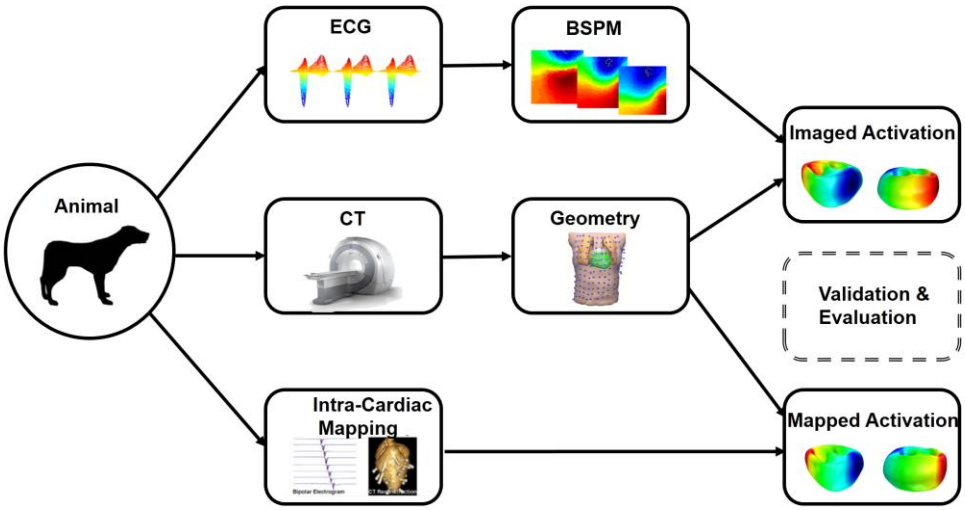

Figure 10: Experimental paradigm of the simultaneous mapping study for both HF and non-HF canines. The animal included in the study underwent CT scans before the mapping study. Intra-cardiac and body surface electrodes were deployed during the simultaneous study. Activation sequences, imaged and measured, were compared quantitatively for evaluation and validation of the imaging technique.

Canines with induced congestive Heart Failure (HF) were also included in the study under the mapping protocol. The HF induction procedure has been previously discussed(Han et al. 2015). In brief, HF was produced by inducing aortic insufficiency with Fogarty balloon catheter under the guidance of fluoroscopy. Constriction of the abdominal aorta was performed after induction with a suture placed to increase the systolic blood pressure gradient by 50 – 60 mmHg. The HF canines had survived two years before the study. The progression of HF was monitored and assessed using Doppler echocardiography on LV end-diastolic dimension, LV end-systolic dimension and LV fractional shortening.

4.2 Reentrant Ventricular Tachycardia in Swine with Myocardial Infarction

The schematic diagram of the swine mapping study and infarction induction process are shown in figure 11. Myocardial infarctions were induced in those included approximately two months prior to the simultaneous mapping study. The infarction induction protocol has been described in detail previously. In brief, the mid-left anterior descending coronary artery was occluded for 150 minutes using a balloon angioplasty catheter via a carotid artery to create myocardial infarction. Structural MRI (1.5x1.5x8 mm, TR=3.72, TE=1.56, Flip Angle=45) and DE-MRI (1.5x1.5x8 mm, TR=7.09, TE=3.08, Flip Angle=20) was performed using a clinical 1.5T MR scanner (Genesis Signa, GE, USA) within a week of the simultaneous mapping study for each swine to identify and visualize the myocardial structure and infarct area. At the day of mapping study, up to 257 unipolar transmural recording electrodes inserted across the myocardium via median sternotomy at a sampling rate of 1000 Hz. Intra-cardiac stimulation catheter was also deployed to induced sustained monomorphic VT through programmed stimulation and burst pacing. Up to 128 body surface electrodes were attached and digitized on the front and back of the swine for BSPM recording in a same protocol used in the canine study.

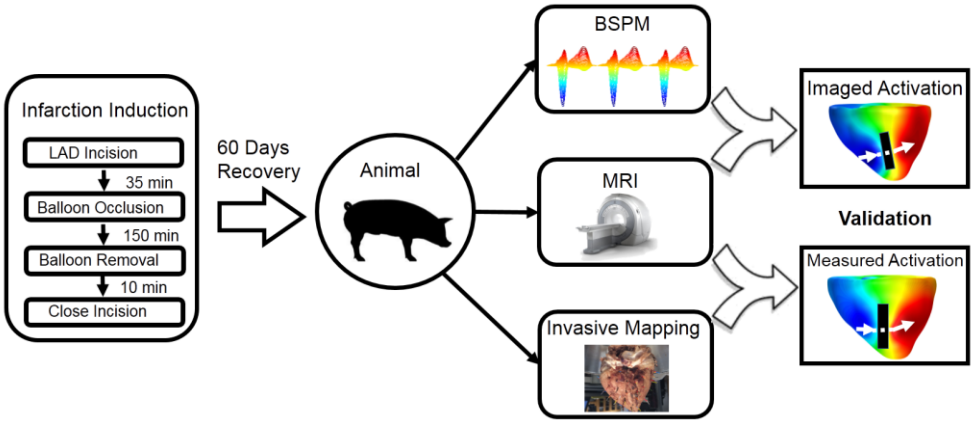

Figure 11: Experimental paradigm of the simultaneous mapping study for both HF and non-HF canines. The animal included in the study underwent CT scans before the mapping study. Intra-cardiac and body surface electrodes were deployed during the simultaneous study. Activation sequences, imaged and measured, were compared quantitatively for evaluation and validation of the imaging technique.

4.3 Data Analysis

The detailed methodology employed by CESI has been described previously in detail(Yu, Zhou, and He 2015). In brief, detailed and individualized geometry on heart, lung and torso of the experimental animal was extracted from the structural images (CT, MRI) assisted by CURRY 6.0 (Compumedics, Charlotte, NC). The extracted ventricular myocardium was tessellated into around 10,000 source grid points. Based on the bidomain theory, Boundary Element Model (BEM) was constructed for each canine including torso, lung, myocardium and blood mass(Jamison et al. 2011; Miller and Geselowitz 1978). By coupling the functional information from ECG recordings and the structural information from CT or MRI, CESI reconstructed the ventricular activation sequence throughout the myocardium in 3D. Exploiting the temporal dynamic the cellular electrophysiology at the depolarization, the temporal sparse promoting imaging technique reconstructs the current density spike

generated at the instant of the cardiac activation directly. The technique has been demonstrated to be able to achieve improved imaging accuracy and robustness against various disturbances.

The time of activation was identified from the intra-cardiac bipolar ECG recordings collected using unipolar or bipolar electrodes aligned on the plunge-in needles. The activation time at a certain location was determined as the instant when the bipolar signal reaches its maximum or the unipolar signal has its steepest decent along the time course. After acquiring the activation time at each recording site, the intra-cardiac electrodes were co-registered with the myocardium volume grid points extracted from structural images and interpolated using Gaussian interpolation method.

The imaging results were then compared with intra-cardiac activation sequences. Numerical data was presented in mean ± SD format. Correlation Coefficient (CC), Relative Error (RE), and Relative Resolution Error (RRE) were defined and computed to quantitatively evaluate the performance of the technique. CC, RE and RRE are defined to assess and quantify the concordance and discrepancy between the invasively mapped and non-invasively imaged activation patterns on the endocardium, defined as:

$$CC = \frac{\sum_i (AT_i - \overline{AT}) \bullet (MT_i - \overline{MT})}{\sqrt{\sum_i (AT_i - \overline{AT})^2} \bullet \sqrt{\sum_i (MT_i - \overline{MT})^2}} \qquad (1)$$

$$RE = \sqrt{\frac{\sum_i (AT_i - MT_i)^2}{\sum_i MT^2}} \qquad (2)$$

where AT_i and MT_i represent the imaged and measured activation times at the ith grid point while $\overline{AT}$ and $\overline{MT}$ represent their average on all grid points. RRE is employed to measure the loss temporal resolution, and is defined as:

$$RRE = \frac{|T_M - T_I|}{T_{total}} \quad (3)$$

where T_M represents the total activation time of measured activation, T_I represents the total activation time of the imaged activation sequence on the co-registered area and T_{total} represents the total activation time from the body surface ECG.

The capability of CESI to localize key area of interest for ablation was also evaluated in a quantitative manner. Localization Error (LE) is defined as the distance between potential ablation targets indicated by imaged results and the intra-cardiac recordings. For automatic VTs, the LE is simply defined as the distance between the imaged and the measured initiation site for each ectopic activation, a well understood and widely practiced target of ablation. For re-entry VTs, LE is defined as the distance between the imaged and measure exit of reentry isthmus, the initiation site of each re-entry cycle.

Myocardial infarction imaging technique was also adapted to visualize the infarct area based on BSPM abnormalities during the S-T segment. The detailed methodology of the imaging technique has been described previously. In brief, due to the damage inflicted by infarction, the weakened myocardium suffers a lowered plateau potential after QRS depolarization phase, generating current flow in macro level detectable in BSPM. By localizing the electrical abnormality, infarction region can be identified and visualized. The imaged infarct area was compared with the segmented

injured area identified in DE-MRI. CC and RE are defined to quantify the concordance between the two modalities as:

$$CC = \frac{\sum_i (IE_i - \overline{IE}) \bullet (IM_i - \overline{IM})}{\sqrt{\sum_i (IE_i - \overline{IE})^2} \bullet \sqrt{\sum_i (IM_i - \overline{IM})^2}} \qquad (4)$$

$$RE = \sqrt{\frac{\sum_i (IM_i - IE_i)^2}{\sum_i IM^2}} \qquad (5)$$

Where IE and IM represent the binary map generated from imaged and segmented results of infarct area inside the myocardium.

4.4 Results

A total of 13 animals - 10 canine and 3 swine - were included in the study. For each experimental animal, individualized geometrical model was built. The ventricles were tessellated into 11292±1317 source points evenly distributed from throughout the 3D myocardium. Averaged over all the mapping studies, 226±10 intra-cardiac electrodes were localized from CT images and analyzed to construct the intra-cardiac activation maps together with 101±15 body surface electrodes deployed on both chest and back of the experiment animals. In sum, CESI achieved a CC of 0.79 and RE of 0.24 over a total of 150 ectopic beats isolated from the simultaneous recordings, indicating a good accuracy in imaging the activation paten of various arrhythmic patterns. The imaged initiation sites are closely localized with an LE of 7.3 mm in average. The loss of temporal resolution shown in the study was minimal with RRE remaining lower than 7%. As can be observed from the table, the statistics vary slightly among various types of arrhythmias. The performance of the technique in the beats with stable

morphologies, such as PVC and MVT is higher than it is in the unstable cases due to instability in cardiac dynamic. Yet, the technique had demonstrated its robustness against various types of arrhythmias including those in HF canines. The infarct areas image electrically is in good concordance with the DE-MRI results. An averaged CC of 0.73 and RE of 0.31 was observed in the swine with myocardial infarction.

Pace Mapping in Healthy Canine

Pace mapping, as a widely adapted clinical method to modulate the heart as well as

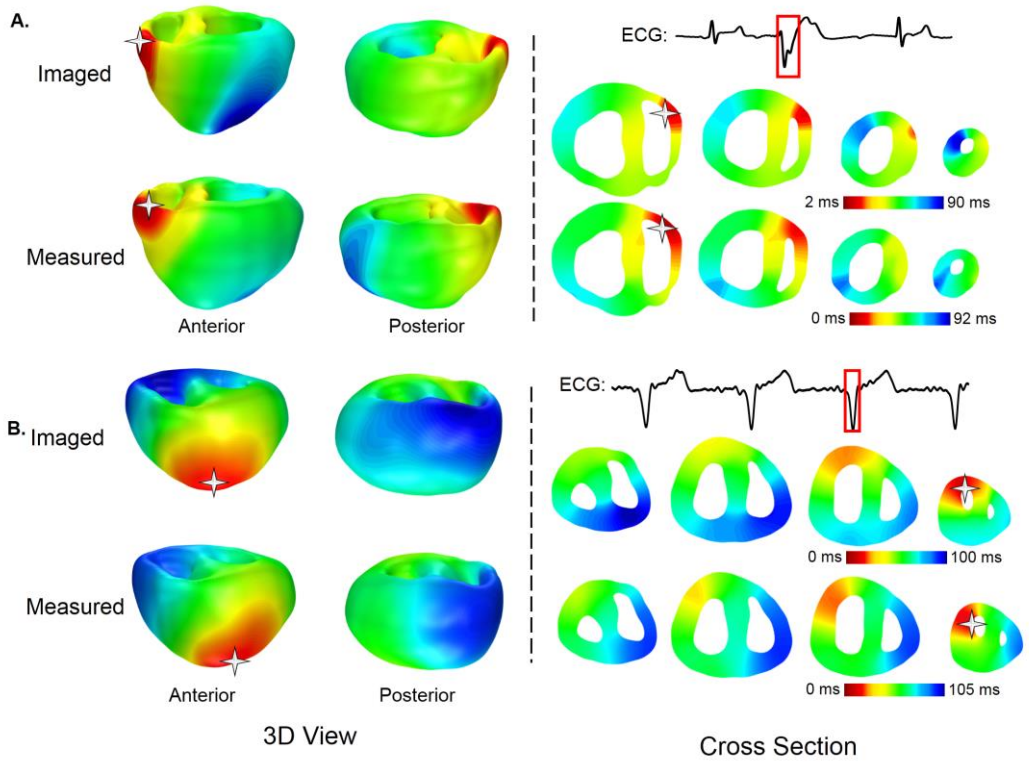

Figure 12: monomorphic arrhythmia beats induced by NE in intact heart. In panel A, the imaged and measured activation sequences for a PVC beat is shown. In panel B, one ectopic beat from a train of MVT is shown. The ECG (Lead-II) is shown on top of each panel.

Monomorphic Automatic VT

To evaluate the performance of the method in more clinical-related circumstances, NE infusion was conducted to induce arrhythmias in the experimental animals. In figure 12, comparisons between imaging and measured activation on different induced arrhythmia cases can be found. In panel A, a PVC beat was isolated and imaged. The initiation can be found in RV free wall and the propagation pattern from RV to LV was imaged with good concordance to the measured activation sequence. Focal initiation from RV free wall was correctly localized and the propagation pathway through the septum was also clearly depicted. The imaged initiation site was localized 4.7 mm away from the imaged origin of the arrhythmia. The global activation patterns also see a CC of 0.82 and RE of 0.19, indicating strong agreement between the results. In the lower panel, one beat selected from train of MVT beat is shown. The beat initiated from the apical area and propagate to the basal posterior of the heart, dissolving at basal free wall. Both the initiation and termination of the activation was corrected imaged. Although minor differences can be found between the imaged and the measured activation, the CC between them remains as high as 0.8 and RE as low as 0.2. The accuracy is well maintained globally and the LE of 6 mm can be found.

Polymorphic Automatic VT

The performance of the method on highly dynamic PVT activities is shown in figure 13 by comparing the imaged and the measured activation sequences on changing rhythms. The activation patterns from panel A and B are selected from a same train of PVT beats. Initiations were correctly identified and localized in different locations. The initiation sites of the two morphologies are 4.3mm and 5.2mm respectively in panel A and B. In panel A, the ectopic beat originated from RV free wall and traveled through the myocardium. The end of the activation can be observed on LV. A relatively larger early activation was imaged as shown in the figure but the foci

of activation was clear and co-localized with the measure results. The CC and RE between the imaged and the measured activation are 0.82 and 0.2 respectively. In the panel B, a different initiation foci located in the apical area and propagated to RV free wall with a CC of 0.79 and RE of 0.23. In both cases, the imaged activation pattern is in good agreement with the measured activation pattern. The performance of the method on a certain arrhythmic pattern is not affected by the frequency of recurrence.

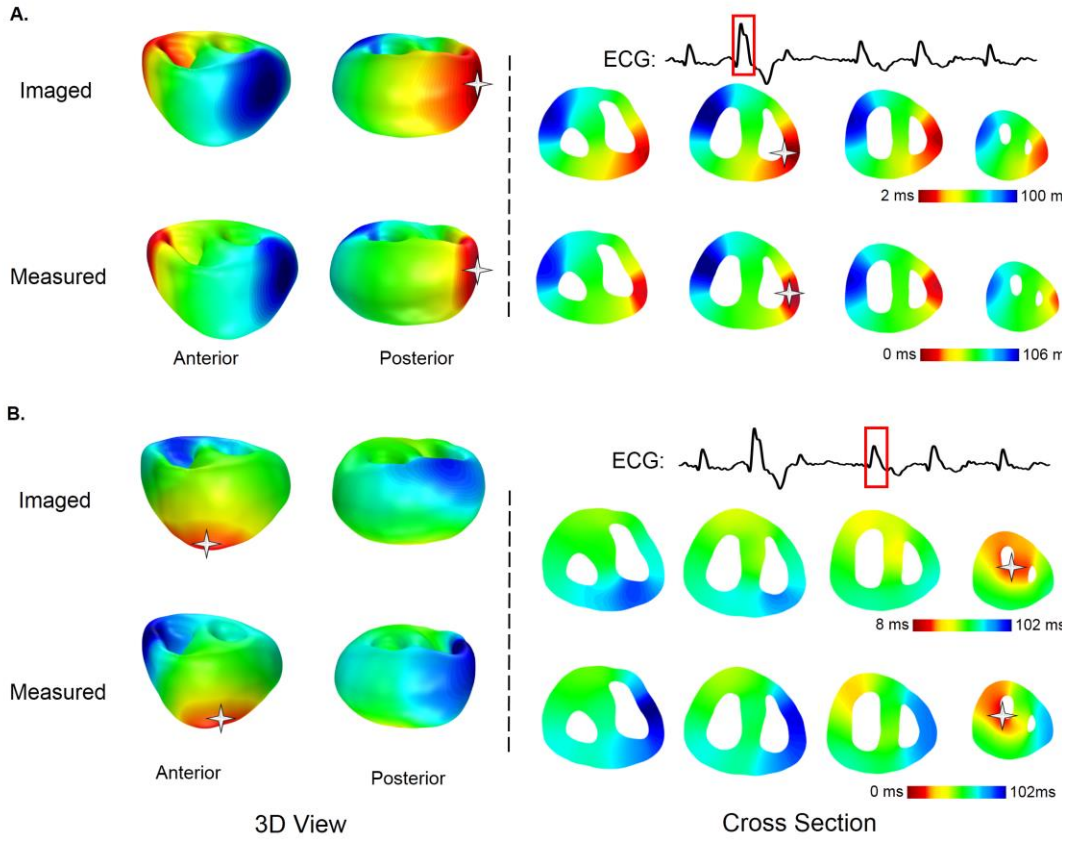

Figure 13: imaging results on arrhythmic activities on HF hearts. The 3D view is shown on left while the cross sections are shown on the opposite. Lead-II ECG is shown on top of each panel. The initiation site is represented by white star.

VT in canine with HF

Figure 14 presents some examples where the method was tested in a more complicated pathological condition, congestive heart failure. As can be observed in the figure, remodeling in myocardium due to the pathology has changed the geometry of

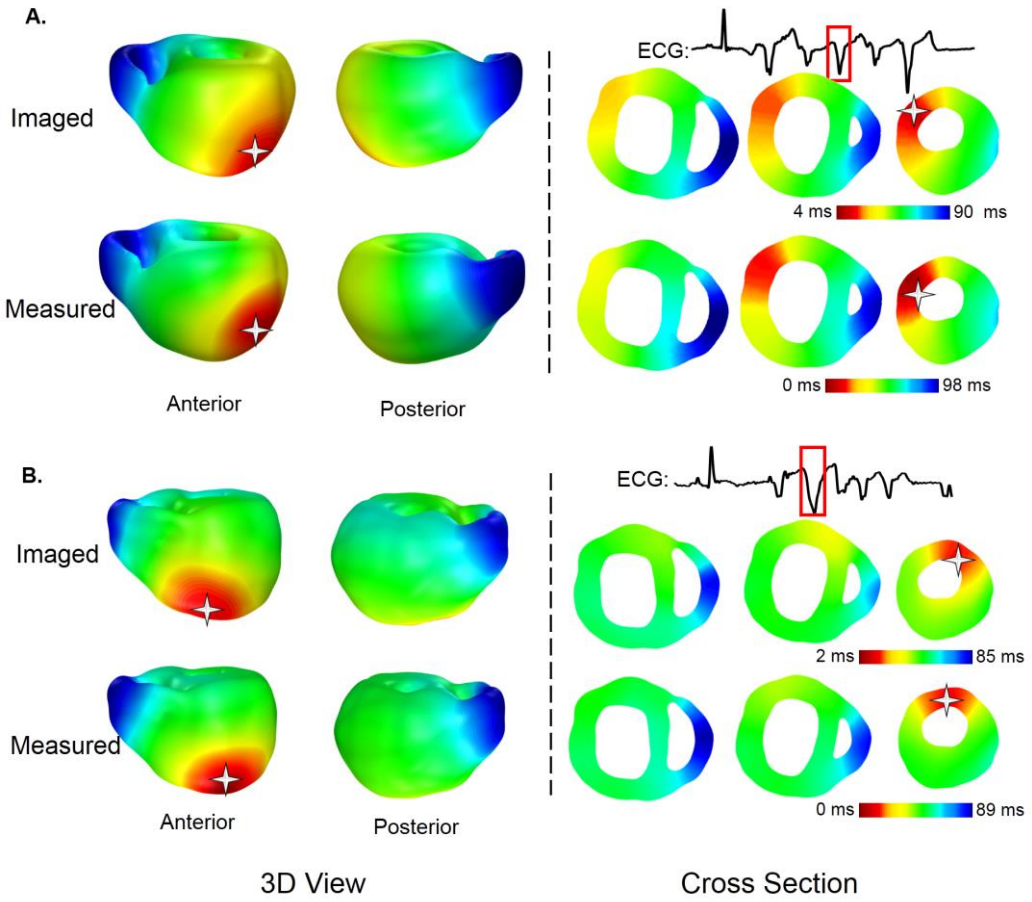

Figure 14: imaging results on arrhythmic activities on HF hearts. The 3D view is shown on left while the cross sections are shown on the opposite. Lead-II ECG is shown on top of each panel. The initiation site is represented by white star.

the heart, leading to hypotrophy myocardium with thicker ventricle wall and septum. However, the technique is shown in the comparisons to be robust against the myocardial remodeling process. In panel A, a VT ectopic beat was initiated from LV lateral apical area. The activation travels through the myocardium and terminated at

RV free wall. In panel B, the VT activation was also initiated in LV but in anterior apical area. Despite the initiation were in different locations, termination patterns of the beats were basically identical. The feature is well captured by the imaging technique. The relatively slower conduction speed was imaged and can be observed in the figure when the activation traveled in the septal area across LV and RV.

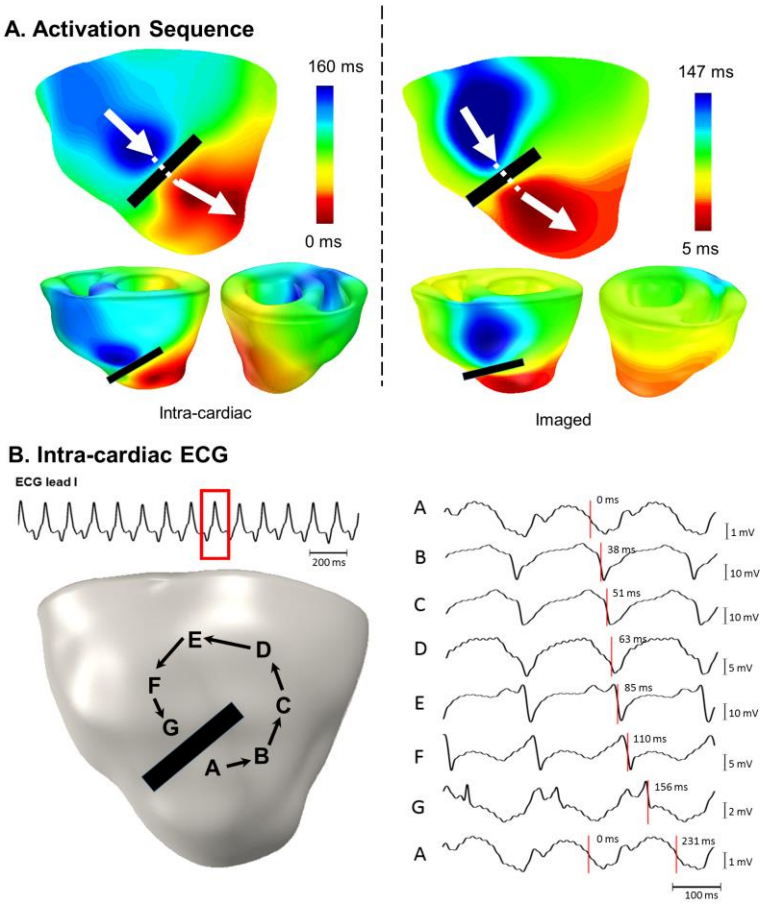

Figure 15: imaging results on arrhythmic activities on HF hearts. The 3D view is shown on left while the cross sections are shown on the opposite. Lead-II ECG is shown on top of each panel. The initiation site is represented by white star.

Reentrant VT in swine with myocardial infarction

An example of reentrant VT and the intra-cardiac electrograms along the reentry pathway is shown in figure 15. In panel A, the eletrograms are selected and shown

along the propagation pathways. The conduction block identified between electrode A and G is marked in black. Two different pathways can be found along these electrodes as marked with black arrows in the figure. The first pathway, initiating from A and travels through B, C, D, E, F along LV while the other through I, J, K, L along RV. The activation time of each site in the reentry cycle is marked with red lines. The reentry pattern is clearly depicted. The general activation patterns are shown in panel B. The reentrant VT propagates counter clockwise around the heart. The conduction block can be identified in anterior sepal area. The reentry pathway is well captured by the imaging technique and the conduction block is identified non-invasively with good accuracy.

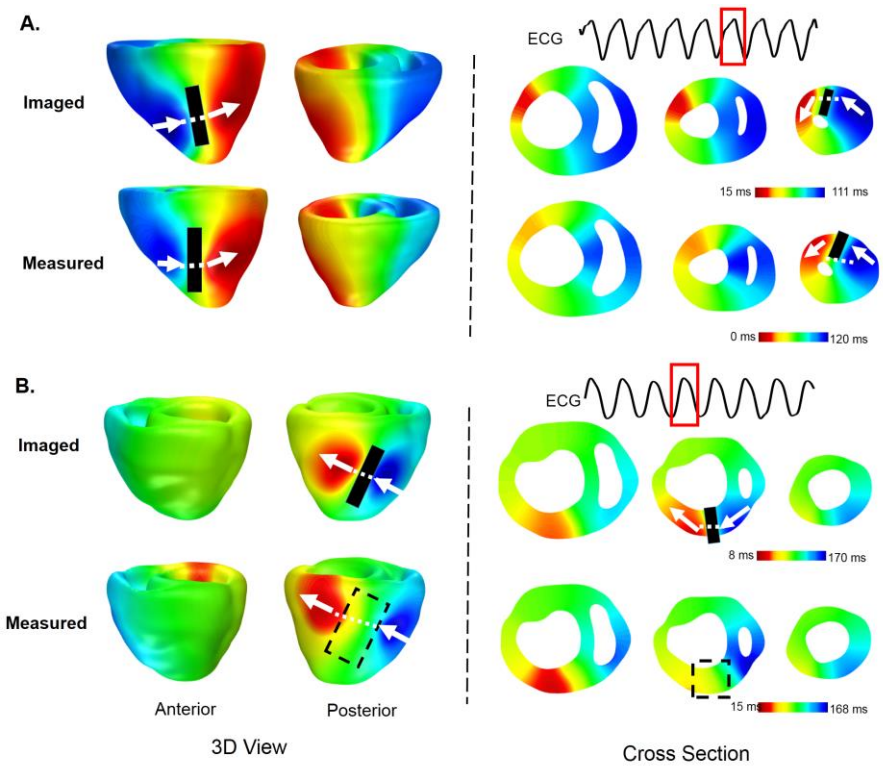

Figure 16: Examples of the imaged and the measure activation sequences during reentrant VTs. Black block is used to mark the potential conduction block shown in the activation sequence and the reentry pathway is identified with white arrow and dashed line.

In figure 16, more imaging results are shown and compared with intra-cardiac activation sequences. In panel A, a counter clockwise macro reentry loop can be identified from the activation sequences. The reentry pathway can be found in anterior septal area. The exit of isthmus lay in middle anterior LV and the propagation traveled through the myocardium, terminating in RV, the entrance of the isthmus. The imaging technique successfully localized the conduction block and exit of the isthmus with high concordance with the intra-cardiac mapping results. In penal B, a posterior clockwise reentrant VT cycle is shown. The macro reentry loop is well shown in both imaged and intra-cardiac activation sequences. Due to the lower density in posterior intra-cardiac electrodes, the exact location of conduction block cannot be pinpointed with transmural electrodes. The imaged conduction block lies well inside the area between the latest and the earliest recorded intra-cardiac activation, indicating a good localization of the reentry isthmus even in posterior hard where the signal is heavily blocked due to its location.

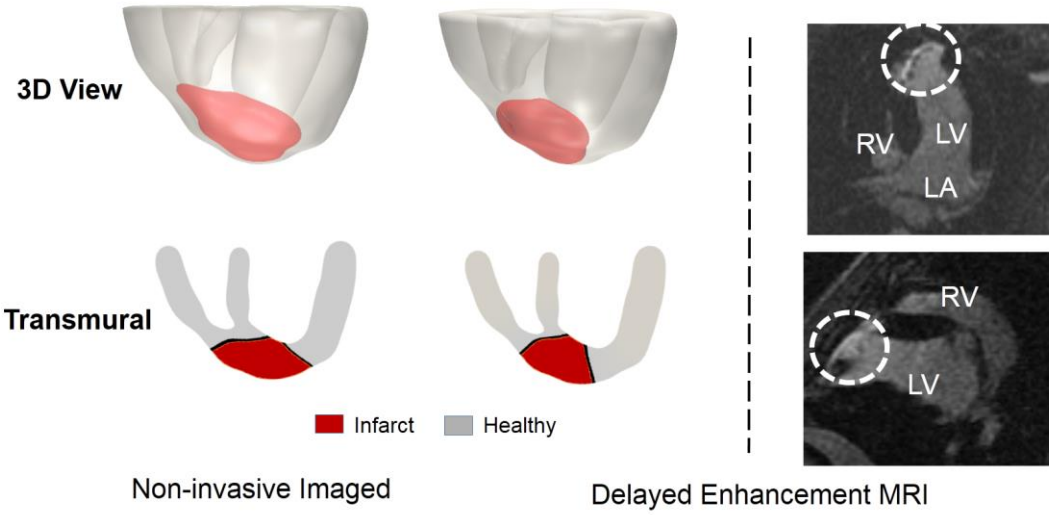

Figure 17: imaged infarct area is compared with the DE-MR imaged region. The 3D visualization and cross section is shown in the left and the DE-MR images are shown in the right. Injured area is marked with white dashed line in MR images.

Infarction imaging in swine

In figure 17 and 18, the imaged infarct area is compared with segmentation results of DE-MRI identified injured area. As can be observed in the figure, the measured and imaged infarct area are in general concordance with each other. In panel A, relatively large area of infarction can be found spreading from anterior septal to posterior RV. Although some discrepancies can be found in mid septal area between DE-MRI and the imaged results, in most area of RV and septum, the infarction is correctly identified. In panel B, the DE-MRI indicates a larger infarct area than the electrically imaged area with major disputed area in the posterior. In mid-anterior apical area, the two modalities are in good agreement.

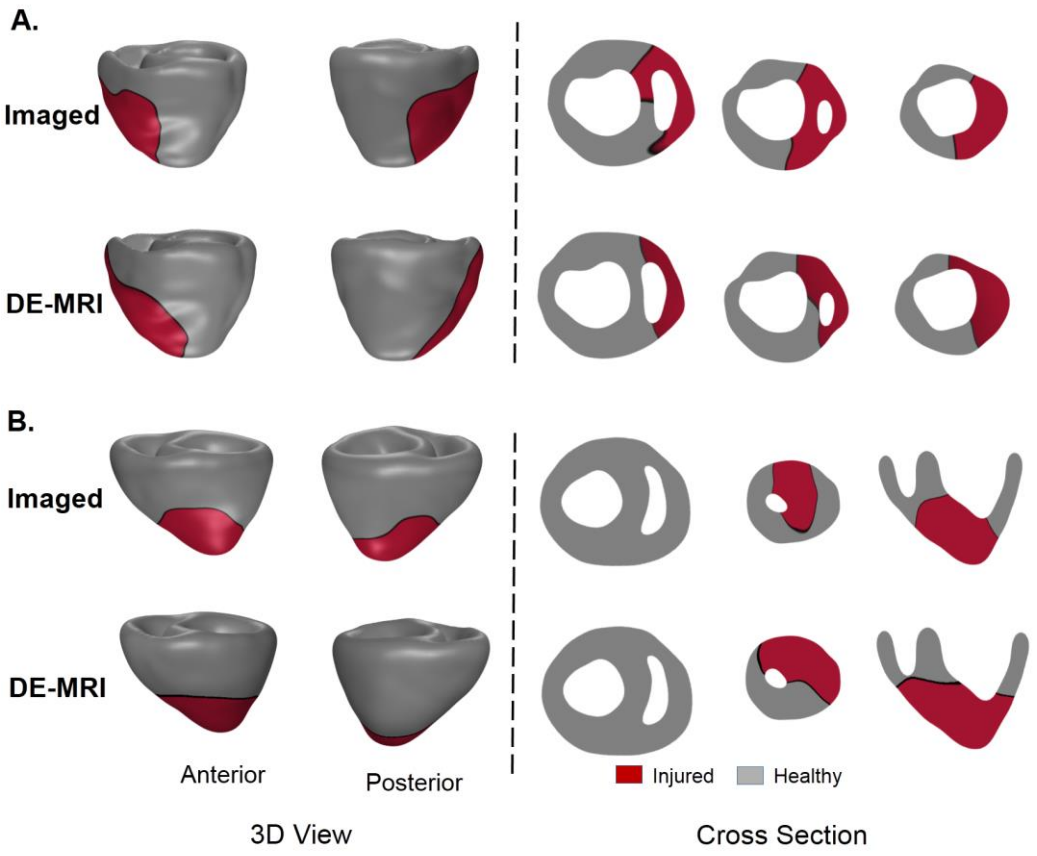

Figure 18: imaged infarct area is visualized and compared with segmented Injured are from DE-MRI. The 3D view of the results is shown in left and the cross section view is shown in the right.

4.5 Discussions

The present study presents a first thorough evaluation and validation of 3D cardiac electrical imaging in large animals with various pathological conditions and mechanisms. The evaluation of the CESI technique was further extended to more complicated pathological conditions in improved animal models to evaluate its performance and clinical potential. On the foundations

laid by the previous numerical and rabbit pacing study(Yu, Zhou, and He 2015), the capability of CESI to localize the ectopic foci and to unveil the arrhythmic pattern throughout the myocardium was examined in various clinically relevant scenarios. On average over the 200 ectopic beats included in the study, a CC of 0.8, RE of 0.23 and LE of 6 mm can be obtained in the isolated arrhythmic beats, indicating good accuracy and robustness of the technique to image the foci and mechanism of the arrhythmias. RRE stayed below 5% in general and therefore the temporal resolution is well maintained. These findings imply that CESI is feasible to reconstruct the 3D ventricular activation sequence of the heart at arrhythmias in the scenarios that highly resemble those in the clinical practice.

Efforts have been undertaken to directly visualize the cardiac electrical activity from body surface ECG from various perspectives(Erem et al. 2014; Oster and Rudy 1992; Vijayakumar et al. 2014; Y. Wang et al. 2011; Bin He, Li, and Zhang 2003; Ghosh et al. 2008; Milanič et al. 2014; Brooks and MacLeod 1997; Nash, Bradley, and Paterson 2003; Pullan et al. 2001; Ohyu, Okamoto, and Kuriki 2002). CESI technique offers an alternative approach to directly visualize the whole heart electrical activity in 3D on a beat-to-beat basis. This feature indicates that the technique can potentially become a unique tool to direct information on the location and depth of the arhythmogenesis not only in the hemodynamically stable rhythms, but the highly dynamic activities such as the PVT beats, a commonly encountering challenge that the sequential mapping procedures are likely to fail. Moreover, the non-invasive nature of the imaging

modality promises relatively low cost and dexterity to adapt for both pre-procedural (diagnostic) and in-procedural (ablation guiding) scenarios, allowing CESI to provide the physicians with helpful information to improve and accelerate the currently ablative procedure while co-existing with current standard protocol. On the technical aspects, the temporal sparse formulation employed in CESI, in contrast to the minimum norm based approaches, counters the ill-posedness, a central challenge of the ECG inverse problem(Okamoto, Teramachi, and Musha 1983), with both mathematical constraints to strengthen uniqueness and electrophysiological knowledge to avoid distortion. This reconstruction strategy avoids the complicated electrophysiological model with its robust biophysics based model while, at the same time, considers the momentary cellular electrophysiological behavior at the activation in the process of imaging. Rather than estimating the activation time based on a continuous inversely computed ECG waveform, CESI directly reconstructs the current density spike generated at the depolarization. It is the preservation of the electrophysiology in reconstruction that permits the temporal resolution to be properly maintained as well as the improved accuracy and robustness.

For an imaging modality, rigorous validation in biological systems has been proved to be critical. The closed chest condition with both intra-cardiac and body surface electrodes enabled a thorough and accurate validation of the recently proposed non-invasive imaging technique. The present validation study is founded on a protocol refined from the previous well established validation

mapping studies and animal model in a procedure where the rigorousness has been well demonstrated. All the activation sequences were collected through in vivo study where the condition and vitals of the animal were closely monitored and the pathology was induced with caution and tightly controlled. Compared to the rabbit heart used previously, the canine heart model is better comparable to human hearts in both its electrical conduction and in its size. Also, due to their size, the experiment conditions with canines better resemble those found clinically. One can observed a comparable, but slightly deteriorated performance compared to the previous numerical and rabbit pacing study. The experimental setup employed in the study involves highly complicated disturbances such as interferences from other monitoring electronics and movement artifact that are as severe, if not more, than the realistic clinical setup. In addition, the sternotomy and close chest procedure employed in the study to achieve three dimensional direct measurements may induce unknown modeling error which will mostly likely to absent clinical applications. Therefore, our finding based on the results in the study indicates that the technique possesses a strong potential to image the activation sequence in the patents as a clinically feasible tool for diagnosis and guiding the ablative procedure.

In aim for a more thorough evaluation of the technique for the clinical challenges from various arrhythmic morphology and pathological conditions, this study extends the coverage on different types of arrhythmias in the validation to a completely new level, including a series of focal, multifocal, and even non-focal arrhythmias in various pathological conditions. The infusion of

NE served as a good resemble of the activation of sympathetic nervous system, producing arrhythmias such as PVC, couplets, MVT, PVT, VF etc. These ectopic activities are commonly seen for patients undergoing EP study with ablation. Repeating runs of PVC may be feasible for current ablation techniques yet it usually takes hours to make a full chamber activation map. However, it is not uncommon that patients have less frequent PVCs so that the procedure has to be delayed by hours or even aborted. PVTs have shown unstable and highly dynamic activities, it is shown in the results that CESI can image the multiple distant initiation site within a short, non-repeating arrhythmic episode. The NE induced VTs resemble the morphology of the idiopathic VTs in patients. The results shown that the origins of the unstable activities can be well captured and localized non-invasively by CESI. The performance of the technique in highly complicated pathological conditions such as congestive heart failure is tested. By comparing the results between structurally healthy hearts and those with HF, one can observe that only minimal deterioration in performance occur to the results with HF, indicating strong robustness of CESI against the complicated EP conditions. Combined with those from non-HF canines, the results laid a solid foundation to expand the evaluation of the technique further to various clinical applications.

Reentry VT represents a significant clinical challenge due to its dynamic nature and the hemodynamic instability during the very lethal arrhythmia. This study is the first time 3D imaging technique is put to practice against reentry VT, a highly dynamic and clinically challenging arrhythmia. With the 3D intra-cardiac

mapping system, it is also the first time to our knowledge reentry VT is not only imaged but also thoroughly validated invasively. As can be observed from figure 15 and figure 16, the non-invasive technique is capable of directly visualizing the reentry pathway with high accuracy and identifies the conduction block for each reentry loop correctly. In contrast to the invasive approaches which demand extensively long operating time and hemodynamic stability that scarcely available, the non-invasive approach can imaging the activation sequence over the whole myocardium with only one complete reentry cycle. This capability can potentially benefit the clinical management of reentrant arrhythmia. The imaged technique, validated by intra-cardiac mapping system, is shown to be capable of localizing the exit of reentry isthmus within 8mm on average and clearly identify the conduction block in each reentry cycle. The information provided can directly assist the ablation to cut off the reentrant activation in the slow conduction area, terminating the VT. Also, a beat-to-beat understanding of the arrhythmia can strongly benefit the understanding of the mechanism, leading to further optimized configuration of defibrillation and anti-arrhythmic pacing with the implantable devices. Comparing to pacing mapping and conduction speed mapping invasively, the non-invasive

Other than activation imaging, the electrical information underlying in BSPM also provides insight into the infarct area through the 3D electrical imaging technique. The comparisons between DE-MRI and the imaged results have demonstrated that the non-invasive electrical imaging technique, a much cost-effective approach, can generate comparable localization of the infarct

area to the more expensive MRI. Moreover, the passive recording electrical imaging technique neither requires contrast injection nor has any interference with other electronics such as pace maker and ICDs. Combining the electrical activation and the imaged infarct area, the 3D non-invasive electrical imaging technique can provide a comprehensive understanding of the electrical activity throughout the myocardium.

In sum, the present section of the dissertational study suggests that CESI approach is feasible to reconstruct various arrhythmic rhythm with good accuracy and demonstrates robustness in realistic experimental setup and complicated pathological conditions as validated by 3D intra-cardiac mapping procedure. These findings imply that CESI can potentially function as a useful clinical tool to aid in localizing the origins of arrhythmogenic substrate and help understanding the mechanism of these arrhythmias.

Chapter 5

Non-invasive imaging and localization of ventricular arrhythmia in patients: pre-ablation and in-procedural clinical investigations

5.1 Introduction

Approximately 400,000 sudden cardiac deaths are reported annually in the United States alone, according to the American Heart Association(Mozaffarian et al. 2015). In addition to the medication routinely administered to suppress the syndromes, cardiac radio frequency (RF) ablation techniques have been used in a growing number of patients to ablate critical sites in the heart that initiate ventricular arrhythmia(Stevenson and Delacretaz 2000). In clinical practice, ventricular arrhythmia is difficult to localize based on 12-lead ECG diagnosis with success rate as low as 60%(Yamada et al. 2015). While catheter-based endocardial mapping approaches have shown the promise of offering a minimally invasive means of localizing and mapping cardiac electrical activity over the endocardial surface, these catheter intervention approaches are time-consuming, limited in hemodynamically unstable arrhythmias, and the success rate in patients with structural heart disease can still be as low as 60%(Sacher et al. 2008). By the very nature of the

procedure, the knowledge on location and propagation pattern of arrhythmia has been proven crucial for a successful ablation. However, the invasive intra-cardiac mapping technology requires the patients to stay prolonged periods in the electrophysiology (EP) lab. In contrast, the non-invasive imaging approaches can offer alternative insights into the mechanism of the arrhythmias and therefore provide important information assisting the therapeutic treatments on a beat-to-beat manner.

Efforts have been made to reconstruct the intra-cardiac electrical activity from the body surface potential maps (BSPMs). Various approaches have been proposed previously in different scopes, such as moving dipole solutions(Armoundas et al. 2003), epicardial potential imaging(Y. Wang et al. 2011; Greensite 2005) and heart surface activation imaging(Berger et al. 2006; Tilg et al. 2002). Evaluation studies on the approaches involve animal experiments and human studies, showing good potential for assisting in clinical practice. However, the origin of the arrhythmic activity is not restricted to only the endocardial or epicardial surfaces but also exists across the myocardium such as the subendocardium, the subepicardium and even the intramural myocardium(Yamada et al. 2015; el-Sherif et al. 1985). The detailed knowledge of intramural electrical activity has proven to be important to the planning and conduct of clinical management in catheter ablation(Yamada et al. 2015), leading to a significant clinical demand of a non-invasive imaging approach that can estimate and visualize the transmural electrical activity directly while invasive techniques lacks the access to transmural locations.

Efforts have been made to image the electrical activities throughout the three-dimensional (3D) ventricles(Li and He 2001; Han et al. 2012; Z. Liu, Liu, and He 2006; Zhang et al. 2005; D. Wang, Kirby, and Johnson 2011; Rahimi and Wang 2015; Skipa et al. 2002; Zhou et al. 2014; Ohyu, Okamoto, and Kuriki 2002; Bin He and Wu 2001). Results from the previous studies have demonstrated that the 3D cardiac electrical imaging technique is capable of localizing the 3D ectopic initiation site of different types of arrhythmia in various healthy and pathological models(Han et al. 2012; Han et al. 2013; Han et al. 2008). Yet clinical challenges remain that demand non-invasive imaging techniques that are capable of achieving high spatiotemporal resolution while at the same time do not heavily depend on a specific pre-defined physiological model that limit the techniques with the risk of model over-fitting and the lack of flexibility against unknown pathologies. A most recent development of the noninvasive 3D cardiac electrical imaging technique - Cardiac Electrical Sparse Imaging (CESI) method - has been proposed to meet these demands and has demonstrated improved performance in numerical and animal studies(Yu, Zhou, and He 2015).

In this chapter, the evaluation of the developed imaging technique is forwarded to a new level based on the previous rigorous animal validation. The CESI technique is tested against real clinical challenges in both pre-ablation procedure and in-procedure studies. The performance of the imaging technique in the clinical setup and its compatibilities with the standing devices in the EP lab. Comprehensive evaluation was conducted by quantitatively comparing the

imaged ventricular activation and the intra-cardiac mapping results directly in patients for the first time. We demonstrated the capability of the noninvasive 3D cardiac activation imaging technique to localize arrhythmic substrate, to help elucidate the arrhythmic mechanism and to reveal crucial information aiding in the ablative therapy as a clinically useful imaging technique.

5.1 Pre-procedure Localization of PVC using non-invasive imaging technique

The mathematical formulation and detailed methodology has been described previously(Yu, Zhou, and He 2015). When a myocardial cell is activated, the trans-membrane potential of the excitable cell rises rapidly from the resting state at around -90 mV to its depolarized plateau potential at about 0 mV. The electric field generated by myocardial depolarization travels through the body, a volume conductor, and manifests on the body surface in the form of detectable ECG. With an array of electrodes that can map the spatial distribution of electrical potential drops across the body surface, the BSPM can be obtained. The patient's individualized volume conductor can be approximated numerically using the boundary element method (BEM), based on the geometry provided by the structural tomography imaging such as computed tomography (CT) and magnetic resonance imaging (MRI). By coupling the function information from BSPM and geometrical information from CT or MR, cardiac electrical imaging methods can inversely reconstruct the cardiac electrical activity, revealing vital information regarding the arrhythmias such as the initiation sites and propagation patterns.

Patient population

A total of 13 patients with ventricular arrhythmias undergoing EP study with catheter ablation treatment participated in the present study. All experimental protocols were approved by the Institutional Review Board of the University of Minnesota and the Shanghai Ruijin Hospital. All the patients were consented with formal written consent forms. All the patients were diagnosed with idiopathic premature ventricular complex (PVC) or ventricular tachycardia (VT) with no other previous or concurrent structural cardiovascular disease identified such as ischemia, infarction or congestive heart failure. Twenty-four hour Holter monitoring was deployed to all patients after being admitted to the hospital. Preliminary diagnosis indicates the patients suffer from frequent PVC (around or above 10,000 PVC/day) originating from different locations including RVOT, RV and LV. Detailed information of the patients is summarized in Table 3.

Patient study protocol

The schematic of the study is shown in Figure 19. Body surface mapping

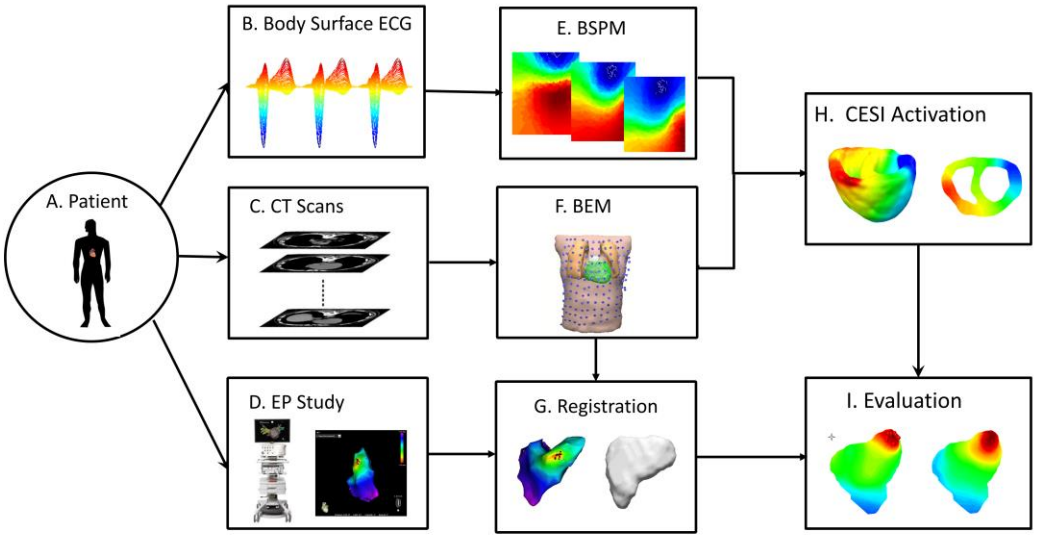

Figure 19: Schematic diagram of the study. A: patients; B: body surface ECG collected pre-surgically including the arrhythmias; C: CT scan with torso and cardiac geometry; D: EP study with catheter ablation by intra-cardiac mapping technique; E: BSPM of the ectopic beats isolated from the ECG recording. F: boundary element model constructed from individual patient's CT images; G: 3D co-registration of CARTO geometry and endocardium from CT; H: 3D CESI activation image; I: quantitative comparisons between the CARTO mapped activation pattern and the CESI activation pattern on corresponding regions.

and CT scanning was performed one day prior to the EP study with ablation. Up to 208 body surface electrodes (2 kHz sampling rate) arranged in strips (ActiveTwo system, BioSemi V.O.F., Amsterdam, the Netherlands.) were evenly distributed to cover the patient's chest (144 electrodes) and back (64 electrodes). Locations of the electrodes and anatomical landmarks identifiable in CT images were digitized with an electromagnetic digitizer (Fastrak, Polhemus Inc, Colchester, VT, USA). Thoracic (0.78x0.78x5 mm) and ECG gated (70% R-R interval) contrast-enhanced cardiac (0.39x0.39x0.75 mm) axial

CT imaging were performed on all patients preceding the ablative procedure within a week of the mapping study.

The EP study with ablation was conducted using a contact endocardial mapping system (CARTO3 system, Biosense Webster, Diamond Bar, CA, USA). The intra-cardiac electrograms were collected sequentially on the endocardium from spontaneous PVC beats. Local activation time (LAT) maps on the endocardium were generated through the sequential mapping of various sites across the entire or partial endocardium surrounding the suspected foci. Ablation was performed on the suspected foci of the arrhythmic activity until all ectopies were eliminated. After the patient's rhythm resumed and maintained normally sinus for 30 minutes, the ablation was then assumed successful. The in-procedural intra-cardiac and 12-lead ECG waveform, LAT maps and the coordinates of the ablation sites were collected after the EP study. All patients were arrhythmia free after the procedure and were discharged within one week.

Data Analysis

Segmentation of patients' CT images and surface triangulations were carried out aided by CURRY 6.0 commercial software package (Compumedics, Charlotte, NC). Triangular meshes of the realistic geometry (torso, lung, epicardium and myocardium) and ECG recordings were exported to the customized CESI software package developed in Matlab 2010a (Math Works, Natick, MA). The entire ventricular myocardium was discretized into approximately 10,000 grid points evenly distributed throughout the entire ventricular myocardium. A distributed equivalent current dipole (ECD) source

model was adopted to represent cardiac electrical activity(Z. Liu, Liu, and He 2006). The transfer function connecting the distributed source model with the BSPM was derived based on the bidomain theory and constructed using the boundary element method(Barr, Ramsey, and Spach 1977). A set of piecewise isotropic electrical conductivities was assumed for all patients in the modeling process: 0.2 S/m for torso, 0.04 S/m for lung cavity, 0.6 S/m for myocardium tissue and 0.8 for blood cavity (Malmivuo and Plonsey 1995). Detailed modeling statistics are summarized in Table 3. With the transfer function built, the BSPM is linearly connected to the electrical activity throughout the myocardium for each patient. Activation sequences can be thereby imaged with the 3D inverse reconstruction algorithm to visualize the electrical activity during the selected arrhythmic beat of interest.

For the purpose of quantitative evaluation of the imaging method, the ablation sites, LAT map and the intra-cardiac geometry were extracted from the EP study and were three dimensionally co-registered with the corresponding CT images based on the digitized anatomical landmarks. The imaged activation was also extracted from the 3D myocardium and projected to the CT endocardium in aligned with endocardial geometry constructed by CARTO.

Six quantitative indices - Localization Error (LE), Nearest Ablation Localization Error (NALE), Correlation Coefficient (CC), Relative Error (RE) and Relative Resolution Error (RRE) - were used in the data analysis to evaluate the accuracy and clinical potential of the imaging technique. Imaged initiation site is defined as the region of earliest activation. LE is defined as the distance

between the imaged activation and the last successful ablation site. NALE is defined as the distance between the imaged initiation site and the nearest ablation site. CC and RE are utilized to assess the concordance and discrepancy between the invasively mapped and non-invasively imaged activation patterns on the endocardium, defined as:

$$CC = \frac{\sum_i (AT_i - \overline{AT}) \bullet (MT_i - \overline{MT})}{\sqrt{\sum_i (AT_i - \overline{AT})^2} \bullet \sqrt{\sum_i (MT_i - \overline{MT})^2}} \qquad (1)$$

$$RE = \sqrt{\frac{\sum_i (AT_i - MT_i)^2}{\sum_i MT^2}} \qquad (2)$$

where AT_i and MT_i represent the imaged and measured activation times at the ith grid point while $\overline{AT}$ and $\overline{MT}$ represent their average on all grid points. RRE is employed to measure the loss temporal resolution, and is defined as:

$$RRE = \frac{|T_M - T_I|}{T_{total}} \qquad (3)$$

where T_M represents the total activation time of measured activation, T_I represents the total activation time of the imaged activation sequence on the co-registered area and T_{total} represents the total activation time from the body surface ECG.

For each patient, multiple ectopic beats were isolated from the BSPM recordings. Ten arrhythmic beats with the same morphology as in the EP study

(CC>95%) were randomly selected from the recording for analysis. To evaluate the robustness of the method, robustness-CC (r-CC) and robustness RE (r-RE) are computed as the average CC and RE respectively between the activation sequences of the 10 selected beats and the averaged activation pattern. A high r-CC and a low r-RE of a certain patient indicate that the results are consistent and therefore capable of evaluating the robustness of the technique.

5.2.2 Results

Patient Population and Summarized Statistics

CT images, BSPMs and EP study records from the 13 patients were analyzed. Multiple ectopic beats were observed during BSPM recordings. Ten PVC beats were randomly selected from each patient for non-invasive imaging. CT based individualized realistic models were built for each patient and 3D co-registered with the CARTO intra-cardiac mapping geometry. BEM related modeling statistics are summarized in Table 3. The CC, RE, LE, NALE and RRE for each patient were computed and summarized in Table 4. The method has achieved good accuracy in the clinical experiment. An average CC of 0.79 and RE of 0.19 indicates a strong concordance between the imaged activation sequence and the intra-cardiac measured LAT. The LE lies below 8 mm and NALE blow 3mm on average, indicating the capability in localization is comparable with the intra-cardiac mapping technique. RRE, as shown in the figure, is well controlled below 3% and the temporal resolution loss is minimal.

CC, RE and RRE of patient 7 are excluded from the summarized statistics with only LE and NALE left due to the inconsistency between the invasive mapping results and the ablation outcomes. In general, the performance of the method is slightly better in RV than RVOT and LV. The variation in the statistics may be due to the differences in initiation locations and consequentially the quality of the signal and complexity of the corresponding structure.

In addition, the aforementioned statistics along with the robustness statistics r-CC and r-RE were summarized in Table 3 and organized according to different regions of initiation (LV, RV, RVOT). The results have demonstrated to be highly robust among the selected beats with similar morphology. As can be observed in the table, the r-CC is as high as 0.97 and r-RE as low as 0.07, indicating the imaged results are stable and robust to the interferences in the clinical setup.

Focal Arrhythmias in RV and LV

Figure 20 displays examples of CESI activation imaging on ectopic beats initiated from the right and left ventricles. Panel A shows an example of a PVC beat originating in the right ventricle near the RVOT while in Panel B, an arrhythmic beat is localized in the left bundle anterior branch. The left column displays a 3D view of the imaged activation sequence color coded from red (early activation), to dark blue (late activation) as shown in the color bars at the

corners of each panel. Cross sections at various axial positions can be found in the middle-left of each panel, sharing an identical color code with the 3D view. In the middle-right column, CARTO intra-cardiac mapping activation sequence and the ablation sites are compared with those extracted from the 3D imaging results after co-registration. The white star represents the imaged initiation. The black circle and the red dots in the figure represent the last successful ablation site and rest of the ablation sites respectively. In Panel A, a focal pattern can be observed from the 3D activation sequence that initiated in the right ventricle and dissolved at the left ventricle wall. From the global activation pattern, cardiac excitation does not travel at an isotropic speed geometrically but rather propagates faster along the right ventricle wall than it does across the septum. A clear progression of activation from the RV to the LV can be observed. As the activation propagates from the RV free wall, a delay occurred when it enters the LV, in contrast to a relative higher faster propagation observed in RV. The two activation frontline met and the beat terminated in LV free wall. On the endocardium shown in the right, the focal pattern is well captured in the imaged results and is consistent with the CARTO activation maps. The intra-cardiac mapped activation sequence displays a relatively diffused pattern in the early activated area, in contrast to a more focused initiation pattern imaged. Note that the sequential intra-cardiac mapping has a much lower spatial resolution in

general and inevitably produces a spread-out pattern without time-consuming further refinement.

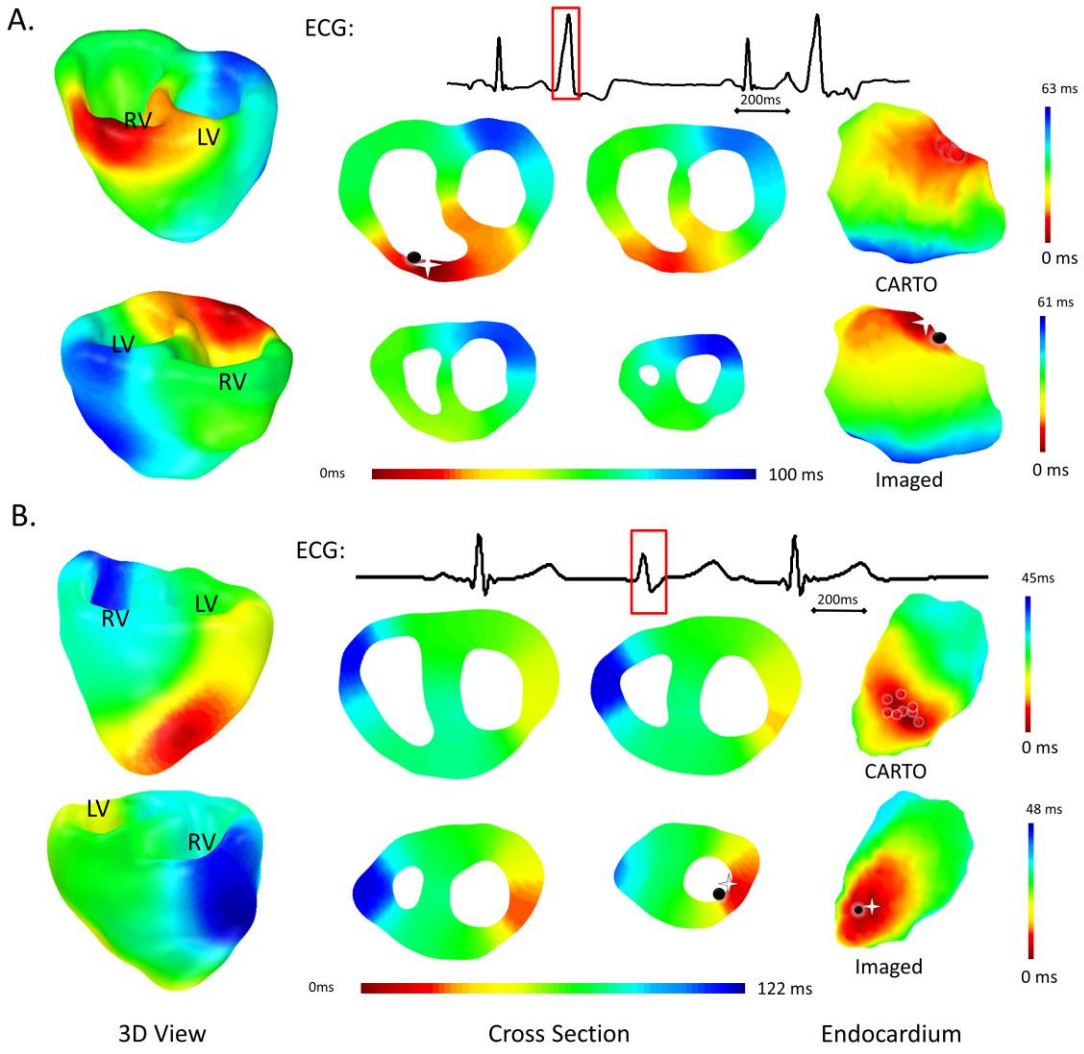

Figure 20: Examples of imaging of activation sequence during ectopic beats originating from the RV (Panel A) and the LV (Panel B). The figure is color coded from red (early activation) to blue (late activation). Black circle represents the last successful ablation site. The white star indicates the site of initiation localized by CESI. The dashed lines shows the ablated area estimated by the ablation sites represented by red circles.

In Panel B, the focal pattern originates in the left anterior wall and is also well imaged globally from the LV to the RV free wall. Multiple trials of ablation

were performed on this patient to terminate the arrhythmic activities. The initiation lies in the LV close to the apical anterior region. The focal propagation pattern can be observed from the results. In the endocardium view, although discrepancy can be found in detailed early activation pattern, the localizations made by the invasive and non-invasive technique agree well with each other. By comparison between the two, one can see that the imaged activation sequence has a clear focal activation pattern whereas the measured one holds more irregularity. The differences between the early activation pattern may originate from the limited spatial resolution of the invasive measurements where the pattern is highly affected by the location of catheter recording.

Focal Arrhythmia in RVOT

Figure 21 shows two more examples on the imaging results of PVCs. In both cases, the ectopic beats originated from the RVOT. In Panel A, the PVC beat initiated near the RV free wall while the beat in panel B initiated at the

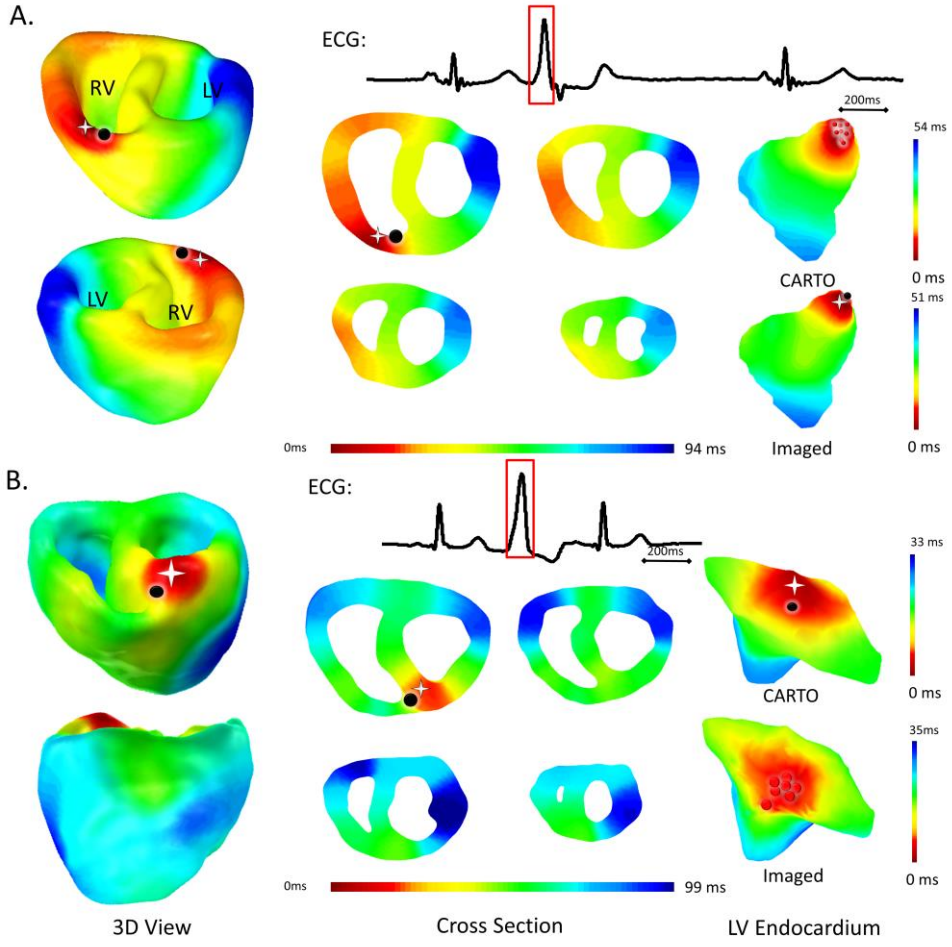

Figure 21: Examples of PVC ectopic beats originating near the RV free wall (Panel A) and septum (Panel B). The figure is color coded from red (early activation) to blue (late activation). Black circle represents the last ablated site recorded. The white star indicates the CESI imaged initiation. The dashed lines shows the ablated area estimated by the ablation sites represented by red circles.

septal side. Both of the activation sequences share a similar body surface ECG pattern as can be observed in the figure. However, the detailed propagation patterns differ from each other. In Panel A, activation initiated from the free wall

RVOT, traveled through the RV and terminated at the LV free wall. Initiating close to the septum, the activation traveled faster on the RV free wall than it did across the septum. Good concordance can be observed on the extracted endocardium together with good accuracy in localization. In Panel B, different from the previous case, the PVC beat originated at the septal RVOT, traveled through septum and the two ventricles, and dissolved at RV and LV respectively. Focal patterns surrounding the RVOT, as shown in the right column, are well captured and in good concordance with ablation outcomes while the differences in detailed activation patterns between the invasive and the non-invasive approaches are clearly depicted. By comparing the limb-lead ECG of the two examples, it can be observed that the ECG pattern of the majority of the beat is similar to each other but differences exist in the termination of the beat. The differences in the terminating period of the beat are captured by the imaging method. In the panel A, the activation terminated in the basal free wall, generating a propagation direction different from the bulk of the beat. Therefore, a small turning point can be found in the end of the limb lead QRS waveform. In contrast, the activation sequence in panel B, although terminated separately in two locations, has a general uniform propagation direction and consequently smoother waveform can be found in the limb lead ECG.

Figure 22 shows some imaging results of which invasive mapping and non-invasive imaging generated discrepant activation patterns (patient 7). The ectopic beats recorded in the EP lab had a correlation of greater than 0.95 to the arrhythmic activities isolated in the BSPMs. The invasive mapping approach

identified multiple early activation sites and suggested a non-focal pattern. Additional mapping sites were selected to remap the suspected early initiation

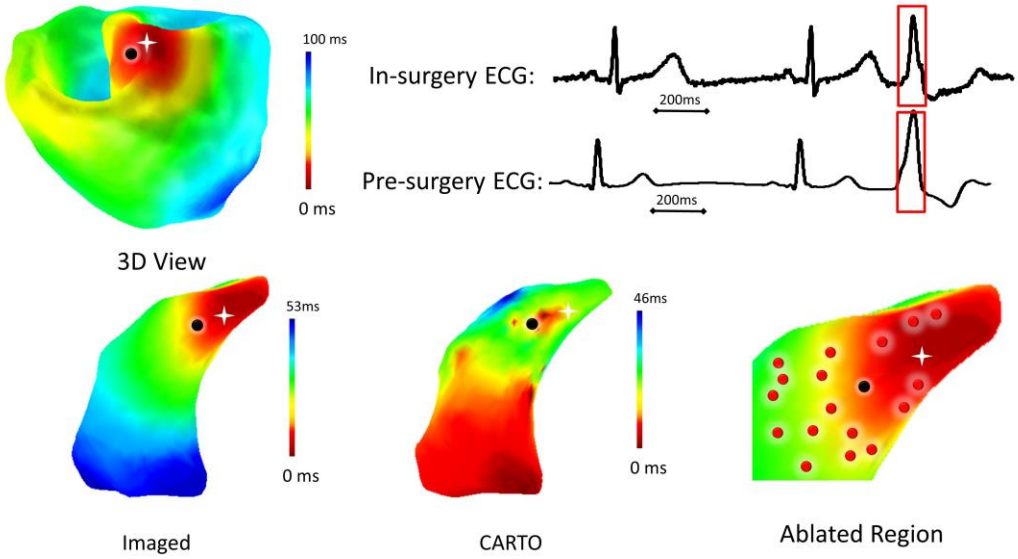

Figure 22: Imaging results from patient 7, whose imaged activation shows discrepancy with invasive mapping. Black circle represents the last successful ablation site recorded. The white star indicates the CESI initiation site. The dashed lines shows the ablated area estimated by the ablation sites represented by red circles.

area after the first round of mapping. It can be observed that due to the proliferated early activation pattern, a total of 45 ablation attempts were performed to eliminate the arrhythmic activity, resulting in a relatively larger injured area. Alternatively, the non-invasive imaging results indicated a better organized focal pattern initiated from the septal RVOT, sharing proper concordance with the procedural outcomes. The imaged initiation site of the ectopic beats was identified well within the injured area inflicted by multiple ablations.

Discussion

This study is the first clinical investigation to demonstrate the performance and the applicability of the 3D cardiac activation imaging approach in patients who underwent EP study with ablation. This is also the first time that 3D activation imaging techniques have advanced into clinical application. As a substantial extension from the previous numerical and animal studies, the 3D activation imaging technique was further evaluated in a realistic clinical environment regarding its potential to reveal critical knowledge about the arrhythmic activity to assist in catheter ablation directly. In general, the focal pattern of the PVC activation propagation is accurately captured non-invasively and the imaged initiation site also demonstrates the concordance to the ablation sites as well as the procedural outcomes. By comparing the intra-cardiac mapping results with the non-invasive imaging results on the endocardium, quantitative evaluation and validation was carried out on the non-invasive imaging technique as a potential clinical tool. On average, a CC of 0.8 and a RE of 0.19 were obtained in 12 out of 13 patients, indicating good accuracy of the imaging technique to directly visualize the arrhythmic activation pattern inside the heart. The imaged initiation sites were localized on average within 8 mm of the last successful ablation sites and within less than 3mm to the nearest ablation sites. The strong agreement between the imaged results and the ablative outcome demonstrates a promising potential for the technique to directly guide the ablation. The temporal resolution is also well preserved with a RRE of less than 2 percent in general. The significant statistical findings

indicate that the non-invasive imaging results are in strong concordance with the records from the EP study and the ablation outcomes. The excellent performance of 3D imaging technique revealed in the evaluation demonstrates that CESI is potentially able to provide a close match to invasive sequential mapping techniques not only on endocardium, but further throughout the myocardium three dimensionally on a beat-to-beat basis.

Rigorousness and clinically relevance have always been key factors in the validation of all non-invasive medical imaging technologies. The present study represents the first comprehensive clinical investigation using quantitative evaluation of a noninvasive activation imaging technique regarding both the concordance to the ablation outcome and the agreement with intra-cardiac mapping activation sequences directly. In this study a series of quantitative indices were used to assess the imaging accuracy and capability in clinical practices. With the two geometries - CT geometry and CARTO mapped geometry – co-registered together, the activation pattern on the endocardium could be compared directly and the results have shown that invasive and non-invasive counterparts are in agreement with each other in both global activation pattern and initiation sites, or suspected target of ablation. Although in some cases, discrepancies can be observed, it is important to note that the intra-cardiac mapping technique essentially has a limited resolution and has to be performed sequentially and in many situations needs manual registration in order to obtain a global activation map. The concordance observed in the comparisons between the imaged results and those from the invasive approach

indicates that CESI does have the potential to image the endocardium activation pattern accurately. For focal arrhythmias such as PVC or automatic VT, the success of the ablative procedure relies heavily on identifying the foci of the ectopic beats. LE, and NALE were defined and used to evaluate the CESI's capability to function in assisting the ablation practice. The results indicate that the imaged initiation lies on average within 8 mm from the last successful ablation sites, thus enabling the electrophysiologists to perform a quick and economical initial localization of the PVC foci before a full-fledged ablation procedure is conducted. Naturally the question may arise whether the reported LE of 8 mm is sufficiently precise to eliminate the arrhythmic activities solely based on non-invasive imaging results. However, by localizing the potential origin of arrhythmia within a sub-centimeter distance, the number of ablation attempts, the invasive mapping time and the damage inflicted due to the ablation can be significantly reduced. Despite the 8 mm distance between the imaged initiation sites and the last successful ablation sites, the imaged initiation sites are on average 2.7 mm away from the nearest ablation sites. Considering the registration error that may arise combining different modalities and the potentially varying conditions of the patients before and during the ablation procedure, the results indicate that the non-invasive CESI can provide an independent pre-procedural source of information for the ablation. Therefore, with the aid of the 3D imaging technique, the area to be mapped with invasive techniques and the ablation area can be further reduced while maintaining the high success rate of the ablative procedure.

Efforts have been made to visualize the cardiac electrical activities based on the body surface recordings (Yu, Zhou, and He 2015; Zhou et al. 2014; L. Wang et al. 2013; Han et al. 2013; Barr, Ramsey, and Spach 1977; Berger et al. 2006; Y. Wang et al. 2011; Skipa et al. 2002; Milanič et al. 2014; Brooks and MacLeod 1997; Okamoto, Teramachi, and Musha 1983; Rahimi et al. 2016). CESI employs a physical model in cardiac imaging and the construction of a distributed current density source model, which enable the technique to image electrical activities three dimensionally throughout the myocardium without relying on any presumed physiological knowledge and therefore intrinsically robust in various pathological conditions. By integrating the temporal dynamics into reconstruction, CESI with its temporal sparse reconstruction method can also suppress the spatiotemporal smoothing effect that traditional minimum norm based methods have suffered from. Instead of a smoothed activity distributed along the time course, CESI is able to reconstruct the current spike at the depolarization, enabling the method to image cardiac electrical activity at an improved spatiotemporal resolution. Besides, the 3D activation sequences generated by CESI are composed of the imaged depolarization instants throughout the myocardium. As a result, CESI has the potential to directly identify the activation pattern and the regions of interest such as ectopic foci or reentrant pathways regardless of their positions or depths inside the heart. Examples in figure 20 show that CESI, as a biventricular imaging technique, can identify the PVCs originating from either of the ventricles without preliminary knowledge of the arrhythmic origin. Results also indicate that CESI can identify

differences in the activation patterns when the body surface ECGs are similar. In Figure 21, both of the PVC beats are initiated in the RVOT but on opposite side of the outflow track: one near the RV free wall and the other near the septum. The BSPM and the limb lead ECG patterns are similar in both cases and the CARTO also identified a similar focal pattern with only slight differences in initiation locations. However, the non-invasive technique managed to discriminate not only the initiation sites, but also different propagation patterns closely related to the detailed structure of the heart. The capability in identification of the different propagation pathways based on similar ECG recordings demonstrated the capability of CESI to effectively integrate functional and structural information to image the arrhythmic mechanisms which play a major role in the treatment of more complicated arrhythmias.

Patient No	Gender	Age	PVC /24h	Myocardium Grid Points	Body Surface Grid Points
1	M	43	10,000	13,248	3,566
2	M	53	25,630	12,114	3,478
3	F	54	13,411	11,663	3,145
4	M	37	27,161	13,011	3,235
5	F	41	15,160	11,840	3,387
6	F	71	21,100	12,589	3,233
7	F	42	26,337	12,773	3,171
8	M	62	20,000	12,011	3,412
9	M	43	39,476	13,222	3,517
10	F	47	10,000	12,544	3,227
11	F	33	51,226	10,212	3,111
12	F	61	8,470	11,255	3,199
13	F	55	31,062	12,014	3,308
Mean±sd		49±11	23,002±12,528	12,192±853	3,307±149

Table 3: Summarized statistics on patients and the modeling details. The myocardium grid points show the number of the myocardial source points considered in the imaging process. The body surface grid points show the number of body surface nodal points considered in the boundary element torso forward modeling.

The robustness of an imaging modality is also crucial to its clinical performance. The imaging results from 13 patients in various age and gender are in good concordance with the procedural outcomes. For each individual, the imaged activation pattern remained stable among the ectopic beats randomly selected from the recording. The observations indicate that CESI is able to provide reliable imaging results in a realistic clinical setting and is robust against the disturbances common in the clinical environments such as movement artifact and the surrounding electronic interferences. The activation patterns from 12 of the 13 patients are also in agreement with the invasive mapping results. In the remaining case where discrepancies were found between the imaged and the intra-cardiac mapped activation patterns, the CESI imaging

results are still in excellent agreement with the procedural outcomes. Based on procedural outcomes and holter ECG, the arrhythmia was suspected to be initiated from the RVOT and had a focal pattern. The sequential mapping result multiple initiation sites were located in the RV, forming a widespread early activation area. The multi-initiation sites with spread-out early activation area observed in invasive mapping that can be explained by various factors, such as limited SNR, physical disturbances inside the ventricular chamber during the procedure or failure in the temporal co-registrations on multiple PVC beats. In contrast, a clear activation focus and the global activation propagation from the RVOT to the LV is clearly identified, which is in agreement with the previous Holter recordings. Given the similarities in body surface in-procedure and pre-procedure ECG and the fact that the imaged initiation lay in the relatively large ablated area, CESI's capability to function as a peri-procedural imaging tool to improve the efficiency and efficacy of ablative procedure can be demonstrated.

As can be observed in the results, CESI is able to non-invasively image the cardiac electrical activities on a beat-to-beat basis in a clinical setting. The focal mechanisms of the ventricular arrhythmias in the current patient populations are well captured in the imaged results. Although in this study, the ectopic beats were mainly isolated PVCs, the technique does not have intrinsic difficulties for imaging arrhythmias with continuous trains of ectopy such as sustainable or unsustainable VT trains, which are usually difficult to map in the EP lab. Much less demanding in medical expertise or effort to wait for or induce recurring arrhythmias to complete a sequential mapping, CESI can image the

ectopic beats in their natural state, relatively free from the possible perturbation in the EP lab. The simple setup and whole heart imaging capability also enables CESI to perform as a long term monitoring modality where detailed information on arrhythmic mechanisms, especially for patients who have a changing dynamic, can be gathered to provide additional information for treatment or diagnosis purposes in various arrhythmia activities.

Previously, the CESI method has been validated via computer simulation and animal studies with simultaneous recording by 3D transmural electrodes. However, for clinical studies, the highly invasive approaches are not applicable in patients. Activation sequences and ablation sites on the endocardium mapped by invasive EP study can be utilized to assess the capability and performance of the method in a clinical environment. The present results have shown that CESI possess the potential to function as a pre-procedural assessment and ablation planning tool with its full overage and simple setup. Moreover, it can be a promising further investigation to evaluate the performance of the CESI technique as an imaging modality function in the EP lab in real time to the ablative procedures.

Patient No	CC	RE	LE (mm)	NALE (mm)	RTS
1	0.78	0.16	8.1	2.7	0.01
2	0.8	0.17	7.5	4.5	0.02
3	0.78	0.21	7.3	1	0.03
4	0.81	0.2	9.2	1.3	0.01
5	0.82	0.18	7.7	4	0
6	0.81	0.16	8.6	4.2	0.03
7	N/A	N/A	6.2	1.7	N/A
8	0.75	0.23	6.6	4.1	0.02
9	0.8	0.18	7.1	4.5	0.01
10	0.81	0.16	8.2	2	0
11	0.77	0.19	9	1.9	0.01
12	0.77	0.22	9.2	3.5	0.02
13	0.78	0.23	8.5	1.5	0.01
Mean±sd	0.79±0.02	0.19±0.03	7.9±0.9	2.8±1.3	0.014±0.01

Table 4: Statistics summarized between CARTO mapped and imaged activation sequence on the CARTO mapped endocardium.

The present study in the chapter investigates for the first time the clinical performance of the noninvasive three dimensional cardiac electrical activation imaging method on a population of 13 patient undergoing catheter ablation with ventricular arrhythmias. Quantitative comparison has been made to the EP study results, ablation sites and ablation outcomes in all patients. Our results show that the non-invasive CESI imaging results have excellent concordance with the invasive mapping results and the ablation outcomes and the technique strongly promises to serve as a clinically capable tool to provide crucial arrhythmia information assisting the ablative procedure noninvasively and highly accurately.

5.2 In-procedure simultaneous mapping study in patients with ventricular arrhythmia

The clinical study protocol in the study was approved by the Institutional Review Board of University of Minnesota and University of Alabama at Birmingham. Intra-cardiac mapping was performed with CARTO invasive mapping system during EP study session following by ablations. Up to 208 body surface ECG electrodes (ActiveTwo system, BioSemi V.O.F., Armsterdam, the Netherlands.) were placed on both the chest and the back of the patients prior to the invasive catheter insertion and kept recording during the EP study. Structural imaging such as CT and MRI for both animal and patients were acquired before the ECG simultaneous mapping study. Body surface mapping were performed within one week to the EP study with ablation. Up to 208 electrodes arranged in strips (ActiveTwo system, BioSemi V.O.F., Amsterdam, the Netherlands.) were evenly distributed to cover the patient's chest and back. Locations of the electrodes and the anatomical landmarks were digitized using an electromagnetic digitizer (Fastrak, Polhemus Inc, Colchester, VT, USA). BSPMs were recorded using 2 kHz sampling rate and a 24 bits analog to digital converter. Thoracic (0.78x0.78x5 mm) and ECG gated (70% R-R interval) contrast-enhanced cardiac (0.39x0.39x0.75 mm) axial CT imaging were performed on all patients preceding the ablative procedure within a week of the mapping study.

The EP study with ablation was conducted using a contact endocardial mapping system (CARTO3 system, Biosense Webster, Diamond Bar, CA, USA). Local activation time (LAT) maps on the endocardium were mapped through the sequential mapping of various sites across the entire or partial endocardium surrounding the suspected foci. Ablation was performed on the suspected foci of the arrhythmic activity

until all ectopies were eliminated. All patients were arrhythmia free after the procedure and were discharged within one week.

Data analysis

The detailed methodology employed by CESI has been described previously in detail(Yu, Zhou, and He 2015). In brief, detailed and individualized geometry on heart, lung and torso of the experimental animal was extracted from the structural images (CT, MRI) assisted by CURRY 6.0 (Compumedics, Charlotte, NC). The extracted ventricular myocardium was tessellated into around 10,000 source grid points. Based on the bidomain theory, Boundary Element Model (BEM) was constructed for each canine including torso, lung, myocardium and blood mass(Jamison et al. 2011; Miller and Geselowitz 1978). By coupling the functional information from ECG recordings and the structural information from CT or MRI, CESI reconstructed the ventricular activation sequence throughout the myocardium in 3D. Exploiting the temporal dynamic the cellular electrophysiology at the depolarization, the temporal sparse promoting imaging technique reconstructs the current density spike generated at the instant of the cardiac activation directly. The technique has been demonstrated to be able to achieve improved imaging accuracy and robustness against various disturbances.

The imaging results were then compared with intra-cardiac activation sequences. Numerical data was presented in mean ± SD format. Correlation Coefficient (CC), Relative Error (RE), and Relative Resolution Error (RRE) were defined and computed to quantitatively evaluate the performance of the technique. CC, RE and RRE are defined to assess and quantify the concordance and discrepancy between the invasively mapped and non-invasively imaged activation patterns on the endocardium, defined as:

$$CC = \frac{\sum_i (AT_i - \overline{AT}) \bullet (MT_i - \overline{MT})}{\sqrt{\sum_i (AT_i - \overline{AT})^2} \bullet \sqrt{\sum_i (MT_i - \overline{MT})^2}} \quad (1)$$

$$RE = \sqrt{\frac{\sum_i (AT_i - MT_i)^2}{\sum_i MT^2}} \quad (2)$$

where AT_i and MT_i represent the imaged and measured activation times at the ith grid point while $\overline{AT}$ and $\overline{MT}$ represent their average on all grid points. RRE is employed to measure the loss temporal resolution, and is defined as:

$$RRE = \frac{|T_M - T_I|}{T_{total}} \quad (3)$$

where T_M represents the total activation time of measured activation, T_I represents the total activation time of the imaged activation sequence on the co-registered area and T_{total} represents the total activation time from the body surface ECG.

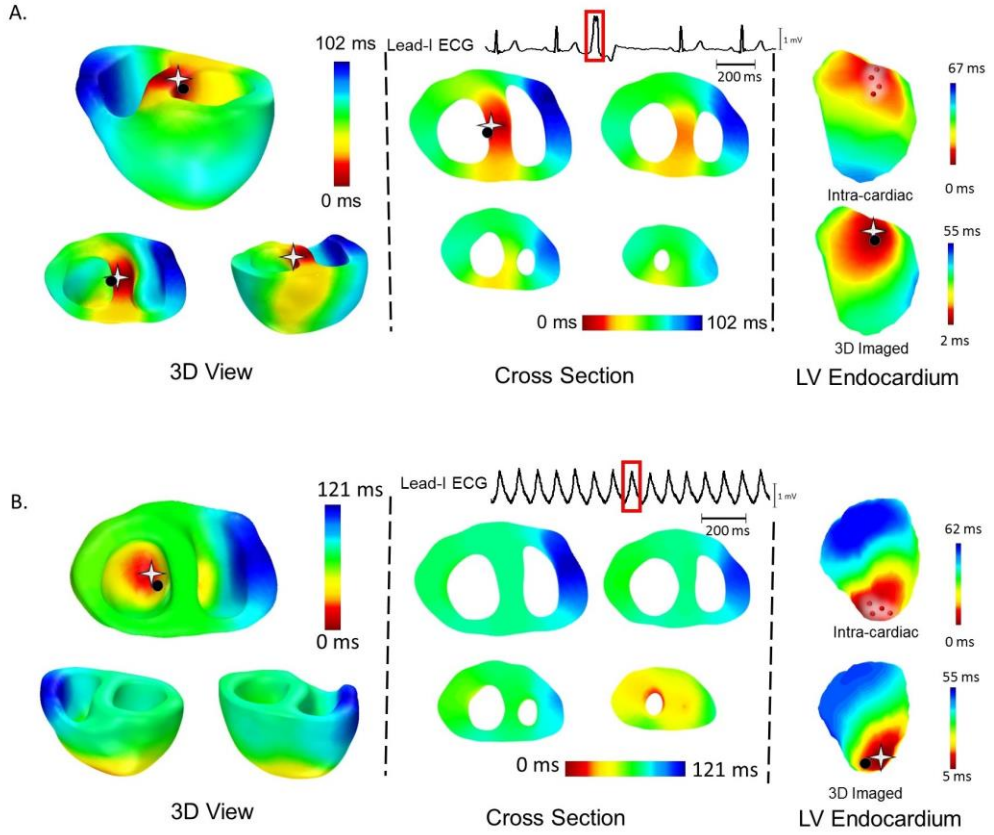

Figure 23: clinical results from in-procedure simultaneous study of ventricular arrhythmias. The activation sequence is color coded from red to blue. The imaged initiation of the ectopic beat is marked with white star. The last ablation site is marked with black dot. The red dot represents the other ablation sites performed during the ablation.

The capability of CESI to localize key area of interest for ablation was also evaluated in a quantitative manner. Localization Error (LE) is defined as the distance between potential ablation targets indicated by imaged results and the intra-cardiac recordings. For automatic VTs, the LE is simply defined as the distance between the imaged and the measured initiation site for each ectopic activation, a well understood and widely practiced target of ablation.

Results

Activation imaging of VT, PVC and pace mapping in patients with ventricular arrhythmias

Some examples are shown in figure 23 on the imaging results of ventricular activation during EP study with ablation. The 3D view of the ventricular myocardium is shown in the left column and the corresponding cross sections are shown in the middle. The activation sequence was color coded from red (early) to blue (late). The imaged initiation site of the ectopic beat is marked with white star while the last ablation site is marked with black sphere. In the right column, CARTO intra-cardiac local activation map is compared with the imaged activation sequence projected on the same endocardial surface. As can be seen from the figure, the focal pattern of the premature ventricular complex and the ventricular tachycardia was clearly depicted with good accuracy compared to the sequential mapping results. The imaged initiation site strongly co-localized with the ablations. Both the arrhythmic beats originated on endocardial surface deep inside the myocardium but the method identified the initiation foci and the propagation pattern in 3D successfully.

Discussion

Efforts have been undertaken to directly visualize the cardiac electrical activity from body surface ECG from various perspectives(Erem et al. 2014; Oster and Rudy 1992; Vijayakumar et al. 2014; Y. Wang et al. 2011; Bin He, Li, and Zhang 2003; Ghosh et al. 2008; Milanič et al. 2014; Brooks and MacLeod 1997; Nash, Bradley, and Paterson 2003; Pullan et al. 2001; Ohyu, Okamoto, and Kuriki 2002). CESI technique offers an alternative approach to directly visualize the whole heart electrical activity in 3D on a beat-to-beat basis. This feature indicates that the technique can potentially become a unique tool to

direct information on the location and depth of the arhythmogenesis not only in the hemodynamically stable rhythms, but the highly dynamic activities such as the PVT beats, a commonly encountering challenge that the sequential mapping procedures are likely to fail. Moreover, the non-invasive nature of the imaging modality promises relatively low cost and dexterity to adapt for both pre-procedural (diagnostic) and in-procedural (ablation guiding) scenarios, allowing CESI to provide the physicians with helpful information to improve and accelerate the currently ablative procedure while co-existing with current standard protocol. On the technical aspects, the temporal sparse formulation employed in CESI, in contrast to the minimum norm based approaches, counters the ill-posedness, a central challenge of the ECG inverse problem(Okamoto, Teramachi, and Musha 1983), with both mathematical constraints to strengthen uniqueness and electrophysiological knowledge to avoid distortion. This reconstruction strategy avoids the complicated electrophysiological model with its robust biophysics based model while, at the same time, considers the momentary cellular electrophysiological behavior at the activation in the process of imaging. Rather than estimating the activation time based on a continuous inversely computed ECG waveform, CESI directly reconstructs the current density spike generated at the depolarization. It is the preservation of the electrophysiology in reconstruction that permits the temporal resolution to be properly maintained as well as the improved accuracy and robustness.

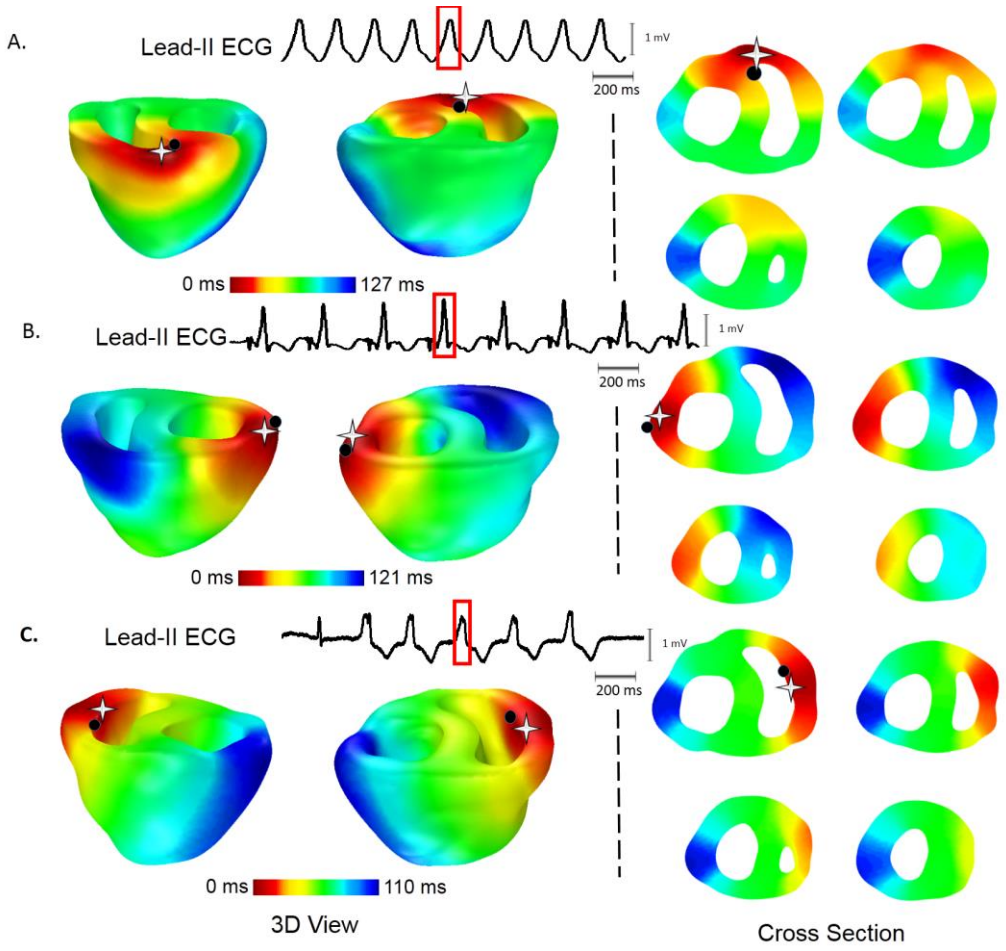

Figure 24: examples of catheter pacing mapping in patients with ventricular arrhythmias. The pacing site is marked using black dot while the imaged initiation site is represented by white star.

For a medical imaging modality, rigorous validation in clinical relevant systems has been proved to be vital to further and wider application of the imaging method. In the study, quantitative validation was performed upon a wide spectrum of scenarios from in-procedural clinical study to invasive animal study with sophisticated pathologies such as heart failure and myocardial infarction. The in-procedural simultaneous mapping study represents, to our knowledge, the most sophisticated clinical validation available where the intra-

cardiac electricity can be directly compared to the imaged results from patient with ventricular arrhythmias. The results have demonstrated that the imaged activation can resemble what was found out later by sequential mapping of the whole ventricle on a beat-to-beat basis. The robustness of the imaging results also indicate that the method can maintain its performance even in the most complicated electronic interferences and that the method is fully compatible with the standing clinical systems, promising and highly applicable for wider clinical application. The animal invasive validation study also represents a most rigorous approach to validate the imaged activation using direct and simultaneous measurements three dimensionally. The closed chest condition with both intra-cardiac and body surface electrodes enabled a thorough and accurate validation of the recently proposed non-invasive imaging technique. The present validation study is founded on a protocol refined from the previous well established validation mapping studies and animal model in a procedure where the rigorousness has been well demonstrated. All the activation sequences were collected through in vivo study where the condition and vitals of the animal were closely monitored and the pathology was induced with caution and tightly controlled. Compared to the rabbit heart used previously, the canine heart model is better comparable to human hearts in both its electrical conduction and in its size. Also, due to their size, the experiment conditions with canines better resemble those found clinically. One can observed a comparable, but slightly deteriorated performance compared to the previous numerical and rabbit pacing study. The experimental setup employed in the

study involves highly complicated disturbances such as interferences from other monitoring electronics and movement artifact that are as severe, if not more, than the realistic clinical setup. In addition, the sternotomy and close chest procedure employed in the study to achieve three dimensional direct measurements may induce unknown modeling error which will mostly likely to absent clinical applications. Therefore, our finding based on the results in the study indicates that the technique possesses a strong potential to image the activation sequence in the patents as a clinically feasible tool for diagnosis and guiding the ablative procedure.

5.3 Depth identification of automatic arrhythmias using Deep-Learning Neural Network

Cardiac ablation has become one of the routine measure against the automatic ventricular arrhythmias. Due to limited penetration of the RF ablation procedure, the depth of the origin of the ectopic activation proved to be crucial for the success of the procedure and misestimating the arrhythmic depth may potentially lead to the failure of the procedure. However, in contrast to other critical information such as rhythm and global morphology, the hints on the depth of the arrhythmic origin has proven to be more challenging due to the general similarities of the epi – endo initiations in ECG waveforms.Efforts has been done in determining the depths of the arrhythmic foci. By reading ECG waveform directly, a rough estimation can be made by assessing the morphologies of early phase of QRS segment. Yet it is a valid and commonly adapted practice, the accuracy of the approach is clouded by limited information

a 12 – lead standard ECG can provide and the complexity the condition may be due to different localization of the arrhythmic foci. 3D cardiac electrical imaging techniques have also had some success but the accuracy is still limited.

In the previous sections, localization of the arrhythmic foci using 3D cardiac imaging technique has been investigated in clinical setup. In this section of the chapter, a deep learning based coevolution neural network depth estimator is developed for the first time as a supporting algorithm to identify the origin depth of the focal arrhythmias. The developed method is evaluated in both numerical and clinical studies.

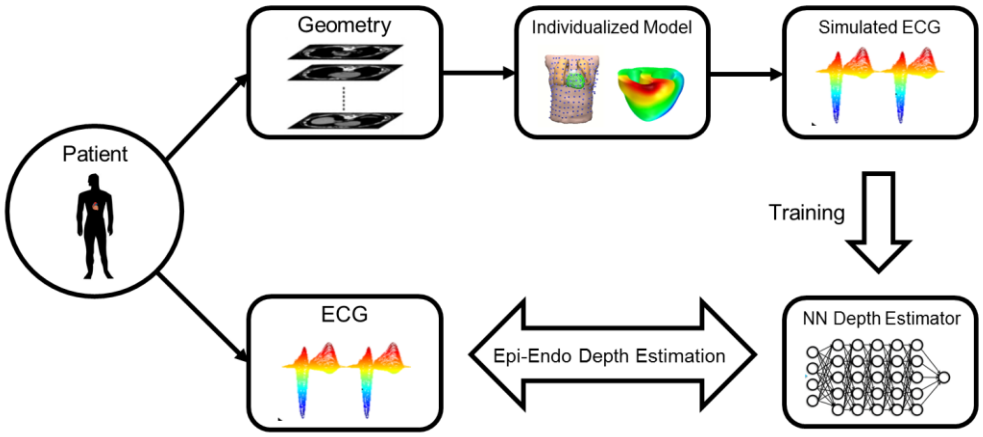

Figure 25: schematic paradigm of deep learning neural network based arrhythmic depth estimation.

The brief schematic paradigm is presented in figure 25. Body surface ECG and images from structural imaging modalities were collected in the same protocol as in section 5.3. Based on the realistic geometry collected from each patient, realistic automaton based heart-torso model was built. The physiological automaton based model can generate activation sequence for

ectopies from different locations. The BSPM generated based on patient geometry was used to train the deep learning based neural network depth estimator. A total of 40000 ectopic beats were initiated from 4000 different epicardial and endocardial sites, covering both LV and RV. Training was assumed to be completed when the depth estimator achieved 95% accuracy in identifying whether an arrhythmia beat is initiated from epicardium or endocardium in a separate simulated date set consisting of 10000 beats from 1000 sites different from those used in training. Other than epi vs endo identification, depth estimation was also performed, defined by the relative ratio of the epi and endo decision weights.

A total of 3 patients are included in the clinical study to evaluate the deep learning based depth estimator. A total of 120 ectopic beats (30 LV pacing, 50 RV pacing and 40 PVCs) were isolated from the BSPM, including pacing and spontaneous PVC beats.

The results is summarized in the figure. In general the accuracy of endo-epi identification in patients with ventricular arrhythmia undergoing cardiac catheter ablation is above 0.9 in general for pacing and PVC cases. The results from the clinical study and the numerical study show comparable accuracy in general.

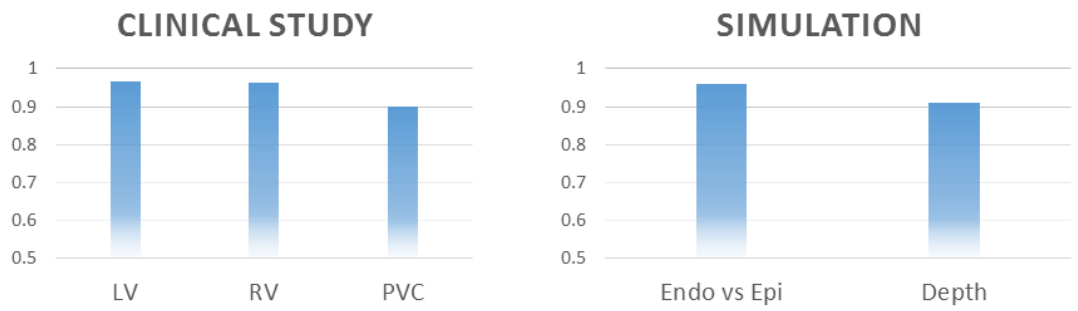

Figure 26: summarized statistics of the clinical study and simulations of depth estimation.

This is the first time a specialized deep learning based neural network estimator is developed and applied to patients with ventricular arrhythmia. The results has demonstrated promising capability of the developed estimator to function as a supplementary part to 3D cardiac electrical imaging technique to further improve the accuracy in the localization of arrhythmias in patients.

Chapter 6 Conclusion and Future Work

6.1 Conclusions

Noninvasive imaging and estimation of cardiac electrical activity can play a vital role in further expanding the efficacy and efficiency of the clinical management of cardiovascular disease such as cardiac arrhythmias and cardiac infarctions. In this dissertation, a line of investigations on the noninvasive imaging techniques are presented covering both methodological designs of the imaging problem and thorough validations and evaluations of the developed imaging techniques in numerical, animal and clinical studies against various realistic challenges.

In the dissertation, spatiotemporal dynamic of the cardiac electrophysiology is for the first time incorporated into reconstruction through spatiotemporal sparse formulation. The further developed imaging formulation improved the spatiotemporal resolution of the imaged activation, allowing the imaging technique to pinpoint the exact activation time along the time course of the arrhythmias. The improved spatiotemporal resolution promises to reveal more detailed information on the arrhythmias that is critical to the success of the clinical management of the cardiac arrhythmias.

The numerical validation studies provided a rigorous evaluation of the developed imaging technique by simulating a broad spectrum of error and disturbances such as various sensor noise and modeling error. The technique has demonstrated improved performance- accuracy, robustness and resolution – in the simulations in imaging cardiac activation throughout the myocardium. Rigorous numerical investigation shown in the dissertation lay a strong foundation on which the further animal and clinical validation will be carried out.

The dissertation also presents a first and a most throughout animal validation studies covering both automatic arrhythmias and the reentrant arrhythmias on animal models with various pathologies such as heart failure and myocardial infarction. By employing the 3D intra-cardiac mapping technology, the imaging results were directly compared with the intra-cardiac real time recorded cardiac electricity and good concordance has been found in various mechanisms such as PVC, MVT, PVT and reentry. The imaging technique has demonstrated the capability to imaging the 3D activation

sequence throughout the myocardium with high accuracy and strong robustness and identify the key clinical targets such as arrhythmia foci and reentrant pathway accurately. Validated rigorously in the animal models, the technique has demonstrated its potential in assisting clinical practice and help elucidate the mechanisms of cardiac arrhythmias.

The dissertation took further steps in evaluating the performance of the developed imaging techniques in clinical setup. For the first time, the 3D electrical imaging technique is applied to patients with ventricular arrhythmias against the fast rhythms such as VTs where the standard contact mapping technique found challenging. With clinical experiment on both pre-procedure imaging and in-procedural simultaneous mapping, the clinical performance of the imaging modality is thoroughly evaluated and the results have demonstrated that the developed imaging technique is capable of imaging the activation sequence of the cardiac arrhythmias in full-fledged clinical environments and provide important information to assist both diagnostic management and potentially in-procedural ablation mapping of cardiac arrhythmias.

In sum, in this dissertation study, a novel spatiotemporal cardiac electrical imaging technique is developed and evaluated in a series of numerical, animal and clinical studies. This is the first time and to our knowledge on an unpreceded level of thoroughness and rigorousness a 3D cardiac electrical imaging method is evaluated. The results covering a wide spectrum of clinically challenging scenarios has shown that the novel imaging technique promises to accurately image the electricity inside the myocardium and provide important information

in both clinical management and mechanism understanding of cardiac arrhythmia.

6.2 Future Work

The present study provide a solid insight into both the technicality and the application capability of the 3D cardiac electrical imaging technique. Yet, further exploration can be made in the future to purse the next generation techniques.

1. Unify spatiotemporal based methodology and frequency/transoform (Fourier, wavelet, etc) based techniques to accommodate complicated cardiac electrical conditions.
2. Expand the imaging substrate from ventricle to the whole myocardium to incorporate whole heart conduction system into reconstruction.
3. Effectively integrate prior knowledge from other imaging modalities such as DE-MRI and PET/SPECT to adapt the imaging technique to more complicate physiological conditions such as heart failure and myocardial infarction.
4. Further explore the direct clinical applications where imaging can contribute significant information such as ICD and CRT.

References:

Armoundas, Antonis A., Andrew B. Feldman, Ramakrishna Mukkamala, and Richard J. Cohen. 2003. “A Single Equivalent Moving Dipole Model: An Efficient Approach for Localizing Sites of Origin of Ventricular Electrical Activation.” *Annals of Biomedical Engineering* 31 (5): 564–76. doi:10.1114/1.1567281.

B, He, and Cohen Rj. 1994. “Body Surface Laplacian Electrocardiographic Mapping--a Review.” *Critical Reviews in Biomedical Engineering* 23 (5–6): 475–510.

Barr, R. C., and M. S. Spach. 1978. “Inverse Calculation of QRS-T Epicardial Potentials from Body Surface Potential Distributions for Normal and Ectopic Beats in the Intact Dog.” *Circulation Research* 42 (5): 661–75. doi:10.1161/01.RES.42.5.661.

Barr, R.C., Maynard Ramsey, and Madison S. Spach. 1977. “Relating Epicardial to Body Surface Potential Distributions by Means of Transfer Coefficients Based on Geometry Measurements.” *IEEE Transactions on Biomedical Engineering* BME-24 (1): 1–11. doi:10.1109/TBME.1977.326201.

Ben-Haim, Shlomo A., Daniel Osadchy, Israel Scnuster, Lior Gepstein, Gal Hayam, and Mark E. Josephson. 1996. “Nonfluoroscopic, in Vivo Navigation and Mapping Technology.” *Nature Medicine* 2 (12): 1393–95. doi:10.1038/nm1296-1393.

Berger, Thomas, Gerald Fischer, Bernhard Pfeifer, Robert Modre, Friedrich Hanser, Thomas Trieb, Franz X. Roithinger, et al. 2006. “Single-Beat Noninvasive Imaging of Cardiac Electrophysiology of Ventricular Pre-Excitation.” *Journal of the American College of Cardiology* 48 (10): 2045–52. doi:10.1016/j.jacc.2006.08.019.

Brooks, D.H., and Robert S. MacLeod. 1997. “Electrical Imaging of the Heart.” *IEEE Signal Processing Magazine* 14 (1): 24–42. doi:10.1109/79.560322.

Cotter, S.F., B.D. Rao, K. Engan, and K. Kreutz-Delgado. 2005. “Sparse Solutions to Linear Inverse Problems with Multiple Measurement Vectors.” *IEEE Transactions on Signal Processing* 53 (7): 2477–88. doi:10.1109/TSP.2005.849172.

Ding, Lei, Ying Ni, John Sweeney, and Bin He. 2011. “Sparse Cortical Current Density Imaging in Motor Potentials Induced by Finger Movement.” *Journal of Neural Engineering* 8 (3): 36008.

el-Sherif, N., W. B. Gough, R. H. Zeiler, and R. Hariman. 1985. “Reentrant Ventricular Arrhythmias in the Late Myocardial Infarction Period. 12. Spontaneous versus Induced Reentry and Intramural versus Epicardial Circuits.” *Journal of the American College of Cardiology* 6 (1): 124–32.

Erem, B., J. Coll-Font, R. Martinez Orellana, P. St’ovicek, and D.H. Brooks. 2014. “Using Transmural Regularization and Dynamic Modeling for Noninvasive Cardiac Potential Imaging of Endocardial Pacing With Imprecise Thoracic Geometry.” *IEEE Transactions on Medical Imaging* 33 (3): 726–38. doi:10.1109/TMI.2013.2295220.

Ghosh, Subham, Edward K. Rhee, Jennifer N. Avari, Pamela K. Woodard, and Yoram Rudy. 2008. “Cardiac Memory in Patients With Wolff-Parkinson-White Syndrome Noninvasive Imaging of Activation and Repolarization Before and After Catheter Ablation.” *Circulation* 118 (9): 907–15. doi:10.1161/CIRCULATIONAHA.108.781658.

Go, Alan S., Dariush Mozaffarian, Véronique L. Roger, Emelia J. Benjamin, Jarett D. Berry, Michael J. Blaha, Shifan Dai, et al. 2014. “Heart Disease and Stroke Statistics--2014 Update: A Report from the American Heart Association.” *Circulation* 129 (3): e28–292. doi:10.1161/01.cir.0000441139.02102.80.

Grant, Michael, Stephen Boyd, and Y. Ye. 2012. “CVX: Matlab Software for Disciplined Convex Programming, Version 2.0 Beta.” *Recent Advances in Learning and Control${}$*, 95–110.

Grant, Michael C., and Stephen P. Boyd. 2008. “Graph Implementations for Nonsmooth Convex Programs.” In *Recent Advances in Learning and Control*, edited by Vincent D. Blondel, Stephen P. Boyd, and Hidenori Kimura, 95–110. Lecture Notes in Control and Information Sciences 371. Springer London. http://link.springer.com/chapter/10.1007/978-1-84800-155-8_7.

Greensite, Fred. 2003. “The Temporal Prior in Bioelectromagnetic Source Imaging Problems.” *IEEE Transactions on Biomedical Engineering* 50 (10): 1152–59. doi:10.1109/TBME.2003.817632.

———. 2005. “Heart Surface Electrocardiographic Inverse Solutions.” In *Modeling and Imaging of Bioelectrical Activity*, edited by Bin He, 119–60. Bioelectric Engineering. Springer US. http://link.springer.com/chapter/10.1007/978-0-387-49963-5_4.

Greensite, Fred, and G. Huiskamp. 1998. “An Improved Method for Estimating Epicardial Potentials from the Body Surface.” *IEEE Transactions on Biomedical Engineering* 45 (1): 98–104. doi:10.1109/10.650360.

Gulrajani, Ramesh M., Fernand A. Roberge, and Pierre Savard. 1984. “Moving Dipole Inverse ECG and EEG Solutions.” *IEEE Transactions on Biomedical Engineering* BME-31 (12): 903–10. doi:10.1109/TBME.1984.325257.

Han, Chengzong, Zhongming Liu, Xin Zhang, S. Pogwizd, and Bin He. 2008. “Noninvasive Three-Dimensional Cardiac Activation Imaging From Body Surface Potential Maps: A Computational and Experimental Study on a Rabbit Model.” *IEEE Transactions on Medical Imaging* 27 (11): 1622–30. doi:10.1109/TMI.2008.929094.

Han, Chengzong, Steven M. Pogwizd, Cheryl R. Killingsworth, and Bin He. 2011. “Noninvasive Imaging of Three-Dimensional Cardiac Activation Sequence during Pacing and Ventricular Tachycardia.” *Heart Rhythm* 8 (8): 1266–72. doi:10.1016/j.hrthm.2011.03.014.

———. 2012. “Noninvasive Reconstruction of the Three-Dimensional Ventricular Activation Sequence during Pacing and Ventricular Tachycardia in the Canine Heart.” *American Journal of Physiology - Heart and Circulatory Physiology* 302 (1): H244–52. doi:10.1152/ajpheart.00618.2011.

Han, Chengzong, Steven M. Pogwizd, Cheryl R. Killingsworth, Zhaoye Zhou, and Bin He. 2013. “Noninvasive Cardiac Activation Imaging of Ventricular Arrhythmias during Drug-Induced QT Prolongation in the Rabbit Heart.” *Heart Rhythm* 10 (10): 1509–15. doi:10.1016/j.hrthm.2013.06.010.

Han, Chengzong, Steven M. Pogwizd, Long Yu, Zhaoye Zhou, Cheryl R. Killingsworth, and Bin He. 2015. “Imaging Cardiac Activation Sequence during Ventricular Tachycardia in a Canine Model of Nonischemic Heart Failure.” *American Journal of Physiology. Heart and Circulatory Physiology* 308 (2): H108-114. doi:10.1152/ajpheart.00196.2014.

Hansen, Per Christian. 1992. “Analysis of Discrete Ill-Posed Problems by Means of the L-Curve.” *SIAM Review* 34 (4): 561–580.

He, B., and G. Li. 2002. “Noninvasive Three-Dimensional Myocardial Activation Time Imaging by Means of a Heart-Excitation-Model.” *Int. J. of Bioelectromagnetism* 4 (2): 87–88.

He, Bin, Guanglin Li, and Xin Zhang. 2002. “Noninvasive Three-Dimensional Activation Time Imaging of Ventricular Excitation by Means of a Heart-Excitation Model.” *Physics in Medicine and Biology* 47 (22): 4063–78.

———. 2003. “Noninvasive Imaging of Cardiac Transmembrane Potentials within Three-Dimensional Myocardium by Means of a Realistic Geometry Anisotropic Heart Model.” *IEEE Transactions on Biomedical Engineering* 50 (10): 1190–1202. doi:10.1109/TBME.2003.817637.

He, Bin, and Dongsheng Wu. 2001. “Imaging and Visualization of 3-D Cardiac Electric Activity.” *IEEE Transactions on Information Technology in Biomedicine* 5 (3): 181–86. doi:10.1109/4233.945288.

Jamison, C., C. Navarro, C. Turner, J. Shannon, J. Anderson, and Jennifer Adgey. 2011. “The Inverse Problem Utilizing the Boundary Element Method for a Nonstandard Female Torso.” *IEEE Transactions on Biomedical Engineering* 58 (4): 876–83. doi:10.1109/TBME.2010.2093525.

Li, Guanglin, and B. He. 2001. “Localization of the Site of Origin of Cardiac Activation by Means of a Heart-Model-Based Electrocardiographic Imaging Approach.” *IEEE Transactions on Biomedical Engineering* 48 (6): 660–69. doi:10.1109/10.923784.

Liebman, J., J. A. Zeno, B. Olshansky, A. S. Geha, C. W. Thomas, Y. Rudy, R. W. Henthorn, M. Cohen, and A. L. Waldo. 1991. “Electrocardiographic Body Surface Potential Mapping in the Wolff-Parkinson-White Syndrome. Noninvasive Determination of the Ventricular Insertion Sites of Accessory Atrioventricular Connections.” *Circulation* 83 (3): 886–901. doi:10.1161/01.CIR.83.3.886.

Liu, Chenguang, M.D. Eggen, C.M. Swingen, P.A. Iaizzo, and Bin He. 2012. “Noninvasive Mapping of Transmural Potentials During Activation in Swine Hearts From Body Surface Electrocardiograms.” *IEEE Transactions on Medical Imaging* 31 (9): 1777–85. doi:10.1109/TMI.2012.2202914.

Liu, Chenguang, and Bin He. 2011. “Noninvasive Estimation of Global Activation Sequence Using the Extended Kalman Filter.” *IEEE Transactions on Biomedical Engineering* 58 (3): 541–49. doi:10.1109/TBME.2010.2066564.

Liu, Chenguang, Nicholas D. Skadsberg, Sarah E. Ahlberg, Cory M. Swingen, Paul A. Iaizzo, and Bin He. 2008. “Estimation of Global Ventricular Activation Sequences by Noninvasive 3-Dimensional Electrical Imaging: Validation Studies in a Swine Model during Pacing.” *Journal of Cardiovascular Electrophysiology* 19 (5): 535–40. doi:10.1111/j.1540-8167.2007.01066.x.

Liu, Chenguang, Xin Zhang, Zhongming Liu, S.M. Pogwizd, and Bin He. 2006. “Three-Dimensional Myocardial Activation Imaging in a Rabbit Model.” *IEEE Transactions on Biomedical Engineering* 53 (9): 1813–20. doi:10.1109/TBME.2006.873701.

Liu, Zhongming, Chenguang Liu, and Bin He. 2006. “Noninvasive Reconstruction of Three-Dimensional Ventricular Activation Sequence from the Inverse Solution of Distributed Equivalent Current Density.” *IEEE Transactions on Medical Imaging* 25 (10): 1307–18. doi:10.1109/TMI.2006.882140.

Malmivuo, Jaakko, and Robert Plonsey. 1995. *Bioelectromagnetism: Principles and Applications of Bioelectric and Biomagnetic Fields*. Oxford University Press.

Messnarz, B., B. Tilg, R. Modre, G. Fischer, and F. Hanser. 2004. “A New Spatiotemporal Regularization Approach for Reconstruction of Cardiac Transmembrane Potential Patterns.” *IEEE Transactions on Biomedical Engineering* 51 (2): 273–81. doi:10.1109/TBME.2003.820394.

Milanič, Matija, Vojko Jazbinšek, Robert S. MacLeod, Dana H. Brooks, and Rok Hren. 2014. “Assessment of Regularization Techniques for Electrocardiographic Imaging.” *Journal of Electrocardiology* 47 (1): 20–28. doi:10.1016/j.jelectrocard.2013.10.004.

Miller, W. T., and D. B. Geselowitz. 1978. “Simulation Studies of the Electrocardiogram. I. The Normal Heart.” *Circulation Research* 43 (2): 301–15. doi:10.1161/01.RES.43.2.301.

Modre, R., B. Tilg, G. Fischer, and P. Wach. 2002. “Noninvasive Myocardial Activation Time Imaging: A Novel Inverse Algorithm Applied to Clinical ECG Mapping Data.” *IEEE Transactions on Biomedical Engineering* 49 (10): 1153–61. doi:10.1109/TBME.2002.803519.

Mozaffarian, Dariush, Emelia J. Benjamin, Alan S. Go, Donna K. Arnett, Michael J. Blaha, Mary Cushman, Sarah de Ferranti, et al. 2015. “Heart Disease and Stroke Statistics—2015 Update A Report From the American Heart Association.” *Circulation* 131 (4): e29–322. doi:10.1161/CIR.0000000000000152.

Nademanee, Koonlawee, and Erol M. Kosar. 1998. “A Nonfluoroscopic Catheter-Based Mapping Technique to Ablate Focal Ventricular Tachycardia.” *Pacing and Clinical Electrophysiology* 21 (7): 1442–47. doi:10.1111/j.1540-8159.1998.tb00216.x.

Nademanee, Koonlawee, Gumpanart Veerakul, Pakorn Chandanamattha, Lertlak Chaothawee, Aekarach Ariyachaipanich, Kriengkrai Jirasirirojanakorn, Khanchit Likittanasombat, Kiertijai Bhuripanyo, and Tachapong Ngarmukos. 2011. “Prevention of Ventricular Fibrillation Episodes in Brugada Syndrome by Catheter Ablation Over the Anterior Right Ventricular Outflow Tract Epicardium.” *Circulation* 123 (12): 1270–79. doi:10.1161/CIRCULATIONAHA.110.972612.

Nash, Martyn P., Chris P. Bradley, and David J. Paterson. 2003. “Imaging Electrocardiographic Dispersion of Depolarization and Repolarization During Ischemia Simultaneous Body Surface and Epicardial Mapping.” *Circulation* 107 (17): 2257–63. doi:10.1161/01.CIR.0000065602.78328.B5.

Nebel, Katharina, Philipp Stude, Holger Wiese, Bernhard Müller, Armin de Greiff, Michael Forsting, Hans-Christoph Diener, and Matthias Keidel. 2005. “Sparse Imaging and Continuous Event-Related fMRI in the Visual Domain: A Systematic Comparison.” *Human Brain Mapping* 24 (2): 130–43. doi:10.1002/hbm.20075.

Nielsen, Bjørn Fredrik, Xing Cai, and Marius Lysaker. 2007. “On the Possibility for Computing the Transmembrane Potential in the Heart with a One Shot Method: An Inverse Problem.” *Mathematical Biosciences* 210 (2): 523–53. doi:10.1016/j.mbs.2007.06.003.

Nielsen, Bjørn Fredrik, Marius Lysaker, and Aslak Tveito. 2007. “On the Use of the Resting Potential and Level Set Methods for Identifying Ischemic Heart Disease: An Inverse Problem.” *Journal of Computational Physics* 220 (2): 772–90. doi:10.1016/j.jcp.2006.05.040.

Ohyu, S., Y. Okamoto, and S. Kuriki. 2002. “Use of the Ventricular Propagated Excitation Model in the Magnetocardiographic Inverse Problem for Reconstruction of Electrophysiological Properties.” *IEEE Transactions on Biomedical Engineering* 49 (6): 509–19. doi:10.1109/TBME.2002.1001964.

Okamoto, Y., Y. Teramachi, and T. Musha. 1983. “Limitation of the Inverse Problem in Body Surface Potential Mapping.” *IEEE Transactions on Biomedical Engineering* BME-30 (11): 749–54. doi:10.1109/TBME.1983.325190.

Oster, Howard S., and Yoram Rudy. 1992. “The Use of Temporal Information in the Regularization of the Inverse Problem of Electrocardiography.” *IEEE Transactions on Biomedical Engineering* 39 (1): 65–75. doi:10.1109/10.108129.

Oster, Howard S., Bruno Taccardi, Robert L. Lux, Philip R. Ershler, and Yoram Rudy. 1998. “Electrocardiographic Imaging Noninvasive Characterization of Intramural

Myocardial Activation From Inverse-Reconstructed Epicardial Potentials and Electrograms." *Circulation* 97 (15): 1496–1507. doi:10.1161/01.CIR.97.15.1496.

Pascual-Marqui, R. D. 1995. "Reply to Comments by Hämäläinen, Ilmoniemi and Nunez." *Source Localization: Continuing Discussion of the Inverse Problem (W. Skrandies, Ed.)*, 16–28.

Pullan, A. J., L. K. Cheng, M. P. Nash, C. P. Bradley, and D. J. Paterson. 2001. "Noninvasive Electrical Imaging of the Heart: Theory and Model Development." *Annals of Biomedical Engineering* 29 (10): 817–36. doi:10.1114/1.1408921.

Rahimi, A., J. Sapp, J. Xu, P. Bajorski, M. Horacek, and L. Wang. 2016. "Examining the Impact of Prior Models in Transmural Electrophysiological Imaging: A Hierarchical Multiple-Model Bayesian Approach." *IEEE Transactions on Medical Imaging* 35 (1): 229–43. doi:10.1109/TMI.2015.2464315.

Rahimi, A., and L. Wang. 2015. "Sensitivity of Noninvasive Cardiac Electrophysiological Imaging to Variations in Personalized Anatomical Modeling." *IEEE Transactions on Biomedical Engineering* 62 (6): 1563–75. doi:10.1109/TBME.2015.2395387.

Ramanathan, Charulatha, Raja N. Ghanem, Ping Jia, Kyungmoo Ryu, and Yoram Rudy. 2004. "Noninvasive Electrocardiographic Imaging for Cardiac Electrophysiology and Arrhythmia." *Nature Medicine* 10 (4): 422–28. doi:10.1038/nm1011.

Sacher, Frédéric, Usha B. Tedrow, Michael E. Field, Jean-Marc Raymond, Bruce A. Koplan, Laurence M. Epstein, and William G. Stevenson. 2008. "Ventricular Tachycardia Ablation Evolution of Patients and Procedures Over 8 Years." *Circulation: Arrhythmia and Electrophysiology* 1 (3): 153–61. doi:10.1161/CIRCEP.108.769471.

Serinağaoğlu, Y., D.H. Brooks, and Robert S. MacLeod. 2005. “Bayesian Solutions and Performance Analysis in Bioelectric Inverse Problems.” *IEEE Transactions on Biomedical Engineering* 52 (6): 1009–20. doi:10.1109/TBME.2005.846725.

Shpun, Shlomo, Lior Gepstein, Gal Hayam, and Shlomo A. Ben-Haim. 1997. “Guidance of Radiofrequency Endocardial Ablation With Real-Time Three-Dimensional Magnetic Navigation System.” *Circulation* 96 (6): 2016–21. doi:10.1161/01.CIR.96.6.2016.

Skipa, O, M Nalbach, F Sachse, C Werner, and O Dossel. 2002. “Transmembrane Potential Reconstruction In Anistropic Heart Model.” *International Journal of Bioelectromagnetism* 4 (2): 17–18.

Soejima, Kyoko, Makoto Suzuki, William H. Maisel, Corinna B. Brunckhorst, Etienne Delacretaz, Louis Blier, Stanley Tung, Hafiza Khan, and William G. Stevenson. 2001. “Catheter Ablation in Patients With Multiple and Unstable Ventricular Tachycardias After Myocardial Infarction Short Ablation Lines Guided by Reentry Circuit Isthmuses and Sinus Rhythm Mapping.” *Circulation* 104 (6): 664–69. doi:10.1161/hc3101.093764.

Stevenson, William G., and Etienne Delacretaz. 2000. “Radiofrequency Catheter Ablation of Ventricular Tachycardia.” *Heart* 84 (5): 553–59. doi:10.1136/heart.84.5.553.

Thiagalingam, Aravinda, Elisabeth M. Wallace, Anita C. Boyd, Vicki E. Eipper, Craig R. Campbell, Karen Byth, David L. Ross, and Pramesh Kovoor. 2004. “Noncontact Mapping of the Left Ventricle:” *Pacing and Clinical Electrophysiology* 27 (5): 570–78. doi:10.1111/j.1540-8159.2004.00489.x.

Tilg, B., G. Fischer, R. Modre, F. Hanser, B. Messnarz, M. Schocke, C. Kremser, T. Berger, F. Hintringer, and F.X. Roithinger. 2002. “Model-Based Imaging of Cardiac Electrical Excitation in Humans.” *IEEE Transactions on Medical Imaging* 21 (9): 1031–39. doi:10.1109/TMI.2002.804438.

Tung, Leslie. 1978. “A Bi-Domain Model for Describing Ischemic Myocardial Dc Potentials.” Massachusetts Institute of Technology. http://dspace.mit.edu/handle/1721.1/16177.

Vijayakumar, Ramya, Jennifer N. A. Silva, Kavit A. Desouza, Robert L. Abraham, Maria Strom, Frédéric Sacher, George F. Van Hare, Michel Haïssaguerre, Dan M. Roden, and Yoram Rudy. 2014. “Electrophysiologic Substrate in Congenital Long QT Syndrome: Noninvasive Mapping with Electrocardiographic Imaging (ECGI).” *Circulation*, October, CIRCULATIONAHA.114.011359. doi:10.1161/CIRCULATIONAHA.114.011359.

Wang, Dafang, R.M. Kirby, and C.R. Johnson. 2011. “Finite-Element-Based Discretization and Regularization Strategies for 3-D Inverse Electrocardiography.” *IEEE Transactions on Biomedical Engineering* 58 (6): 1827–38. doi:10.1109/TBME.2011.2122305.

Wang, Dafang, Robert M. Kirby, Rob S. MacLeod, and Chris R. Johnson. 2013. “Inverse Electrocardiographic Source Localization of Ischemia: An Optimization Framework and Finite Element Solution.” *Journal of Computational Physics* 250 (October): 403–24. doi:10.1016/j.jcp.2013.05.027.

Wang, Jia-Zhu, S.J. Williamson, and L. Kaufman. 1992. “Magnetic Source Images Determined by a Lead-Field Analysis: The Unique Minimum-Norm Least-Squares Estimation.” *IEEE Transactions on Biomedical Engineering* 39 (7): 665–75. doi:10.1109/10.142641.

Wang, Linwei, F. Dawoud, Sai-Kit Yeung, Pengcheng Shi, K.C.L. Wong, Huafeng Liu, and A.C. Lardo. 2013. “Transmural Imaging of Ventricular Action Potentials and Post-Infarction Scars in Swine Hearts.” *IEEE Transactions on Medical Imaging* 32 (4): 731–47. doi:10.1109/TMI.2012.2236567.

Wang, Linwei, Heye Zhang, K.C.L. Wong, Huafeng Liu, and Pengcheng Shi. 2010. “Physiological-Model-Constrained Noninvasive Reconstruction of Volumetric Myocardial Transmembrane Potentials.” *IEEE Transactions on Biomedical Engineering* 57 (2): 296–315. doi:10.1109/TBME.2009.2024531.

Wang, Yong, Phillip S. Cuculich, Junjie Zhang, Kavit A. Desouza, Ramya Vijayakumar, Jane Chen, Mitchell N. Faddis, Bruce D. Lindsay, Timothy W. Smith, and Yoram Rudy. 2011. “Noninvasive Electroanatomic Mapping of Human Ventricular Arrhythmias with Electrocardiographic Imaging.” *Science Translational Medicine* 3 (98): 98ra84-98ra84. doi:10.1126/scitranslmed.3002152.

Wittkampf, Fred H.m., and Hiroshi Nakagawa. 2006. “RF Catheter Ablation: Lessons on Lesions.” *Pacing and Clinical Electrophysiology* 29 (11): 1285–97. doi:10.1111/j.1540-8159.2006.00533.x.

Yamada, Takumi, William R. Maddox, H. Thomas McElderry, Harish Doppalapudi, Vance J. Plumb, and G. Neal Kay. 2015. “Radiofrequency Catheter Ablation of Idiopathic Ventricular Arrhythmias Originating from Intramural Foci in the Left Ventricular Outflow Tract: Efficacy of Sequential versus Simultaneous Unipolar Catheter Ablation.” *Circulation. Arrhythmia and Electrophysiology* 8 (2): 344–52. doi:10.1161/CIRCEP.114.002259.

Yamashita, Yasuo, and David B. Geselowitz. 1985. “Source-Field Relationships for Cardiac Generators on the Heart Surface Based on Their Transfer Coefficients.” *IEEE Transactions on Biomedical Engineering* BME-32 (11): 964–70. doi:10.1109/TBME.1985.325647.

Yu, Long, Zhaoye Zhou, and Bin He. 2015. “Temporal Sparse Promoting Three Dimensional Imaging of Cardiac Activation.” *IEEE Transactions on Medical Imaging* 34 (11): 2309–19. doi:10.1109/TMI.2015.2429134.

Zhang, Xin, Indiresha Ramachandra, Zhongming Liu, Basharat Muneer, Steven M. Pogwizd, and Bin He. 2005. “Noninvasive Three-Dimensional Electrocardiographic Imaging of Ventricular Activation Sequence.” *American Journal of Physiology - Heart and Circulatory Physiology* 289 (6): H2724–32. doi:10.1152/ajpheart.00639.2005.

Zhou, Z., C. Han, T. Yang, and B. He. 2014. “Noninvasive Imaging of 3-Dimensioal Myocardial Infarction from the Inverse Solution of Equivalent Current Density in Pathological Hearts.” *IEEE Transactions on Biomedical Engineering* PP (99): 1–1. doi:10.1109/TBME.2014.2358618.